ELSEVIER

Progress in Nuclear Magnetic Resonance Spectroscopy 38 (2001) 197–266

PROGRESS IN NUCLEAR MAGNETIC RESONANCE SPECTROSCOPY

www.elsevier.nl/locate/pnmrs

NMR studies of Brownian tumbling and internal motions in proteins

D.M. Korzhnev[a,b], M. Billeter[c], A.S. Arseniev[b], V.Y. Orekhov[a,*]

[a]*Swedish NMR Centre at Göteborg University, Box 465, 405 30 Göteborg, Sweden*
[b]*Shemyakin and Ovchinikov Institute of Bioorganic Chemistry, Russian Academy of Sciences, 16/10 Miklukho-Maklaya str., 117871 Moscow, Russian Federation*
[c]*Göteborg University, Lundberg Laboratory, Biochemistry and Biophysics, Box 462, 405 30 Göteborg, Sweden*

Received 29 June 2000

Contents

Abbreviations: NMR: nuclear magnetic resonance; DD: dipole–dipole; CSA: chemical shift anisotropy; RF: radio frequency; MD: molecular dynamics

* Corresponding author. Tel.: +46-317733886; fax: +46-317733880.
E-mail address: orov@bcbp.gu.se (V.Y. Orekhov).

PII: S0079-6565(00)00028-5

Keywords: Relaxation theory; Cross-correlation; CSA; Backbone dynamics; Hydrodynamics; Diffusion anisotropy; Model-free; Rotating frame; Conformational exchange; Molecular dynamics; Normal mode

Introduction

Bio-macromolecules and their assembles are generally thought of as molecular machines functioning under certain conditions. This definition provides NMR spectroscopists with two major arguments that validate their necessity for intellectual reading of the 'book of life' written in the genome. First, for this purpose one needs spatial structures (co-ordinates of atoms) of bio-molecules at physiological conditions or in media, which mimic them as far as possible. In this respect high-resolution NMR in liquids provides much better opportunities than does its close competitors. Moreover, the complexity of the bio-molecular systems studied by NMR techniques and the accuracy of the NMR structures have grown steadily over the last 15 years. Second, for our understanding of the functioning of bio-molecules not only accurate coordinates of atoms but also the time-scales and amplitudes of their motions are required. There is no doubt about the importance of the internal motions for recognition, binding, signalling, catalysis and other events occurring in living organisms or biotechnological systems and for the proper folding and stabilisation of bio-molecules. In this respect NMR can provide unique information about bio-molecular

dynamics and their response to an external stimulus. Indeed heteronuclear relaxation experiments of isotope (^{15}N and/or ^{13}C) enriched bio-molecules have become widely accepted tools for characterisation of their global and internal motions. Despite the remarkable increase in the number of publications dealing with NMR relaxation studies of bio-molecular dynamics the progress in this area has been much slower as compared to structural NMR. In principle this might indicate that NMR approaches to the analysis of internal dynamics of bio-molecules require a fundamental reconsideration. Therefore this review should not be taken as an account of the progress already achieved, but rather as a practical guidance and discussion of complications in studies of macromolecular motions based on NMR relaxation data. ^{15}N relaxation studies have become routine for analysis of protein intramolecular motions. Therefore, the review is focused on the two-spin ^{1}H–^{15}N system found in a protein backbone. In Section 1 we consider the current state of NMR relaxation theory in liquids and its application to the analysis of relaxation in the two spin 1/2 system, practical aspects of relaxation measurements for a protein backbone ^{1}H–^{15}N group and the parameters governing relaxation in this system. In Section 2 the effect of Brownian rotational diffusion on NMR relaxation is discussed. Attention is paid to computational methods for analysis of macromolecular hydrodynamics and their application to proteins. In Section 3 we discuss the problems, range of validity and advances in the development of the approaches used for analysis of ^{15}N relaxation data in proteins.

1. NMR relaxation in liquids

NMR relaxation is the process that brings a system of nuclear spins back to the equilibrium state. NMR relaxation is a consequence of the coupling of the spin system to the surrounding media (termed the lattice or thermal bath). In particular, different kinds of spin interactions alter upon random molecular motions and perturb the Hamiltonian of the spin system resulting in relaxation of the ensemble of nuclear spins. Spin interactions, modulated by random molecular motions, provide the means for exchange of energy between the spin system and the thermal bath (e.g. overall rotation or intramolecular vibrations). Therefore, the relaxation rates for the spin system depend on the parameters of molecular motions.

The first phenomenological theories of relaxation [1,2] appeared in the very beginning of the development of the NMR method. Semi-classical relaxation theory appears to be the most useful for modern NMR applications [3–8]. This theory considers the system of nuclear spins from a quantum mechanical point of view using the density operator formalism (see [9]) whereas the lattice is treated classically. A theory considering both the lattice and the spin system from a quantum mechanical point of view was also developed (see Ref. [5]). However, in most aspects the semi-classical and quantum mechanical considerations provide identical results. An exception is that the semi-classical theory cannot correctly describe the equilibrium state of the system.

In this section we concisely review general aspects of semi-classical relaxation theory and its application to relaxation in a two-spin heteronuclear system. Chemical exchange phenomena, affecting the measured transverse relaxation rates, are also discussed. In the last two sub-sections of this section we consider heteronuclear two-spin systems of the protein backbone. In particular, some technical aspects of relaxation measurements for protein backbone ^{15}N nuclei are discussed and parameters governing relaxation in backbone ^{15}N–^{1}H and $^{13}C^{\alpha}$–^{1}H systems are reviewed.

1.1. Fundamentals of semi-classical relaxation theory

1.1.1. Master equation

The evolution of a spin system, considered from a quantum mechanical point of view, is described by the density operator $\rho(t)$, whose time dependence is given by the Liouville–von Neumann equation:

$$\frac{\mathrm{d}}{\mathrm{d}t}\rho(t) = -\mathrm{i}[\mathsf{H}_0 + \mathsf{H}_1(t), \rho(t)], \tag{1.1}$$

where H_0 is the time independent part of the Hamiltonian of the spin system and $\mathsf{H}_1(t)$ is the Hamiltonian for a random perturbation, with $\langle \mathsf{H}_1(t) \rangle = 0$. The Hamiltonians in Eq. (1.1) are written in units of the Plank constant $\hbar$. The perturbation due to a random dynamic process, $\mathsf{H}_1(t)$, causes a relaxation of the system towards equilibrium. The stationary

component H_0 of the Hamiltonian can be excluded when considering the system in the *interaction representation* (this corresponds to switching to the rotating frame in classical considerations). An arbitrary operator A in this representation is written as:

$$\mathsf{A}^I(t) = \mathrm{e}^{\mathrm{i}\mathsf{H}_0 t}\mathsf{A}\,\mathrm{e}^{-\mathrm{i}\mathsf{H}_0 t}. \tag{1.2}$$

The Liouville–von Neumann equation in the interaction representation becomes:

$$\frac{\mathrm{d}}{\mathrm{d}t}\rho^I(t) = -\mathrm{i}[\mathsf{H}_1^I(t), \rho^I(t)]; \tag{1.3}$$

it is solved by successive approximations:

$$\rho^I(t) = \rho_0^I(t) + \rho_1^I(t) + \rho_2^I(t) + \cdots \tag{1.4a}$$

where

$$\rho_0^I = \rho^I(0) \qquad \text{and}$$
$$\rho_{i+1}^I(t) = -\mathrm{i}\int_0^t [\mathsf{H}_1^I(t'), \rho_i^I(t')]\,\mathrm{d}t'. \tag{1.4b}$$

To second-order the solution of Eq. (1.3) is given by:

$$\frac{\mathrm{d}}{\mathrm{d}t}\rho^I(t) = -\mathrm{i}[\mathsf{H}_1^I(t), \rho^I(0)] - \int_0^t [\mathsf{H}_1^I(t)[\mathsf{H}_1^I(t-\tau), \rho^I(0)]]\,\mathrm{d}\tau, \tag{1.5}$$

where $\tau = t - t'$ (here the time derivative of $\rho^I(t)$ in Eq. (1.4a) is taken). The observable behaviour of the system is described by the average density operator $\sigma^I(t) = \langle\rho^I(t)\rangle$, whose time evolution is obtained by averaging both sides of Eq. (1.5) over the ensemble of all random Hamiltonians $\mathsf{H}_1^I(t)$. Since $\langle\mathsf{H}_1^I(t)\rangle = 0$, the first term in Eq. (1.5) vanishes. A further simplification of Eq. (1.5) is allowed when using the following assumptions:

1. $\mathsf{H}_1^I(t)$ and $\rho^I(t)$ are uncorrelated and can be averaged separately.
2. The evolution of the density operator $\rho^I(t)$ caused by a random Hamiltonian $\mathsf{H}_1^I(t)$ is slow and $\rho^I(0)$ on the right-hand side of Eq. (1.5) can be replaced by $\rho^I(t)$.
3. It is permissible to replace the upper limit of the integral in Eq. (1.5) by $+\infty$.
4. It is permissible to neglect the higher-order approximations in Eq. (1.5).

In general, these assumptions are valid for weak perturbations $\mathsf{H}_1^I(t)$ and short correlation times τ_c of the random processes. A detailed discussion of the range of validity of these assumptions can be found in Ref. [5]. Averaging of both sides of Eq. (1.5) using the assumptions (1)–(3) results in the master equation written in the following form:

$$\frac{\mathrm{d}}{\mathrm{d}t}\sigma^I(t) = -\int_0^\infty \langle[\mathsf{H}_1^I(t)[\mathsf{H}_1^I(t-\tau), \sigma^I(t)]]\rangle\,\mathrm{d}\tau. \tag{1.6}$$

Since semi-classical theory cannot correctly describe the equilibrium state of the system (i.e. it predicts equal populations for the states, which would correspond to an infinite temperature), the density operator $\sigma^I(t)$ in Eq. (1.6) is usually replaced by $\sigma^I(t) - \sigma_0$, where σ_0 is the equilibrium density operator written as:

$$\sigma_0 = \frac{\mathrm{e}^{-\mathsf{H}_0/k_\mathrm{B}T}}{\mathrm{Tr}[\mathrm{e}^{-\mathsf{H}_0/k_\mathrm{B}T}]}, \tag{1.7}$$

k_B is the Boltzmann constant, T the temperature and Tr means the trace operation.

1.1.2. Operator form of the master equation. Correlation functions

The Hamiltonian of the random perturbation $\mathsf{H}_1(t)$ can be written in the following form:

$$\mathsf{H}_1(t) = \sum_m T_m F_m(t) = \sum_m T_m^+ F_m^*(t), \tag{1.8}$$

where the T_m are operators acting on spin variables, $F_m(t)$ are stationary random functions describing the lattice, and the cross and asterisk denote Hermitian and complex conjugate operations, respectively. The dual form of $\mathsf{H}_1(t)$ in Eq. (1.8) indicates that $\mathsf{H}_1(t)$ is a Hermitian operator. The spin operators T_m are the components of an irreducible tensor operator of rank l, and the random functions $F_m(t)$ are proportional to spherical harmonics of rank l (see Appendix A). The value of l depends on the relaxation mechanisms considered. In particular, for dipole–dipole relaxation, relaxation due to the chemical shift anisotropy and for quadrupolar relaxation $l = 2$. The transformation of spin operators T_m to the interaction

representation results in:

$$T_m^I = \mathrm{e}^{\mathrm{i}\mathsf{H}_0 t} T_m \, \mathrm{e}^{-\mathrm{i}\mathsf{H}_0 t} = \sum_n T_m^n \, \mathrm{e}^{\mathrm{i}\omega_m^n t} m, \tag{1.9}$$

where T_m^n meet the relationship $[\mathsf{H}_0, T_m^n] = \omega_m^n T_m^n$, and ω_m^n are the differences between the eigenfrequencies of the Hamiltonian H_0 (see Ref. [10]). The Hamiltonian of a random perturbation in the interaction representation $\mathsf{H}_1^I(t)$ is then expressed as:

$$\mathsf{H}_1^I(t) = \sum_m T_m^l F_m(t) = \sum_{m,n} T_m^n F_m(t) \, \mathrm{e}^{\mathrm{i}\omega_m^n t}. \tag{1.10}$$

Substitution of $\mathsf{H}_1^I(t)$ from Eq. (1.10) into Eq. (1.6) results in the master equation written in operator form:

$$\frac{\mathrm{d}}{\mathrm{d}t}\sigma^I(t) = - \sum_{m,m',n,n'} (-1)^{m'} \, \mathrm{e}^{\mathrm{i}(\omega_m^n + \omega_{m'}^{n'})t} [T_{m'}^{n'}[T_m^n, \sigma^I(t) - \sigma_0]] \times \int_0^\infty \langle F_m(t) F_{-m'}^*(t+\tau)\rangle \, \mathrm{e}^{-\mathrm{i}\omega_m^n \tau} \, \mathrm{d}\tau. \tag{1.11}$$

Since the random process resulting in relaxation is stationary, the factor $\langle F_m(t) F_{-m'}^*(t+\tau)\rangle$ on the right-hand side of Eq. (1.11) can be replaced by $\langle F_m(0) F_{-m'}^*(\tau)\rangle$. Moreover, for spherical harmonics, S_{lm} and $V_{l'm'}$ of ranks l and l', averaging over the ensemble results in the following relationship [7,11]:

$$\langle S_{l'm'}(0) V_{lm}(t)\rangle = \delta_{l',l}\delta_{m',-m}(-1)^m \langle S_{l0}(0) V_{l0}(t)\rangle, \tag{1.12a}$$

where δ is the Kronecker delta. Therefore, the factor $\langle F_m(0) F_{-m'}^*(\tau)\rangle$ in Eq. (1.11) can be written as:

$$\langle F_m(0) F_{-m'}^*(\tau)\rangle = \delta_{m',-m} \langle F_0(0) F_0(\tau)\rangle, \tag{1.12b}$$

which allows to us avoid the summation over the index m' in the right-hand side of Eq. (1.11) by replacing m' by $-m$.

A further simplification of Eq. (1.11) is obtained by the *secular approximation*: due to the rapidly oscillating factors $\mathrm{e}^{\mathrm{i}(\omega_m^n + \omega_{-m}^{n'})t}$ the terms with $\omega_m^n + \omega_{-m}^{n'} \neq 0$ in Eq. (1.11) are averaged to zero before the relaxation occurs and, thus, may be neglected. The remaining secular terms in Eq. (1.11) fit the condition $n = n'$, which holds in the absence of degenerate eigenfrequencies of the Hamiltonian H_0 (i.e. if all $\omega_m^n + \omega_{-m}^{n'} (n \neq n')$ exceed the value $\langle|\mathsf{H}_1^I(t)|\rangle^2 \tau_c$, that determines the characteristic rate for change of $\sigma^I(t)$).

Let us now introduce the concepts of the *correlation function* $C(\tau)$ and the *spectral density function* $J(\omega)$, which is the cosine Fourier transform of the correlation function $C(\tau)$:

$$C(\tau) = \langle F_0(0) V_0(\tau)\rangle, \tag{1.13a}$$

$$J(\omega) = \int_0^\infty C(\tau) \cos(\omega\tau) \, \mathrm{d}\tau. \tag{1.13b}$$

Here F and V are proportional to spherical harmonics of the same rank. If $F(t) \equiv V(t)$ the functions $C(\tau)$ and $J(\omega)$ are referred to as auto-correlation, otherwise they are termed as cross-correlation. Let us also define the quantity $k(\omega)$ as:

$$k(\omega) = \int_0^\infty C(\tau) \sin(\omega\tau) \, \mathrm{d}\tau. \tag{1.13c}$$

The integral in the right-hand side of Eq. (1.11) is equal to $J(\omega) - \mathrm{i}k(\omega)$. However, it can be shown [5,6] that the complex part of the integral results in small second-order shifts of the eigenvalues of the Hamiltonian (the so-called dynamic frequency shift), which may be safely neglected when considering relaxation.

Finally, applying the above mentioned simplifications to Eq. (1.11), one can write the operator form of the master equation:

$$\frac{\mathrm{d}}{\mathrm{d}t}\sigma^I(t) = - \sum_{m,n} (-1)^m J(\omega_m^n)[T_{-m}^n, [T_m^n, \sigma^I(t) - \sigma_0]], \tag{1.14a}$$

$$\frac{\mathrm{d}}{\mathrm{d}t}\sigma(t) = -\mathrm{i}[\mathsf{H}_0, \sigma(t)] - \sum_{m,n} (-1)^m J(\omega_m^n) \times [T_{-m}^n, [T_m^n, \sigma(t) - \sigma_0]], \tag{1.14b}$$

where Eq. (1.14b) is written in the Schrödinger representation (laboratory frame).

1.1.3. Master equation for mean values

Experimentally observable quantities are connected with the spin operators Q by the following relationships:

$$\langle Q\rangle(t) = \mathrm{Tr}[Q\sigma(t)], \tag{1.15a}$$

$$\langle Q\rangle^I(t) = \mathrm{Tr}[Q\sigma^I(t)]. \tag{1.15b}$$

For studies of slow changes of $\langle Q\rangle$ due to the relaxation process it is convenient to consider the time evolution of $\langle Q\rangle$ in the interaction representation. If the operator Q commutes with the Hamiltonian H_0, Eqs. (1.15a) and (1.15b) provide identical results. The time dependence of $\langle Q\rangle^I$ is calculated by multiplying both sides of Eq. (1.14a) with Q and performing the trace operation:

$$\frac{\mathrm{d}}{\mathrm{d}t}\langle Q\rangle^I(t) = -(\mathrm{Tr}[\hat{\Gamma}(Q)\sigma^I(t)] - \mathrm{Tr}[\hat{\Gamma}(Q)\sigma_0])$$
$$= \langle\hat{\Gamma}(Q)\rangle^I(t) - \langle\hat{\Gamma}(Q)\rangle_0, \tag{1.16a}$$

where $\hat{\Gamma}$ is the relaxation super-operator given by:

$$\hat{\Gamma}(Q) = \sum_{m,n}(-1)^m J(\omega_m^n)[T_m^n,[T_{-m}^n, Q]]. \tag{1.16b}$$

Using Eqs. (1.16a) and (1.16b) one can easily derive the expressions for relaxation rates for any observable quantity connected with a spin operator Q. A basis of spin operators, Bs_i, may be defined. For the complete analysis of relaxation in a particular spin system it is convenient to derive the expressions for relaxation rates for all basis operators $\langle Bs_i\rangle$:

$$\frac{\mathrm{d}}{\mathrm{d}t}\langle\mathbf{Bs}\rangle^I(t) = \mathbf{R}(\langle\mathbf{Bs}\rangle^I(t) - \langle\mathbf{Bs}\rangle_0^I), \tag{1.17}$$

where $\mathbf{B}$ is the vector composed of basis operators Bs_i, $\mathbf{R}$ is the matrix comprising auto- and cross-relaxation rates for $\langle Bs_i\rangle$, which is referred to as the relaxation matrix. For the computations it is convenient to use the matrix forms of operators T_m^n and Bs_i.

The following computational procedure may be used:

1. Represent the Hamiltonian of a random process $\mathsf{H}_1^I(t)$ as a product of random functions $F_m(t)$, proportional to spherical harmonics, with components of an irreducible tensor operator T_m^n (Eq. (1.10)). Calculate the eigenfrequencies ω_m^n.
2. Evaluate $\hat{\Gamma}(Q)$ for a given operator Q by applying the double commutators of Eq. (1.16b). Calculate the right-hand side of Eq. (1.16a).
3. If a basis of spin operators, Bs_i, has been defined, one may expand the result over this basis. The coefficients of the expansion will correspond to the rates of cross-relaxation from $\langle Q\rangle$ to $\langle Bs_i\rangle$.

1.2. Relaxation in a heteronuclear two-spin 1/2 system

Below we consider a spin system composed of two unlike spin-1/2 nuclei **I** and **S**. The relaxation in this system is due to dipole–dipole (DD) interactions between the two spins and their chemical shift anisotropy (CSA), modulated by random molecular motions. A typical example of a two-spin heteronuclear system is a ^{15}N–^{1}H nuclear pair of a protein backbone amide group. For such a group, the relaxation rates, derived here for an ideal two-spin system, could be modified to account for: (i) the DD relaxation from the amide proton to other protons; and (ii) contributions of the conformational exchange on a micro millisecond time scale (Section 1.3). Below we derive the expressions for the relaxation rates for all Cartesian product operators of a two-spin 1/2 system. In some cases the expressions for shift basis and single-transition basis operators are also presented. Special attention is paid to the effect of cross-correlation between DD and CSA interactions, and to the cross-correlation between the CSA interactions of the spins **I** and **S**.

1.2.1. Hamiltonian for dipole–dipole interactions

The most important mechanism expected to cause relaxation is the DD interaction between magnetic moments of neighbouring nuclei, modulated by random molecular motions. The Hamiltonian for two spins **I** and **S**, interacting by the dipolar mechanism, is given by:

$$\mathsf{H}_1^{\mathrm{D}}(t) = \frac{\mu_0}{4\pi}\frac{\gamma_I\gamma_S\hbar}{r^3(t)}\left(\mathbf{I}\cdot\mathbf{S} - \frac{3}{r^2(t)}(\mathbf{I}\cdot\mathbf{r}(t))(\mathbf{S}\cdot\mathbf{r}(t))\right). \tag{1.18}$$

Here **I** and **S** denote the operators of spin angular momentum for the nuclei, γ_I and γ_S are their gyromagnetic ratios, $\mathbf{r}(t)$ is the internuclear unit vector, $r(t)$ is the internuclear distance, μ_0 is the permeability of free space. By transforming $\mathbf{r}(t)$ to polar co-ordinates one can write the Hamiltonian $\mathsf{H}_1^{\mathrm{D}}(t)$ in a form analogous to Eq. (1.8). Corresponding components of the irreducible tensor operator T_m, acting on spin variables, and the random functions $F_m(t)$ (Eq. (1.8))

are given by:

$$T_m = \sqrt{\frac{3}{10}}\frac{\mu_0}{4\pi}\gamma_I\gamma_S\hbar\langle r^{-3}\rangle T_{2m} \tag{1.19a}$$

$$T_{2,0} = -\frac{1}{\sqrt{6}}(4I_zS_z - (I_+S_- + I_-S_+))$$

$$T_{2,\pm1} = \pm(I_zS_\pm + I_\pm S_z)$$

$$T_{2,\pm2} = -I_\pm S_\pm$$

$$F_m(t) = \sqrt{4\pi}Y^*_{2m}(\theta(t),\varphi(t)), \tag{1.19b}$$

where I_i and S_i $(i = x, y, z)$ are the components of operators **I** and **S**, $I_\pm$ and $S_\pm$ are shift operators defined as $I_\pm = I_x \pm iI_y$ and $S_\pm = S_x \pm iS_y$, Y_{2m} are spherical harmonics of rank 2 (see Appendix A), $\theta(t)$ and $\varphi(t)$ are time-dependent polar angles defining the orientation of the vector $\mathbf{r}(t)$ in the laboratory co-ordinate frame, and the index m runs over $(-2,2)$. It is worth noting that Eqs. (1.19a) and (1.19b) are valid only if the orientation of the internuclear vector changes much more slowly than the internuclear distance (see Refs. [12,13]), or if the amplitudes of vibrations involving the internuclear distance are negligibly small. Otherwise, the following definitions for T_m and $F_m(t)$ should be used:

$$T_m = \sqrt{\frac{3}{10}}\frac{\mu_0}{4\pi}\gamma_I\gamma_S\hbar\langle r^{-6}\rangle^{1/2}T_{2m}$$
$$F_m(t) = \sqrt{4\pi}\langle r^{-6}\rangle^{-1/2}\frac{Y^*_{2m}(\theta(t),\varphi(t))}{r^3(t)}. \tag{1.19c}$$

In Eqs. (1.19b) and (1.19c)) $F_m(t)$ are normalised in such a manner that the correlation function $C(t) = \langle F_0(0)F_0(t)\rangle$ (Eq. (1.13a)) is equal to 1 at $t = 0$.

It can be shown that for isotropic media the dipolar Hamiltonian is averaged to zero by the random molecular motions, i.e. $\langle \mathsf{H}_1^{\mathrm{D}}(t)\rangle = 0$. Thus, for the dipolar relaxation the time-independent Hamiltonian H_0 (Eq. (1.1)) corresponds to the Zeeman Hamiltonian for nuclear moments interacting with the permanent magnetic field $\mathbf{B}_0$ directed along the z-axis:

$$\mathsf{H}_0 = -\gamma_I(\mathbf{B}_0\cdot\mathbf{I}) - \gamma_S(\mathbf{B}_0\cdot\mathbf{S}) = \omega_I I_z + \omega_S S_z, \tag{1.20}$$

where $\omega_I = \gamma_I B_0$ and $\omega_S = \gamma_S B_0$ are the Larmor frequencies of spins **I** and **S**. Using the relationships:

$$e^{i\mathsf{H}_0 t}I_z\, e^{-i\mathsf{H}_0 t} = I_z$$

$$e^{i\mathsf{H}_0 t}I_\pm\, e^{-i\mathsf{H}_0 t} = I_\pm\, e^{\pm i\omega_I t}$$

$$e^{i\mathsf{H}_0 t}S_z\, e^{-i\mathsf{H}_0 t} = S_z$$

$$e^{i\mathsf{H}_0 t}S_\pm\, e^{-i\mathsf{H}_0 t} = S_\pm\, e^{\pm i\omega_S t} \tag{1.21}$$

one can easily transform the Hamiltonian $\mathsf{H}_1^{\mathrm{D}}(t)$ to the interaction representation. The spin operators T_m (Eqs. (1.19a)–(1.19c)) in the interaction representation are written as:

$$T_0^I = \underbrace{-\frac{4A_{\mathrm{D}}}{\sqrt{6}}I_zS_z}_{T_0^1;\omega_0^1=0} + \underbrace{\frac{A_{\mathrm{D}}}{\sqrt{6}}I_+S_-\, e^{i(\omega_I-\omega_S)t}}_{T_0^2;\omega_0^2=\omega_I-\omega_S} + \underbrace{\frac{A_{\mathrm{D}}}{\sqrt{6}}I_-S_+\, e^{-i(\omega_I-\omega_S)t}}_{T_0^3;\omega_0^3=-(\omega_I-\omega_S)} \tag{1.22a}$$

$$T_{\pm1}^I = \underbrace{\pm A_{\mathrm{D}}I_zS_\pm\, e^{\pm i\omega_I t}}_{T_{\pm1}^1;\omega_{\pm1}^1=\pm\omega_I}\ \underbrace{\pm A_{\mathrm{D}}I_\pm S_z\, e^{\pm i\omega_S t}}_{T_{\pm1}^2;\omega_{\pm1}^2=\pm\omega_S}$$

$$T_{\pm2}^1 = \underbrace{A_{\mathrm{D}}I_\pm S_\pm\, e^{\pm i(\omega_I+\omega_S)t}}_{T_{\pm2}^1;\omega_{\pm2}^1=\pm(\omega_I+\omega_S)},$$

where

$$A_{\mathrm{D}} = \sqrt{\frac{3}{10}}\frac{\mu_0}{4\pi}\gamma_I\gamma_S\hbar\langle r^{-3}\rangle, \tag{1.22b}$$

assuming that Eqs. (1.19a) and (1.19b) are valid. Eqs. (1.22a) and (1.22b) allows us to express the Hamiltonian $(\mathsf{H}_1^{\mathrm{D}})^I(t)$ in a form analogous to Eq. (1.10), which is required for the derivation of the relaxation rates. The corresponding T_m^n and ω_m^n are written below each term in Eq. (1.22a).

1.2.2. Hamiltonian for anisotropic chemical shift

The local electronic environment produces an additional magnetic field at the location of the nucleus being placed in a strong magnetic field. This effect is termed nuclear shielding. The local electronic environment of the nucleus is, in general, not isotropic. Thus, the changes in nuclear shielding upon random molecular reorientation are expected to result in relaxation. The Hamiltonian for nuclear shielding is a bilinear combination with respect to the

components of the external field $\mathbf{B}_0$ and the spin $\mathbf{I}$:

$$\mathsf{H}^{\mathrm{CS}}_{1(\mathbf{I})} = \gamma_I \mathbf{B}_0 \cdot \boldsymbol{\Omega} \cdot \mathbf{I}. \tag{1.23}$$

Here, $\boldsymbol{\Omega}$ denotes the *chemical shielding tensor*. Eq. (1.23) is written in a molecular co-ordinate frame, rigidly attached to the eigenvectors of the shielding tensor.

The chemical shielding tensor may be represented as a sum of isotropic and anisotropic parts, $\boldsymbol{\Omega}_{\mathrm{is}}$ and $\boldsymbol{\Omega}_{\mathrm{a}}$. The isotropic part $\boldsymbol{\Omega}_{\mathrm{is}}$ does not change with the rotation of the co-ordinate system and has all three eigenvalues equal to Ω (below we assume that $|\Omega| \ll 1$). The anisotropic part $\boldsymbol{\Omega}_{\mathrm{a}}$, is the second-rank symmetric traceless tensor referred to as the *shielding anisotropy tensor* (here and in the following we neglect the anti-symmetric part of the shielding tensor [14]). $\boldsymbol{\Omega}_{\mathrm{a}}$ has the eigenvalues δ_z, $\delta_x = -1/2(1-\eta)\delta_z$ and $\delta_y = -1/2(1+\eta)\delta_z$, where $\eta = (\delta_x - \delta_y)/\delta_z$ is the termed the asymmetry parameter. Thus, the Hamiltonian $\mathsf{H}^{\mathrm{CS}}_{1(\mathbf{I})}$ (Eq. (1.23)) can be separated into two parts corresponding to isotropic and anisotropic shielding $-\mathsf{H}^{\mathrm{CSI}}_{1(\mathbf{I})}$ and $\mathsf{H}^{\mathrm{CSA}}_{1(\mathbf{I})}$. The isotropic part $\mathsf{H}^{\mathrm{CSI}}_{1(\mathbf{I})}$ does not change with molecular motions and can be included into the Zeeman Hamiltonian (in this case the Larmor frequency for spin $\mathbf{I}$ is given by $\omega_I = (1 - \Omega)\gamma_I B_0 \approx \gamma_I B_0$). The anisotropic part $\mathsf{H}^{\mathrm{CSA}}_{1(\mathbf{I})}$ changes during random molecular motions and results in relaxation. For an isotropic media it can be shown that $\langle \mathsf{H}^{\mathrm{CSA}}_{1(\mathbf{I})}(t) \rangle = 0$.

Transformation of Eq. (1.23) to the laboratory frame, where the magnetic field $\mathbf{B}_0$ is directed along z-axis, results in $\mathsf{H}^{\mathrm{CSA}}_{1(\mathbf{I})}$ written in a form analogous to Eq. (1.8):

$$\mathsf{H}^{\mathrm{CSA}}_{1(\mathbf{I})} = \sum_{m=-2}^{2} T_m F_m, \tag{1.24a}$$

where

$$T_0 = -\frac{A_{\mathrm{CSA}(\mathbf{I})}}{\sqrt{6}}(4B_z I_z - (B_+ I_- + B_- I_+)) = -\frac{4A_{\mathrm{CSA}(\mathbf{I})}}{\sqrt{6}} B_0 I_z$$

$$T_{\pm 1} = \pm A_{\mathrm{CSA}(\mathbf{I})}(B_z I_\pm + I_z B_\pm) = \pm A_{\mathrm{CSA}(\mathbf{I})} B_0 I_\pm$$

$$T_{\pm 2} = -A_{\mathrm{CSA}(\mathbf{I})} B_\pm I_\pm = 0 \tag{1.24b}$$

$$F_m(t) = (1 + \eta^2/3)^{-\frac{1}{2}}(\sqrt{4\pi} Y^*_{2m}(\beta, \alpha) + \sqrt{5/6\eta}(D^2_{m,2}(\alpha, \beta, \gamma) + D^2_{m,-2}(\alpha, \beta, \gamma))) \tag{1.24c}$$

$$A_{\mathrm{CSA}(\mathbf{I})} = -\sqrt{\frac{3}{10}}\frac{1}{2}\gamma_I \delta_z (1 + \eta^2/3)^{\frac{1}{2}} \tag{1.24d}$$

where T_m are the components of an irreducible tensor operator of rank 2, α, β and γ are the time-dependent Euler angles defining the orientation of the molecular co-ordinate frame with respect to the laboratory frame, $D^2_{mm'}(\alpha, \beta, \gamma)$ are Wigner functions (see Appendix A). As in the case of dipolar interactions, the $F_m(t)$ are normalised to meet the condition $C(t) = 1$ at $t = 0$ (see Eq. (1.13a)). In the case of an asymmetric shielding anisotropy tensor (here and below 'asymmetric' means that $\delta_x \neq \delta_y$ and $\eta \neq 0$) it is cumbersome to calculate the correlation function $C(t)$ from $F_m(t)$ given by Eq. (1.24c). This can be avoided by representing $\boldsymbol{\Omega}_{\mathrm{a}}$ as a sum of two axially symmetric tensors that are considered as independent sources of relaxation [15]. For an axially symmetric shielding anisotropy tensor Eq. (1.24c) is reduced to:

$$F_m(t) = \sqrt{4\pi} Y^*_{2m}(\beta, \alpha) \tag{1.24e}$$

which is equivalent to Eq. (1.19b) for the dipolar relaxation (with the exception that β and α here are the polar angles defining the orientation of the symmetry axis of the shielding anisotropy tensor).

Using Eq. (1.21) one can easily write the spin operators T_m (Eq. (1.24b)) in the interaction representation:

$$(T_0)^I = \underset{T^0_0;\omega^0_0=0}{-\frac{4A_{\mathrm{CSA}(\mathbf{I})}B_0 I_z}{\sqrt{6}}}$$

$$(T_{\pm 1})^I = \underset{T^0_1;\omega^0_1=\pm\omega_I}{\pm A_{\mathrm{CSA}(\mathbf{I})} B_0 I_\pm \, \mathrm{e}^{\pm \mathrm{i}\omega_I t}} \tag{1.25}$$

$$(T_{\pm 2})^I = 0$$

Eq. (1.25) allows us to express $(\mathsf{H}^{\mathrm{CSA}}_{1(\mathbf{I})})^I$ in a form analogous to Eq. (1.10), which is required for the derivation of the relaxation rates (the corresponding T^n_m and ω^n_m are written below each term in Eq. (1.25)).

1.2.3. Expressions for relaxation rates

Let us now derive the expressions for all auto- and cross-relaxation rates for the mean values of Cartesian product operators of a two spin 1/2 system[1] relaxing by the DD and CSA mechanisms. Below it is assumed that: (i) the distance between the nuclei changes much faster than the orientation of the internuclear vector; and (ii) the shielding anisotropy tensors for the spins are axially symmetric ($\eta_I = \eta_S = 0$).

The existence of several relaxation mechanisms in the two-spin system considered causes effects of relaxation interference (or cross-correlation effects). Two relaxation mechanisms A and B might be accounted for independently when the cross-correlation function $C_{AB}(\tau) = \langle F_0^A(0)F_0^B(\tau)\rangle$ is zero. This condition holds if: (i) $F_m^A(t)$ and $F_m^B(t)$ are proportional to the spherical harmonics of different ranks; or (ii) $F_m^A(t)$ and $F_m^B(t)$ are uncorrelated. Otherwise, expressions for the relaxation rates would depend both on the auto-correlation and cross-correlation spectral density functions (Eqs. (1.13a), (1.13b)). The effects of cross-correlation account for cross-relaxation pathways, which are prohibited when the relaxation is considered for each mechanism independently. The cross-correlated cross-relaxation often results in complex multi-exponential decays for the components of magnetisation, which complicates the analysis of the relaxation data. On the other hand the rates of the cross-correlated cross-relaxation might provide useful information about the molecular motions. Examples of cross-correlation effects are interference between the dipolar interactions for two nuclear pairs in a multi-spin system [5,16] or interference between dipolar and CSA interactions [15]. The effects of DD–CSA **I**, DD–CSA **S** and CSA **I**–CSA **S** cross-correlation will be considered here for a two-spin 1/2 system.

The master equation for mean values of the Cartesian product operators (Eqs. (1.16a)–(1.17)) is easily obtained using the expressions for the spin operators T_m^n and the frequencies ω_m^n for the DD (Eqs. (1.22a) and (1.22b)) and CSA (Eq. (1.25)) relaxation mechanisms. The right-hand side of the master equation (Eq. (1.16a)) contains the relaxation super-operator $\hat{\Gamma}(Q)$ (Eq. (1.16b)) given by:

$$\hat{\Gamma}(Q) = \hat{\Gamma}_{\mathrm{D}}(Q) + \hat{\Gamma}_{\mathrm{CSA(I)}}(Q) + \hat{\Gamma}_{\mathrm{CSA(S)}}(Q) + \hat{\Gamma}_{\mathrm{D,CSA(I)}}(Q) + \hat{\Gamma}_{\mathrm{D,CSA(S)}}(Q) + \hat{\Gamma}_{\mathrm{CSA(I),CSA(S)}}(Q), \tag{1.26}$$

where Q is the product operator considered. The terms composing the relaxation super-operator (Eq. (1.26)) are summarised in Table 1. As it is seen from Table 1 the terms in Eq. (1.26) depend on the auto- and cross-correlation spectral density functions $J_{\mathrm{D}}(\omega)$, $J_{\mathrm{CSA(I)}}(\omega)$, $J_{\mathrm{CSA(S)}}(\omega)$, $J_{\mathrm{D,CSA(I)}}(\omega)$, $J_{\mathrm{D,CSA(S)}}(\omega)$, $J_{\mathrm{CSA(I),CSA(S)}}(\omega)$ describing reorientation of the internuclear vector and the principal axes of the shielding anisotropy tensors of the spins **I** and **S**. However, it can be shown (see e.g. Ref. [17]) that for isotropic rotation diffusion and/or for small angles $\theta_{\mathrm{D,CSA(I)}}$, $\theta_{\mathrm{D,CSA(S)}}$, $\theta_{\mathrm{CSA(I),CSA(S)}}$ a good approximation for the spectral density functions is provided by:

$$J(\omega) = J_{\mathrm{D}}(\omega) = J_{\mathrm{CSA(I)}}(\omega) = J_{\mathrm{CSA(S)}}(\omega) = \frac{J_{\mathrm{D,CSA(I)}}(\omega)}{P_2(\cos\theta_{\mathrm{D,CSA(I)}})} = \frac{J_{\mathrm{D,CSA(S)}}(\omega)}{P_2(\cos\theta_{\mathrm{D,CSA(S)}})} = \frac{J_{\mathrm{CSA(I),CSA(S)}}(\omega)}{P_2(\cos\theta_{\mathrm{CSA(I),CSA(S)}})}, \tag{1.27}$$

where $P_2(x) = (3x^2 - 1)/2$ is a second-rank Legendre polynomial. By calculating $\langle\hat{\Gamma}(Q)\rangle(t)$ and $\langle\hat{\Gamma}(Q)\rangle_0$ (Eq. (1.16a)), and expanding the result over the basis of Cartesian product operators one can fill the relaxation matrix **R** (Eq. (1.17)) for the Cartesian product operators by the relaxation rates.

According to the block structure of the relaxation matrix **R** in a two-spin 1/2 system the Cartesian product operators can be separated into several groups. The group (I_z, S_z, $2I_zS_z$) is composed of longitudinal coherences for spins **I** and **S** and longitudinal two spin-order. The groups (I_x, $2I_xS_z$), (I_y, $2I_yS_z$), (S_x, $2I_zS_x$), (S_y, $2I_zS_y$) are composed of transverse in-phase and anti-phase coherences. The groups ($2I_xS_x$, $2I_yS_y$) and ($2I_xS_y$, $2I_yS_x$) consist of two-spin coherences, which are linear combinations of zero-quantum I_+S_-, I_-S_+ and double-quantum I_+S_+, I_-S_- coherences.

The relaxation in the group (I_z, S_z, $2I_zS_z$) (termed as

[1] Cartesian product operators for two-spin 1/2 system are $E/2$, I_x, I_y, I_z, S_x, S_y, S_z, $2I_xS_x$, $2I_yS_x$, $2I_zS_x$, $2I_yS_x$, $2I_yS_y$, $2I_yS_z$, $2I_zS_x$, $2I_zS_y$, $2I_zS_z$ where E is the identity operator.

Table 1
Relaxation super-operators for a two-spin 1/2 system (Here it is assumed that $\mathbf{B}_0$ is directed along the z-axis; A_D, $A_{CSA(I)}$ and $A_{CSA(S)}$ are given by Eqs. (1.22b) and (1.24d); the auto and cross-correlation spectral density functions $J_D(\omega)$,$J_{CSA(I)}(\omega)$, $J_{CSA(S)}(\omega)$, $J_{D,CSA(I)}(\omega)$, $J_{D,CSA(S)}(\omega)$, $J_{CSA(I),CSA(S)}(\omega)$ are the cosine Fourier transforms of the correlation functions (Eqs. (1.13a), (1.13b)), composed from the lattice random functions $F_m(t)$ for the corresponding interactions ($F_m(t)$ are given by Eq. (1.19b) for dipolar interactions and by Eq. (1.24e) for CSA interactions)

Dipolar relaxation
$\hat{\Gamma}_D(Q) = \frac{8}{3}A_D^2 J_D(0)[I_zS_z[I_zS_z,Q]] + \frac{1}{6}A_D^2 J_D(\omega_I-\omega_S)([I_-S_+[I_+S_-,Q]] + [I_+S_-[I_-S_+,Q]]) + A_D^2 J_D(\omega_I)([I_-S_z[I_+S_z,Q]] + [I_+S_z[I_-S_z,Q]]) + A_D^2 J_D(\omega_S)([I_zS_-[I_zS_+,Q]] + [I_zS_+[I_zS_-,Q]]) + A_D^2 J_D(\omega_I+\omega_S)([I_-S_-[I_+S_+,Q]] + [I_+S_+[I_-S_-,Q]])$

CSA relaxation of spin **I**
$\hat{\Gamma}_{CSA(I)}(Q) = \frac{8}{3}A_{CSA(I)}^2 B_0^2 J_{CSA(I)}(0)[I_z[I_z,Q]] + A_{CSA(I)}^2 B_0^2 J_{CSA(I)}(\omega_I)([I_-[I_+,Q]] + [I_+[I_-,Q]])$

CSA relaxation of spin **S**
$\hat{\Gamma}_{CSA(S)}(Q) = \frac{8}{3}A_{CSA(S)}^2 B_0^2 J_{CSA(S)}(0)[S_z[S_z,Q]] + A_{CSA(S)}^2 B_0^2 J_{CSA(S)}(\omega_S)([S_-[S_+,Q]] + [S_+[S_-,Q]])$

DD–CSA **I** cross-correlation
$\hat{\Gamma}_{D,CSA(I)}(Q) = \frac{8}{3}A_D A_{CSA(I)} B_0 J_{D,CSA(I)}(0)([I_z[I_zS_z,Q]] + [I_zS_z[I_z,Q]]) + A_D A_{CSA(I)} B_0 J_{D,CSA(I)}(\omega_I)([I_-[I_+S_z,Q]] + [I_+S_z[I_-,Q]] + [I_+[I_-S_z,Q]] + [I_-S_z[I_+,Q]])$

DD–CSA **S** cross-correlation
$\hat{\Gamma}_{D,CSA(S)}(Q) = \frac{8}{3}A_D A_{CSA(S)} B_0 J_{D,CSA(S)}(0)([S_z[I_zS_z,Q]] + [I_zS_z[S_z,Q]]) + A_D A_{CSA(S)} B_0 J_{D,CSA(S)}(\omega_S)([S_-[I_zS_+,Q]] + [I_zS_+[S_-,Q]] + [S_+[I_zS_-,Q]] + [I_zS_-[S_+,Q]])$

CSA **I**–CSA **S** cross-correlation
$\hat{\Gamma}_{CSA(I),CSA(S)}(Q) = \frac{8}{3}A_{CSA(I)} A_{CSA(S)} B_0^2 J_{CSA(I),CSA(S)}(0)([S_z[I_z,Q]] + [I_z[S_z,Q]])$

longitudinal) is described by the equation:

$$\frac{d}{dt}\begin{bmatrix}\langle I_z\rangle - I_{z0}\\ \langle S_z\rangle - S_{z0}\\ \langle 2I_zS_z\rangle\end{bmatrix} = -\begin{bmatrix}R_{1\mathbf{I}}^{D}+R_{1\mathbf{I}}^{CSA} & \rho_D & \rho_{D,CSA(\mathbf{I})}\\ \rho_D & R_{1\mathbf{S}}^{D}+R_{1\mathbf{S}}^{CSA} & \rho_{D,CSA(\mathbf{S})}\\ \rho_{D,CSA(\mathbf{I})} & \rho_{D,CSA(\mathbf{S})} & R_{1\mathbf{I}}^{CSA}+R_{1\mathbf{S}}^{CSA}+\lambda\end{bmatrix} \times \begin{bmatrix}\langle I_z\rangle - I_{z0}\\ \langle S_z\rangle - S_{z0}\\ \langle 2I_zS_z\rangle\end{bmatrix}, \quad (1.28a)$$

where

$$R_{1\mathbf{I}}^{D} = A_D^2(\tfrac{1}{3}J(\omega_I-\omega_S) + J(\omega_I) + 2J(\omega_I+\omega_S))$$

$$R_{1\mathbf{S}}^{D} = A_D^2(\tfrac{1}{3}J(\omega_I-\omega_S) + J(\omega_S) + 2J(\omega_I+\omega_S)) \quad (1.28b)$$

$$R_{1\mathbf{I}}^{CSA} = 4A_{CSA(I)}^2 B_0^2 J(\omega_I) \qquad R_{1\mathbf{S}}^{CSA} = 4A_{CSA(S)}^2 B_0^2 J(\omega_S) \quad (1.28c)$$

$$\rho_D = A_D^2(2J(\omega_I+\omega_S) - \tfrac{1}{3}J(\omega_I-\omega_S)) \quad (1.28d)$$

$$\rho_{D,CSA(\mathbf{I})} = 4A_D A_{CSA(I)} P_2(\cos\theta_{D,CSA(I)}) B_0 J(\omega_I)$$

$$\rho_{D,CSA(\mathbf{S})} = 4A_D A_{CSA(S)} P_2(\cos\theta_{D,CSA(S)}) B_0 J(\omega_S) \quad (1.28e)$$

$$\lambda = A_D^2(J(\omega_I) + J(\omega_S)). \quad (1.28f)$$

Here A_D, $A_{CSA(I)}$ and $A_{CSA(S)}$ are given by Eqs. (1.22b) and (1.24d). The cross-relaxation $I_z \rightarrow 2I_zS_z$, $2I_zS_z \rightarrow I_z$ is caused by DD–CSA **I** cross-correlation. The cross-relaxation $S_z \rightarrow 2I_zS_z$, $2I_zS_z \rightarrow S_z$ is due to DD–CSA **S** cross-correlation. The cross-relaxation $I_z \rightarrow S_z$ and $S_z \rightarrow I_z$, referred to as the *nuclear Overhauser effect*, is the consequence of dipole–dipole interactions between spins **I** and **S**. It can be shown that the steady-state magnetisation for spin **S** under the condition of saturation of spin **I** (i.e. at $\langle I_z\rangle(t) \equiv 0$) is given by:

$$\lim_{t\rightarrow\infty}(\langle S_z\rangle(t) - S_{z0}) = \frac{\rho_D}{R_{1\mathbf{S}}^{D}+R_{1\mathbf{S}}^{CSA}} I_{z0} = \frac{\gamma_I}{\gamma_S}\frac{\rho_D}{R_{1\mathbf{S}}^{D}+R_{1\mathbf{S}}^{CSA}} S_{z0} \quad (1.29a)$$

$$\lim_{t\to\infty}\frac{\langle S_z\rangle(t)}{S_{z0}} = 1 + \frac{\gamma_I}{\gamma_S}\frac{\rho_D}{R_{1S}^D + R_{1S}^{CSA}}, \tag{1.29b}$$

where the quantity given by Eq. (1.29b) is referred to as the value of the nuclear Overhauser effect — NOE (the steady state NOE for the spin **I** can be written by analogy to Eqs. (1.29a) and (1.29b), where one should exchange the symbols **S** and **I**).

The relaxation in the groups (I_x, $2I_xS_z$), (S_x, $2I_zS_x$), (I_y, $2I_yS_z$), (S_y, $2I_zS_y$) (known as transverse) is described by:

$$\frac{d}{dt}\begin{bmatrix}\langle I_x\rangle^I\\ \langle 2I_xS_z\rangle^I\end{bmatrix} = -\begin{bmatrix}R_{2\mathbf{I}}^D + R_{2\mathbf{I}}^{CSA} & \eta_{D,CSA(\mathbf{I})}\\ \eta_{D,CSA(\mathbf{I})} & R_{2\mathbf{I}}^D + R_{2\mathbf{I}}^{CSA} + R_{1\mathbf{S}}^{CSA} - \mu_I\end{bmatrix}\times\begin{bmatrix}\langle I_x\rangle^I\\ \langle 2I_xS_z\rangle^I\end{bmatrix} \tag{1.30a}$$

$$\frac{d}{dt}\begin{bmatrix}\langle S_x\rangle^I\\ \langle 2I_zS_x\rangle^I\end{bmatrix} = -\begin{bmatrix}R_{2\mathbf{S}}^D + R_{2\mathbf{S}}^{CSA} & \eta_{D,CSA(\mathbf{S})}\\ \eta_{D,CSA(\mathbf{S})} & R_{2\mathbf{S}}^D + R_{2\mathbf{S}}^{CSA} + R_{1\mathbf{I}}^{CSA} - \mu_S\end{bmatrix}\times\begin{bmatrix}\langle I_x\rangle^I\\ \langle 2I_zS_x\rangle^I\end{bmatrix},$$

where

$$R_{2\mathbf{I}}^D = A_D^2\left(\tfrac{2}{3}J(0) + \tfrac{1}{6}J(\omega_I - \omega_S) + \tfrac{1}{2}J(\omega_I) + J(\omega_S) + J(\omega_I + \omega_S)\right) \tag{1.30b}$$

$$R_{2\mathbf{S}}^D = A_D^2\left(\tfrac{2}{3}J(0) + \tfrac{1}{6}J(\omega_I - \omega_S) + J(\omega_I) + \tfrac{1}{2}J(\omega_S) + J(\omega_I + \omega_S)\right)$$

$$R_{2\mathbf{I}}^{CSA} = A_{CSA(\mathbf{I})}^2 B_0^2\left(\tfrac{8}{3}J(0) + 2J(\omega_I)\right) \tag{1.30c}$$

$$R_{2\mathbf{S}}^{CSA} = A_{CSA(\mathbf{S})}^2 B_0^2\left(\tfrac{8}{3}J(0) + 2J(\omega_S)\right)$$

$$\eta_{D,CSA(\mathbf{I})} = A_D A_{CSA(\mathbf{I})} P_2(\cos\theta_{D,CSA(\mathbf{I})}) B_0\left(\tfrac{8}{3}J(0) + 2J(\omega_I)\right)$$

$$\eta_{D,CSA(\mathbf{S})} = A_D A_{CSA(\mathbf{S})} P_2(\cos\theta_{D,CSA(S)}) B_0\left(\tfrac{8}{3}J(0) + 2J(\omega_S)\right) \tag{1.30d}$$

$$\mu_I = A_D^2 J(\omega_S) \qquad \mu_S = A_D^2 J(\omega_I). \tag{1.30e}$$

Here A_D, $A_{CSA(I)}$ and $A_{CSA(S)}$ are given by Eqs. (1.22b) and (1.24d), $R_{1\mathbf{I}}^{CSA}$ and $R_{1\mathbf{S}}^{CSA}$ are given by Eq. (1.28c). The cross-relaxation $I_x \rightarrow 2I_xS_z$, $2I_xS_x \rightarrow I_x$is caused by DD–CSA **I** cross-correlation. The cross-relaxation $S_x \rightarrow 2I_zS_x$, $2I_xS_x \rightarrow S_x$ is due to DD–CSA **S** cross-correlation. The terms μ_I and μ_S are related with the cross-relaxation rates between doublet components for spin **I** and **S**, respectively (see below).

The relaxation in groups ($2I_xS_x$, $2I_yS_y$) and ($2I_xS_y$, $2I_yS_x$) composed of double spin operators, which are linear combinations of zero-quantum I_+S_-, I_-S_+ and double-quantum I_+S_+, I_-S_- coherences, is described by:

$$\frac{d}{dt}\begin{bmatrix}\langle 2I_xS_x\rangle^I\\ \langle 2I_yS_y\rangle^I\end{bmatrix} = -\begin{bmatrix}\mu_{mq} + R_{2\mathbf{I}}^{CSA} + R_{2\mathbf{S}}^{CSA} & -\eta_{mq} - \eta_{CSA(\mathbf{I}),CSA(\mathbf{S})}\\ -\eta_{mq} - \eta_{CSA(\mathbf{I}),CSA(\mathbf{S})} & \mu_{mq} + R_{2\mathbf{I}}^{CSA} + R_{2\mathbf{S}}^{CSA}\end{bmatrix}\times\begin{bmatrix}\langle 2I_xS_x\rangle^I\\ \langle 2I_yS_y\rangle^I\end{bmatrix} \tag{1.31a}$$

$$\frac{d}{dt}\begin{bmatrix}\langle 2I_xS_y\rangle^I\\ \langle 2I_yS_x\rangle^I\end{bmatrix} = -\begin{bmatrix}\mu_{mq} + R_{2\mathbf{I}}^{CSA} + R_{2\mathbf{S}}^{CSA} & \eta_{mq} + \eta_{CSA(\mathbf{I}),CSA(\mathbf{S})}\\ \eta_{mq} + \eta_{CSA(\mathbf{I}),CSA(\mathbf{S})} & \mu_{mq} + R_{2\mathbf{I}}^{CSA} + R_{2\mathbf{S}}^{CSA}\end{bmatrix}\times\begin{bmatrix}\langle 2I_xS_y\rangle^I\\ \langle 2I_yS_x\rangle^I\end{bmatrix}$$ where,

$$\mu_{mq} = A_D^2\left(\tfrac{1}{6}J(\omega_I - \omega_S) + \tfrac{1}{2}J(\omega_I) + \tfrac{1}{2}J(\omega_S) + J(\omega_I + \omega_S)\right) \tag{1.31b}$$

$$\eta_{mq} = A_{\mathrm{D}}^2(J(\omega_I + \omega_S) - \tfrac{1}{6}J(\omega_I - \omega_S)) = \tfrac{1}{2}\rho_{\mathrm{D}} \tag{1.31c}$$

$$\eta_{\mathrm{CSA(I)},\mathrm{CSA(S)}} = \tfrac{16}{3}A_{\mathrm{CSA(I)}}A_{\mathrm{CSA(S)}}P_2(\theta_{\mathrm{CSA(I)},\mathrm{CSA(S)}})J(0). \tag{1.31d}$$

Here A_{D}, $A_{\mathrm{CSA(I)}}$ and $A_{\mathrm{CSA(S)}}$ are given by Eqs. (1.22b) and (1.24d), $R_{1\mathbf{I}}^{\mathrm{CSA}}$ and $R_{1\mathbf{S}}^{\mathrm{CSA}}$ are given by Eq. (1.28c), ρ_{D} is given by Eq. (1.28d). The cross-relaxation term $\eta_{\mathrm{CSA(I)},\mathrm{CSA(S)}}$ in Eq. (1.31d) is caused by CSA **I**–CSA **S** cross-correlation. For the analysis of the relaxation in the $(2I_xS_x, 2I_yS_y)$ and $(2I_xS_y, 2I_yS_x)$ groups it is convenient to use the shift instead of the Cartesian product operators. The evolution of the mean values of the zero-quantum I_+S_-, I_-S_+ and double-quantum I_+S_+, I_-S_- coherences are mono-exponential decays with the rate constants R_{dq} and R_{zq}, respectively:

$$\begin{aligned}
&\frac{\mathrm{d}}{\mathrm{d}t}\langle I_+S_+\rangle^I = -R_{dq}\langle I_+S_+\rangle^I \\
&\frac{\mathrm{d}}{\mathrm{d}t}\langle I_-S_-\rangle^I = -R_{dq}\langle I_-S_-\rangle^I \\
&\frac{\mathrm{d}}{\mathrm{d}t}\langle I_+S_-\rangle^I = -R_{zq}\langle I_+S_-\rangle^I \\
&\frac{\mathrm{d}}{\mathrm{d}t}\langle I_-S_+\rangle^I = -R_{zq}\langle I_-S_+\rangle^I,
\end{aligned} \tag{1.32a}$$

where

$$R_{dq} = R_{2\mathbf{I}}^{\mathrm{CSA}} + R_{2\mathbf{S}}^{\mathrm{CSA}} + \mu_{mq} + \eta_{mq} + \eta_{\mathrm{CSA(I)},\mathrm{CSA(S)}}, \tag{1.32b}$$

$$R_{zq} = R_{2\mathbf{I}}^{\mathrm{CSA}} + R_{2\mathbf{S}}^{\mathrm{CSA}} + \mu_{mq} - \eta_{mq} - \eta_{\mathrm{CSA(I)},\mathrm{CSA(S)}}. \tag{1.32c}$$

Here $R_{1\mathbf{I}}^{\mathrm{CSA}}$, $R_{1\mathbf{S}}^{\mathrm{CSA}}$ are given by Eq. (1.28c), μ_{mq}, η_{mq}, $\eta_{\mathrm{CSA(I)},\mathrm{CSA(S)}}$ are given by Eqs. (1.31b)–(1.31d).

The existence of weak scalar coupling between spins **I** and **S**, described by the Hamiltonian $\mathsf{H}_s = JI_zS_z$, gives rise for each spin to a doublet of resonance lines with frequencies $\omega_I \pm J/2$ for spin **I** and $\omega_S \pm J/2$ for spin **S**. It was noted long ago [18] that the consequence of DD–CSA **I** and DD–CSA **S** cross-correlation is a difference in the line-width for the doublet components. For the consideration of this effect, it is convenient to use single-transition basis operators $I_\pm^{(1)} = I_\pm(1/2 + S_z)$, $I_\pm^{(2)} = I_\pm(1/2 - S_z)$, $S_\pm^{(1)} = I_\pm(1/2 + I_z)$, $S_\pm^{(2)} = S_\pm(1/2 - I_z)$ (see [15]). In terms of these operators the differential equations for transverse relaxation (see Eq. (1.30a)) in a system with scalar interactions are written as:

$$\begin{aligned}
\frac{\mathrm{d}}{\mathrm{d}t}\begin{bmatrix}\langle I_\pm^{(1)}\rangle^I \\ \langle I_\pm^{(2)}\rangle^I\end{bmatrix} &= i\frac{J}{2}\begin{bmatrix}\mp\langle I_\pm^{(1)}\rangle^I \\ \mp\langle I_\pm^{(2)}\rangle^I\end{bmatrix} \\
&\quad - \begin{bmatrix}R_{I(1)} & \xi_I \\ \xi_I & R_{I(2)}\end{bmatrix}\begin{bmatrix}\langle I_\pm^{(1)}\rangle^I \\ \langle I_\pm^{(2)}\rangle^I\end{bmatrix}
\end{aligned} \tag{1.33a}$$

$$\begin{aligned}
\frac{\mathrm{d}}{\mathrm{d}t}\begin{bmatrix}\langle S_\pm^{(1)}\rangle^I \\ \langle S_\pm^{(2)}\rangle^I\end{bmatrix} &= i\frac{J}{2}\begin{bmatrix}\mp\langle S_\pm^{(1)}\rangle^I \\ \mp\langle S_\pm^{(2)}\rangle^I\end{bmatrix} \\
&\quad - \begin{bmatrix}R_{S(1)} & \xi_S \\ \xi_S & R_{S(2)}\end{bmatrix}\begin{bmatrix}\langle S_\pm^{(1)}\rangle^I \\ \langle S_\pm^{(2)}\rangle^I\end{bmatrix},
\end{aligned}$$

where

$$\begin{aligned}
R_{I(1)} &= R_{2\mathbf{I}}^{\mathrm{D}} + R_{2\mathbf{I}}^{\mathrm{CSA}} + \frac{R_{1\mathbf{S}}^{\mathrm{CSA}} - \mu_I}{2} + \eta_{\mathrm{D,CSA(I)}} \\
R_{S(1)} &= R_{2\mathbf{S}}^{\mathrm{D}} + R_{2\mathbf{S}}^{\mathrm{CSA}} + \frac{R_{1\mathbf{I}}^{\mathrm{CSA}} - \mu_S}{2} + \eta_{\mathrm{D,CSA(S)}}
\end{aligned} \tag{1.33b}$$

$$\begin{aligned}
R_{I(2)} &= R_{2\mathbf{I}}^{\mathrm{D}} + R_{2\mathbf{I}}^{\mathrm{CSA}} + \frac{R_{1\mathbf{S}}^{\mathrm{CSA}} - \mu_I}{2} - \eta_{\mathrm{D,CSA(I)}} \\
R_{S(2)} &= R_{2\mathbf{S}}^{\mathrm{D}} + R_{2\mathbf{S}}^{\mathrm{CSA}} + \frac{R_{1\mathbf{I}}^{\mathrm{CSA}} - \mu_S}{2} - \eta_{\mathrm{D,CSA(S)}}
\end{aligned} \tag{1.33c}$$

$$\xi_I = \frac{\mu_I - R_{1\mathbf{S}}^{\mathrm{CSA}}}{2} \qquad \xi_S = \frac{\mu_S - R_{1\mathbf{I}}^{\mathrm{CSA}}}{2}. \tag{1.33d}$$

Here $R_{1\mathbf{I}}^{\mathrm{CSA}}$, $R_{1\mathbf{S}}^{\mathrm{CSA}}$ are given by Eq. (1.28c), $R_{2\mathbf{I}}^{\mathrm{D}}$, $R_{2\mathbf{S}}^{\mathrm{D}}$, $R_{2\mathbf{I}}^{\mathrm{CSA}}$, $R_{2\mathbf{S}}^{\mathrm{CSA}}$, $\eta_{\mathrm{D,CSA(I)}}$, $\eta_{\mathrm{D,CSA(S)}}$, μ_I and μ_S are given by Eqs. (1.30a)–(1.30e), ξ_I and ξ_S denote the rates of cross-relaxation between doublet components of spin **I** and **S**, respectively (if spin **I** relaxation due to CSA mechanism is negligible the cross-relaxation rate ξ_S is equal to $\mu_S/2$ and vice versa). The relaxation rates $R_{I(1)}$, $R_{I(2)}$, $R_{S(1)}$, and $R_{S(2)}$, determine the line-width for the doublet components of spin **I** and **S**, respectively.

Differential line broadening for the doublet components, caused by DD–CSA cross-correlation, gives rise to the development of heteronuclear NMR

experiments based on the TROSY (transverse relaxation optimised spectroscopy) principle. TROSY experiments, which make use of the narrowest spectral component for the transfer and detection, have been proposed for protein backbone ^{15}N–^{1}H and aromatic side-chain ^{13}C–^{1}H moieties [19,20]. Narrow line-widths in ^{1}H–^{15}N TROSY spectra are obtained because of nearly complete compensation of transverse relaxation at magnetic fields of 21.0–23.0 T (see Eqs. (1.33b) and (1.33c)). The compensation effect for the relaxation of zero-quantum coherence (see Eq. (1.32c)) due to CSA–CSA cross-correlation might also be used to obtain narrow line-widths as it is proposed in the ZQ-(^{15}N,^{1}H)-TROSY pulse scheme [21].

The measurement of cross-correlated cross-relaxation rates provide the means for estimating the parameters governing relaxation in ^{1}H–^{15}N two-spin system. In particular, DD–CSA ^{15}N cross-correlated relaxation rates have been used for the characterisation of the shielding anisotropy tensor for the backbone ^{15}N nuclei [17,22,23]. Measurements of CSA–CSA cross-correlated relaxation for backbone ^{1}H–^{15}N and ^{15}N–^{13}CO systems have also been reported [24–26].

1.2.4. Relaxation under off-resonance RF irradiation

Measurements of the relaxation rates in the presence of transverse spin-locking radio-frequency (RF) field, applied with the carrier in the vicinity of spin **I** and/or **S** resonance, provide additional information about molecular motions (for a recent review see Ref. [27]). The laboratory frame Hamiltonian for a two-spin 1/2 system subjected to a RF spin-locking field applied along the x-axis with the carrier frequencies $\omega_I - \Delta\omega_I$ and $\omega_S - \Delta\omega_S$ and amplitudes ω_{1I} and ω_{1S} for spins **I** and **S**, respectively, is given by:

$$\mathsf{H}(t) = \mathsf{H}_Z + \mathsf{H}_{RF}(t) + \mathsf{H}_1(t), \tag{1.34a}$$

$$\mathsf{H}_{RF}(t) = \omega_{1I}(I_x \cos(\omega_I - \Delta\omega_I)t + I_y \sin(\omega_I - \Delta\omega_I)t) + \omega_{1S}(S_x \cos(\omega_S - \Delta\omega_S)t + S_y \sin(\omega_S - \Delta\omega_S)t), \tag{1.34b}$$

where H_Z is the Zeeman Hamiltonian given by Eq. (1.20), $\mathsf{H}_1(t)$ is the Hamiltonian of random perturbation resulting in relaxation (Eqs. (1.18) and (1.23)). The Hamiltonians H_Z and $\mathsf{H}_{RF}(t)$ vanish in the interaction representation given by the unitary transformation:

$$\mathsf{U} = \mathsf{U}_I\mathsf{U}_S, \tag{1.35a}$$

where

$$\mathsf{U}_I = e^{i\omega_{eI}I_z t}\, e^{i\theta_I I_y}\, e^{i(\omega_I - \Delta\omega_I)I_z t},$$
$$\mathsf{U}_S = e^{i\omega_{eS}S_z t}\, e^{i\theta_S S_y}\, e^{i(\omega_S - \Delta\omega_S)S_z t}, \tag{1.35b}$$

$$\theta_I = \arctan\frac{\omega_{1I}}{\Delta\omega_I}, \quad \theta_S = \arctan\frac{\omega_{1S}}{\Delta\omega_S}, \tag{1.35c}$$

$$\omega_{eI} = \sqrt{\omega_{1I}^2 + \Delta\omega_I^2}, \quad \omega_{eS} = \sqrt{\omega_{1S}^2 + \Delta\omega_S^2}. \tag{1.35d}$$

This interaction representation defines the frame rotating with the frequencies ω_{eI} and ω_{eS} about the effective field tilted with respect to the permanent magnetic field $\mathbf{B}_0$ (directed along the z-axis) by angles θ_I and θ_S for spins **I** and **S**, respectively. The effective field is directed in the xz-plane of the frame, rotating about the z-axis of the laboratory frame with frequencies $\omega_I - \Delta\omega_I$ and $\omega_S - \Delta\omega_S$ for spins **I** and **S**, respectively. The interaction representation given by Eqs. (1.35a)–(1.35d) thus corresponds to a doubly rotating frame.

Let us consider the relaxation of magnetisation locked along the effective field (which is different for spins **I** and **S**) in the doubly rotating frame, i.e. the relaxation for $I'_z = I_z \cos\theta_I + I_x \sin\theta_I$, $S'_z = S_z \cos\theta_S + S_x \sin\theta_S$ and $2I'_zS'_z$, where I_x and S_x are given in the frame rotating about the z-axis with frequencies $\omega_I - \Delta\omega_I$ and $\omega_S - \Delta\omega_S$ for spins **I** and **S**, respectively. The master equation for mean values of I'_z, S'_z and $2I'_zS'_z$ (Eqs. (1.16a) and (1.16b)) is derived using the expressions for the DD and CSA Hamiltonians $\mathsf{H}_1(t)$ (Eqs. (1.18) and (1.23)), written in the doubly rotating frame (Eqs. (1.35a)–(1.35d)) in terms of spin operators T_m^n and the frequencies ω_m^n (see Eq. (1.10)). The derivation of the relaxation rates in the doubly rotating frame is analogous to that in the previous section and will not be repeated here. The expressions for relaxation rates in the presence of an RF spin-locking field depend on the values of spectral density functions at linear combinations of ω_I, ω_S, ω_{eI} and ω_{eS}. However, due to the correlation time τ_c of random processes causing DD and CSA relaxation being sufficiently short that $\omega_{eI}\tau_c \ll 1$, $\omega_{eS}\tau_c \ll 1$,

the frequencies ω_{eI} and ω_{eS} in the expressions for relaxation rates can be safely set to zero. The master equation for longitudinal relaxation in the doubly rotating frame is then written in a form analogous to Eq. (1.28a) [27–29]:

$$\frac{\mathrm{d}}{\mathrm{d}t}\begin{bmatrix} \langle I'_z\rangle - I'_{z0} \\ \langle S'_z\rangle - S'_{z0} \\ \langle 2I'_zS'_z\rangle \end{bmatrix} = -\begin{bmatrix} R^{\mathrm{D}}_{1\rho,\mathbf{I}} + R^{\mathrm{CSA}}_{1\rho,\mathbf{I}} & \rho_{\rho,\mathrm{D}} & \rho_{\rho,\mathrm{D,CSA(I)}} \\ \rho_{\rho,\mathrm{D}} & R^{\mathrm{D}}_{1\rho,\mathbf{S}} + R^{\mathrm{CSA}}_{1\rho,\mathbf{S}} & \rho_{\rho,\mathrm{D,CSA(S)}} \\ \rho_{\rho,\mathrm{D,CSA(I)}} & \rho_{\rho,\mathrm{D,CSA(S)}} & R^{\mathrm{CSA}}_{1\rho,\mathbf{I}} + R^{\mathrm{CSA}}_{1\rho,\mathbf{S}} + \lambda_\rho \end{bmatrix} \times \begin{bmatrix} \langle I'_z\rangle - I'_{z0} \\ \langle S'_z\rangle - S'_{z0} \\ \langle 2I'_zS'_z\rangle \end{bmatrix}, \tag{1.36a}$$

where I'_{z0} and S'_{z0} are the values of steady-state magnetisation in the doubly rotating frame depending on the RF irradiation conditions and on the relaxation rates [27,30]; the following relationships hold here for rotating-frame auto-relaxation rates:

$$R^{\mathrm{D}}_{1\rho,\mathbf{I}} = R^{\mathrm{D}}_{1\mathbf{I}}c_I^2 + R^{\mathrm{D}}_{2\mathbf{I}}s_I^2 \qquad R^{\mathrm{CSA}}_{1\rho,\mathbf{I}} = R^{\mathrm{CSA}}_{1\mathbf{I}}c_I^2 + R^{\mathrm{CSA}}_{2\mathbf{I}}s_I^2 \tag{1.36b}$$

$$R^{\mathrm{D}}_{1\rho,\mathbf{S}} = R^{\mathrm{D}}_{1\mathbf{S}}c_S^2 + R^{\mathrm{D}}_{2\mathbf{S}}s_S^2 \qquad R^{\mathrm{CSA}}_{1\rho,\mathbf{S}} = R^{\mathrm{CSA}}_{1\mathbf{S}}c_S^2 + R^{\mathrm{CSA}}_{2\mathbf{S}}s_S^2$$

$$\begin{aligned}\lambda_\rho = A^2_{\mathrm{D}}(&\tfrac{2}{3}(s_I^2c_S^2 + c_I^2s_S^2)J(0) + \tfrac{1}{2}((1+c_I^2)c_S^2 \\ &+ s_I^2s_S^2)J(\omega_I) + \tfrac{1}{2}((1+c_S^2)c_I^2 + s_I^2s_S^2)J(\omega_S) \\ &+ \tfrac{1}{2}((1+c_I^2)s_S^2 + (1+c_S^2)s_I^2)J(\omega_I+\omega_S) \\ &+ \tfrac{1}{12}((1+c_I^2)s_S^2 + (1+c_S^2)s_I^2)J(\omega_I-\omega_S)),\end{aligned}$$

where $c_I = \cos\theta_I$, $c_S = \cos\theta_S$, $s_I = \sin\theta_I$, $s_S = \sin\theta_S$, $R^{\mathrm{D}}_{1\mathbf{I}}$ and $R^{\mathrm{CSA}}_{1\mathbf{I}}$ are given by Eqs. (1.28b) and (1.28c), $R^{\mathrm{D}}_{2\mathbf{I}}$ and $R^{\mathrm{CSA}}_{2\mathbf{I}}$ are given by Eqs. (1.30b) and (1.30c); the rotating-frame cross-relaxation rates are given by:

$$\begin{aligned}\rho_{\rho,\mathrm{D}} &= c_Ic_S\rho_{\mathrm{D}} \\ \rho_{\rho,\mathrm{D,CSA(I)}} &= c_S(\rho_{\mathrm{D,CSA(I)}}c_I^2 + \eta_{\mathrm{D,CSA(I)}}s_I^2) \\ \rho_{\rho,\mathrm{D,CSA(S)}} &= c_I(\rho_{\mathrm{D,CSA(S)}}c_S^2 + \eta_{\mathrm{D,CSA(S)}}s_S^2),\end{aligned} \tag{1.36c}$$

where ρ_{D} is given by Eq. (1.28d), $\rho_{\mathrm{D,CSA(S)}}$ and $\rho_{\mathrm{D,CSA(I)}}$ are given by Eq. (1.28e), $\eta_{\mathrm{D,CSA(S)}}$ and $\eta_{\mathrm{D,CSA(I)}}$ are given by Eq. (1.30d). It should be noted that in relaxation studies of scalar coupled systems with RF irradiation applied for both spins one should carefully avoid the conditions where Hartmann–Hahn coherence transfer takes place (see, e.g. [10]).

1.3. Conformational (chemical) exchange

It is well known that chemical exchange of a nucleus between sites in different molecules or intramolecular conformational exchange modulating isotropic part of the chemical shielding tensor (chemical shift) of the nucleus can contribute to the measured relaxation rates. If the exchange is fast, i.e. if the exchange rate constants k_{ex} are much higher than the differences between the Larmor frequencies of the nucleus in the different states one should observe a single resonance in the NMR spectra. In view of relaxation measurements this resonance provides cumulative information on relaxation rates in different states and characteristics of the exchange processes. If the exchange is slow one can study the relaxation for resonances corresponding to different states. Both fast and slow conformational exchange can be accounted for using the modified Bloch equations [31–33]. Fast exchange can be also treated from a quantum mechanical point of view (see [34–36]). In this section we present a quantum mechanical consideration of fast exchange and list some useful equations describing the effect of conformational (chemical) exchange on relaxation rates measured in spin-echo experiments.

1.3.1. Fast exchange from a quantum mechanical point of view

Let us consider fast exchange of spin **I** between states with different chemical shifts as a mechanism of relaxation in terms of the semi-classical theory of relaxation (Section 1.1). In a static magnetic field $\mathbf{B}_0$ the Hamiltonian for spin **I** participating in an exchange process is represented as a sum of a time independent part H_0 and a random perturbation $\mathsf{H}_1(t)$ [35]:

$$\mathsf{H}_0 = -\sum_i p_i\gamma_I(1-\Omega_i)(\mathbf{B}_0\cdot\mathbf{I}), \tag{1.37a}$$

$$\mathsf{H}_1(t) = -\sum_i \gamma_I(f_i(t)-p_i)(1-\Omega_i)(\mathbf{B}_0\cdot\mathbf{I}), \tag{1.37b}$$

where the index i runs over the number of conformational states, Ω_i is the value of the chemical shift of the nucleus in the ith state, p_i is the population of ith state, $f_i(t)$ are random functions that have the property $f_i(t) = 1$ if the nucleus is in ith state and $f_i(t) = 0$ otherwise. From the definition of $\mathsf{H}_1(t)$ it is clear that $\langle \mathsf{H}_1(t) \rangle = 0$. For the simplest case of exchange between two states A and B with populations p_A and p_B and a chemical shift difference $\Delta_{ex(I)} = \Omega_A - \Omega_B$ the Hamiltonian $\mathsf{H}_1(t)$ is given by:

$$\mathsf{H}_1(t) = (f_A(t) - p_A)\gamma_I(\mathbf{B}_0\cdot\mathbf{I})\Delta_{ex(I)} = -(f_B(t) - p_B)\gamma_I(\mathbf{B}_0\cdot\mathbf{I})\Delta_{ex(I)}, \quad (1.37c)$$

where $f_A(t) = 1 - f_B(t)$. $\mathsf{H}_1(t)$ can be written in a form similar to Eq. (1.8) in terms of random functions $F_m(t)$ and components T_m of an irreducible tensor operator of rank 0 (see Appendix A). For a two-state exchange T_m and $F_m(t)$ are given by:

$$T_0 = A_{ex(I)}(\mathbf{B}_0\cdot\mathbf{I}) = A_{ex(I)}(B_zI_z + \tfrac{1}{2}(B_+I_- + B_-I_+)) = A_{ex(I)}B_0I_z, \quad (1.38a)$$

where

$$A_{ex(I)} = \sqrt{p_Ap_B}\gamma_I\Delta_{ex(I)}, \quad (1.38b)$$

$$F_0(t) = \frac{f_A(t) - p_A}{\sqrt{p_Ap_B}} = -\frac{f_B(t) - p_B}{\sqrt{p_Ap_B}}, \quad (1.38c)$$

$F_0(t)$ is normalised such that the correlation function $C(t) = \langle F_0(0)F_0(t)\rangle$ (Eqs. (1.13a), (1.13b)) is equal to 1 at $t = 0$, $\mathbf{B}_0$ is directed along the z-axis. Transformation of Eqs. (1.38a)–(1.38c) to the interaction representation provides T_m^n and ω_m^n (Eq. (1.10)) required for the calculation of relaxation rates:

$$(T_0)^I = \frac{A_{ex(I)}B_0I_z}{T_0^0;\omega_0^0=0}. \quad (1.39)$$

For a two-spin 1/2 system with exchange between states with different chemical shifts, the relaxation super-operator $\hat{\Gamma}(Q)$ (Eq. (1.26); Table 1) in the master equation (Eqs. (1.16a) and (1.16b)) includes three additional terms:

$$\hat{\Gamma}_{ex(I)}(Q) = A^2_{ex(I)}B_0^2J_{ex(I)}(0)[I_z[I_z, Q]] \quad (1.40a)$$

$$\hat{\Gamma}_{ex(S)}(Q) = A^2_{ex(S)}B_0^2J_{ex(S)}(0)[S_z[S_z, Q]] \quad (1.40b)$$

$$\hat{\Gamma}_{ex(I),ex(S)}(Q) = A_{ex(I)}A_{ex(S)}B_0^2J_{ex(I),ex(S)}(0)([S_z[I_z, Q]] + [I_z[S_z, Q]]), \quad (1.40c)$$

where $\hat{\Gamma}_{ex(I)}(Q)$ and $\hat{\Gamma}_{ex(S)}$ are responsible for relaxation due to the exchange mechanism for spins **I** and **S**, respectively; $\hat{\Gamma}_{ex(I),ex(S)}(Q)$ is due to cross-correlation between the exchanges of spins **I** and **S** [26]. The spectral density functions $J_{ex(I)}(\omega)$, $J_{ex(S)}(\omega)$ and $J_{ex(I),ex(S)}(\omega)$ are the cosine Fourier transforms of the corresponding auto- and cross-correlation functions (Eq. (1.13a)), composed of the random functions $F_0(t)$ for the exchanges of spins **I** and **S**. Using Eq. (1.38c) for $F_0(t)$ one can show that for the exchange between two states A and B, occurring simultaneously for spins **I** and **S** with the rate constant $k_{ex} = k_{A\to B}/p_B = k_{B\to A}/p_A$, the spectral density functions in Eqs. (1.40a)–(1.40c) are given by:

$$J_{ex}(\omega) = J_{ex(I)}(\omega) = J_{ex(S)}(\omega) = J_{ex(I),ex(S)}(\omega) = \frac{k_{ex}}{k_{ex}^2 + \omega^2}. \quad (1.41)$$

Substituting shift-basis operators for a two-spin 1/2 system into Eqs. (1.40a)–(1.40c) one can show that fast conformational exchange does not contribute to the relaxation of $\langle I_z\rangle$, $\langle S_z\rangle$ and $\langle 2I_zS_z\rangle$; contributes as $R_{ex(I)}$ and $R_{ex(S)}$ to the auto-relaxation rates of $\langle I_\pm\rangle$, $\langle 2I_\pm S_z\rangle$ and $\langle S_\pm\rangle$, $\langle 2I_zS_\pm\rangle$, respectively; and contributes as $R_{ex(I)} + R_{ex(S)} - \eta_{ex(I),ex(S)}$ and $R_{ex(I)} + R_{ex(S)} + \eta_{ex(I),ex(S)}$ to auto-relaxation rates of zero-quantum $\langle 2I_+S_-\rangle$, $\langle 2I_-S_+\rangle$ and double-quantum $\langle 2I_+S_+\rangle$, $\langle 2I_-S_-\rangle$ coherences, respectively. The relaxation rates $R_{ex(I)}$, $R_{ex(S)}$ and $\eta_{ex(I),ex(S)}$ are given by:

$$R_{ex(I)} = A^2_{ex(I)}B_0^2J_{ex(I)}(0),\ \ R_{ex(S)} = A^2_{ex(S)}B_0^2J_{ex(S)}(0), \quad (1.42)$$

$$\eta_{ex(I),ex(S)} = 2A_{ex(I)}A_{ex(S)}B_0^2J_{ex(I),ex(S)}(0),$$

where $A_{ex(I)}$, $A_{ex(S)}$ are given by Eq. (1.38b) and $J_{ex(I)}(\omega)$, $J_{ex(S)}(\omega)$, $J_{ex(I),ex(S)}(\omega)$ are given by Eq. (1.41), provided that the exchange occurs between the two states A and B simultaneously for spins **I** and **S**. Eq. (1.42) characterises the exchange under free precession.

Let us now consider the exchange-mediated relaxation of magnetisation locked by the transverse spin-locking RF field with amplitude ω_{1I} and the carrier frequency $\omega_I - \Delta\omega_I$ along the effective field in a doubly rotating frame (see Section 1.2.4), i.e. the relaxation for $I'_z = I_z \cos\theta_I + I_x \sin\theta_I$, where I_x is given in the frame rotating about the z-axis with frequency $\omega_I - \Delta\omega_I$. The relaxation rate for $\langle I'_z \rangle$ is derived using the expression for the conformational exchange Hamiltonian $\mathsf{H}_1(t)$ (Eq. (1.37b) and (1.37c)), written in the doubly rotating frame (Eqs. (1.35a)–(1.35d)) in terms of spin operators T_m^n and frequencies ω_m^n (see Eq. (1.10)). In contrast to DD and CSA relaxation (Section 1.2), for the exchange-mediated relaxation the condition $\omega_{eI}\tau_{ex} = \omega_{eI}/k_{ex} \ll 1$ may be violated and the relaxation rate $R_{\rho,ex(\mathbf{I})}$ for the mean value of I'_z appears to be dependent on ω_{eI} (Eq. (1.35d)). The rate $R_{\rho,ex(\mathbf{I})}$ for exchange-mediated relaxation of $\langle I'_z \rangle$ is given by:

$$R_{\rho,ex(\mathbf{I})} = A^2_{ex(\mathbf{I})} B_0^2 \sin^2\theta_I J_{ex(\mathbf{I})}(\omega_{eI}), \tag{1.43}$$

where ω_{eI} and θ_I are given by Eqs. (1.35c) and (1.35d), $A_{ex(\mathbf{I})}$ is given by Eq. (1.38b) and $J_{ex(\mathbf{I})}(\omega)$ is given by Eq. (1.41), provided that the exchange occurs between two states A and B.

It is worth noting that the expressions for relaxation rates due to conformational exchange derived here (Eqs. (1.42) and (1.43)) are valid under the assumptions of semi-classical theory of relaxation (Section 1.1), namely, if the conditions $\omega_I^2\Delta^2_{ex(\mathbf{I})}/k^2_{ex} \ll 1$, $\omega_S^2\Delta^2_{ex(\mathbf{S})}/k^2_{ex} \ll 1$ hold.

1.3.2. Effect of exchange on spin-echo experiments

Conformational exchange is known to affect transverse relaxation rates measured in spin-echo experiments (Section 1.4). In particular, the dependence of the transverse relaxation rate on the separation 2δ between the 180° pulses of the CPMG sequence [37,38] is often used for characterisation of microsecond–millisecond exchange. The amplitudes of CPMG echoes for nucleus **I**, exchanging between n states with different chemical shifts, are given by the sum of n exponential terms [39–42]. For fast exchange the actual decay of the amplitudes of CPMG echoes is well approximated by one exponent depending on the apparent rate constant $R^*_{2(\mathbf{I})}$. Below we list several analytic expressions for $R^*_{2(\mathbf{I})}$ without describing the cumbersome details of their derivation. These expressions make it possible to extract the parameters of the exchange from transverse relaxation rates obtained using CPMG sequence. Here we assume that the exchange is fast, whereas the exchange times $\tau_{ex} = 1/k_{ex}$ are much slower than the correlation times τ_c of random processes causing other relaxation mechanisms (e.g. DD and CSA).

Luz and Meiboom [43] were the first to derive an analytic expression for the apparent rate constant $R^*_{2(\mathbf{I})}$ measured using the CPMG sequence for the nucleus exchanging between states with different chemical shifts. For a two-state exchange this rate is given by:

$$R^*_{2(\mathbf{I})} = R_{2(\mathbf{I})} + R_{ex}, \tag{1.44a}$$

$$R_{ex} = \frac{p_A p_B \Delta^2_{ex(\mathbf{I})}\omega_I^2}{k_{ex}}\left(1 - \frac{\tanh(k_{ex}\delta)}{k_{ex}\delta}\right), \tag{1.44b}$$

where p_A and p_B are populations of the states, $\Delta_{ex(\mathbf{I})} = \Omega_{A(\mathbf{I})} - \Omega_{B(\mathbf{I})}$ is the chemical shift difference between the states, $k_{ex} = k_{A\to B}/p_B = k_{B\to A}/p_A$ is the rate constant for exchange process, δ is the delay of the δ-180°-δ CPMG block, $R_{2(\mathbf{I})}$ is the transverse relaxation rate in the absence of the exchange assumed to be the same in states A and B. Another useful expression for $R^*_{2(\mathbf{I})}$ is given by Bloom et al. [39] (see also Refs. [44,45]):

$$R^*_{2(\mathbf{I})} = R_{2(\mathbf{I})} + R_{ex}, \tag{1.45a}$$

where

$$\begin{aligned}
R_{ex} &= \frac{k_{ex}}{2} - \frac{1}{2\delta}\sinh^{-1}\left(\frac{k_{ex}}{\xi}\sinh(\delta\xi)\right) \\
&\quad \text{if } k^2_{ex} < 4p_A p_B \Delta^2_{ex(\mathbf{I})}\omega_I^2 \\
R_{ex} &= \frac{k_{ex}}{2} - \frac{1}{2\delta}\sinh^{-1}(k_{ex}\delta) \\
&\quad \text{if } k^2_{ex} = 4p_A p_B \Delta^2_{ex(\mathbf{I})}\omega_I^2 \\
R_{ex} &= \frac{k_{ex}}{2} - \frac{1}{2\delta}\sinh^{-1}\left(\frac{k_{ex}}{\xi}\sin(\delta\xi)\right) \\
&\quad \text{if } k^2_{ex} > 4p_A p_B \Delta^2_{ex(\mathbf{I})}\omega_I^2
\end{aligned} \tag{1.45b}$$

$$\xi = \sqrt{|k^2_{ex} - 4p_A p_B \Delta^2_{ex(\mathbf{I})}\omega_I^2|}. \tag{1.45c}$$

Note that Eqs. (1.45a)–(1.45c) was validated only for the case of equally populated states: $p_A = p_B = 0.5$. If the exchange occurs between the two states with different relaxation rates $R_{2A(\mathbf{I})}$ and $R_{2B(\mathbf{I})}$ it is convenient to use the following expression for $R^*_{2(\mathbf{I})}$ [36,42,46]:

$$R^*_{2(\mathbf{I})} = \frac{1}{2}\left(R_{2A(\mathbf{I})} + R_{2B(\mathbf{I})} + k_{\mathrm{ex}} - \frac{1}{2\delta}\cosh^{-1}(D_+ \cosh \eta_+ - D_- \cosh \eta_-)\right), \tag{1.46a}$$

where

$$D_\pm = \frac{1}{2}\left(\frac{\psi + 2\Delta^2_{\mathrm{ex}(\mathbf{I})}\omega_I^2}{\sqrt{\psi^2 + \zeta^2}} \pm 1\right) \tag{1.46b}$$

$$\eta_\pm = \sqrt{2}\delta\sqrt{\sqrt{\psi^2 + \zeta^2} \pm \psi}$$

$$\psi = (R_{2A(\mathbf{I})} - R_{2B(\mathbf{I})} - p_A k_{\mathrm{ex}} + p_B k_{\mathrm{ex}})^2 - \Delta^2_{\mathrm{ex}(\mathbf{I})}\omega_I^2 + 4p_A p_B k^2_{\mathrm{ex}}$$

$$\zeta = 2\Delta_{\mathrm{ex}(\mathbf{I})}\omega_I(R_{2A(\mathbf{I})} - R_{2B(\mathbf{I})} - p_A k_{\mathrm{ex}} + p_B k_{\mathrm{ex}}).$$

1.4. Experimental aspects of relaxation measurements

Protein studies often focus on the relaxation of the backbone ^{15}N and ^{13}C nuclei. The relaxation of the nitrogen and carbon nuclei in ^{15}N–^{1}H and ^{13}C$^{\alpha}$–^{1}H systems occurs mostly due to the dipolar interactions with the covalently bound proton and by the CSA mechanism (Here and below we will refer to the ^{15}N, ^{13}C nuclei as **S**, and ^{1}H as **I**.) The protons in these systems relax also by to the dipolar interactions with remote protons in the protein, which hinder an unambiguous interpretation of the relaxation for the coherences involving the proton operators. Therefore, a commonly used set of experimental relaxation data for ^{15}N–^{1}H or ^{13}C$^{\alpha}$–^{1}H systems of the protein backbone includes only longitudinal (R_1) and transverse (R_2) relaxation rates for ^{15}N or ^{13}C$^{\alpha}$ nuclei and the value of the heteronuclear Overhauser effect (NOE) (Eq. (1.29b)).

For the backbone ^{15}N nuclei the contribution from other mechanisms of relaxation is less than 1–2%. Thus, the formulae derived in Section 1.2 for longitudinal (Eqs. (1.28b) and (1.28c)) and transverse (Eqs. (1.30b) and (1.30c)) relaxation may be applied for the backbone ^{15}N nuclei without any modification, provided that the ^{15}N nuclei considered are not affected by conformational exchange in the microsecond–millisecond time-scale. In an analysis of ^{13}C$^{\alpha}$ relaxation in uniformly ^{13}C-enriched proteins the relaxation due to dipolar interactions of ^{13}C$^{\alpha}$ with the adjacent ^{13}C should also be taken into account. In addition, special care should be taken to avoid the effects of scalar ^{13}C–^{13}C coupling (see [47,48]).

Below we focus on the relaxation measurements for the backbone ^{15}N nuclei and discuss the conventional heteronuclear relaxation experiments.

1.4.1. The heteronuclear NMR relaxation measurements

The experimental schemes for the measurements of ^{15}N R_1, R_2 and ^{15}N{^{1}H} NOE are well documented [49–51]. Numerous experiments for measurement of the relaxation rates of the other coherences, i.e. the anti-phase, longitudinal two-spin order, zero- and double quantum coherences, and cross-correlated cross-relaxation rates have also been described (see, e.g. [17,24,52–55]). Here we briefly discuss the common principles of the heteronuclear relaxation experiments. For a more comprehensive discussion on the basic principles of modern heteronuclear multidimensional NMR spectroscopy see Chapter 7 in Ref. [8].

The general scheme of 2D experiments for heteronuclear relaxation measurements is shown in Fig. 1. The scheme includes the following steps:

1. *Preparation.* The experiment starts from the proton (spin **I**) magnetisation. This increases the sensitivity of the experiment by a factor γ_I/γ_S in comparison with experiments starting from magnetisation of the heteronucleus (spin **S**). The desirable coherence is created using magnetisation transfer through scalar coupling, e.g. using an INEPT transfer step [56].
2. *Delay for the relaxation.* This is a delay of variable length T for auto- or cross-relaxation of the selected coherence. Several spectra with different

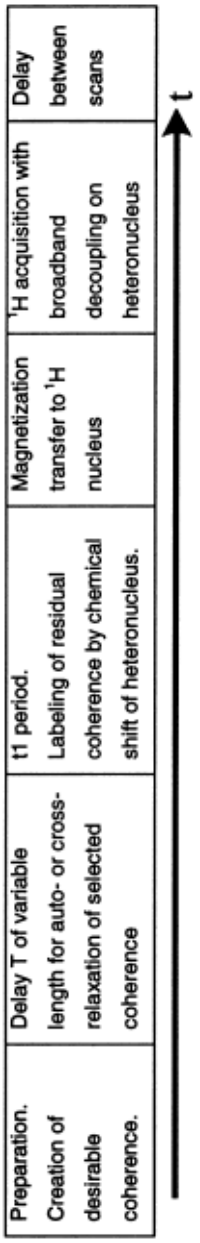

Fig. 1. Schematic representation of 2D experiments for heteronuclear relaxation measurements.

values of T are usually recorded. The desired auto- or cross-relaxation rate is then obtained from the dependence of the peak intensities in the spectra on the value of the relaxation delay T. It is important to ensure that only the selected auto- or cross-relaxation process occurs during the relaxation period T. Therefore, mixing of magnetisation components due to unwanted cross-relaxation or scalar coupling should be carefully avoided.

3. A t_1 *period* is introduced in order to label the residual coherence by the frequency of the heteronucleus.
4. *Reverse magnetisation transfer.* Transfer of magnetisation back to the proton. Detection on protons enhances the sensitivity of the experiment by the factor $(\gamma_I/\gamma_S)^{3/2}$. After the t_1 period the magnetisation in the rotating frame consists of two orthogonal components weighted as $\cos(\Omega_S t_1)$ and $\sin(\Omega_S t_1)$ (Ω_S is the chemical shift of the heteronucleus). Most of the relaxation experiments include the detection of both components using the 'preservation of equivalent pathway' principle (sensitivity enhancement) [57,58]. This increases the sensitivity of the experiment by $\sqrt{2}$ in comparison with the experiment using only one of the components. The reverse magnetisation transfer may also include gradient selection of a coherence transfer pathway [59–61].
5. *Detection.* During this period the proton transverse magnetisation is detected. Broadband decoupling from the heteronucleus is commonly applied here (for a review see [62]).
6. *Delay between the scans.* In the experiments for relaxation rate measurements this delay should be selected to obtain maximal sensitivity of the experiment. In practice, a compromise between complete recovery of the proton magnetisation after the preceding scan and a maximum number of scans collected per unit time should be considered.

This scheme does not cover all available types of relaxation experiments for the ^{15}N–^{1}H two-spin system. In particular, in heteronuclear NOE measurements only two spectra are recorded starting from equilibrium magnetisation of ^{15}N and from steady-state magnetisation of ^{15}N under the condition of proton saturation (see below).

1.4.2. ^{15}N R_1, R_2 and NOE experiments

The commonly used pulse sequences for measurements of ^{15}N R_1, R_2 and $^{15}N\{^1H\}$ NOE [51] are presented in Fig. 2. A modification of the ^{15}N R_1 experiment allowing off-resonance rotating-frame relaxation measurements is also shown (see, e.g. [63]).

The pulse field gradients $g1$ in R_1 and R_2 experiments defocus the initial ^{15}N magnetisation, $g3$ in R_1 and R_2 and $g5$ in R_1 experiments defocus the transverse coherences when the desired magnetisation is of the form $2I_zS_z$ and S_z, respectively. Equal gradients are placed on both sides of the simultaneous 180° $^1H/^{15}N$ pulses to reduce effects of pulse imperfection [64]. The gradient pulses $g6$ and $g9$ in R_1, $g5$ and $g8$ in R_2 and $g1$ and $g4$ in NOE experiments are used for the selection of a coherence transfer pathway [59–61]. The length and strength of these gradients are adjusted in such a manner that the ratio of areas of encoding and decoding gradient pulses is equal to γ_S/γ_I.

The preservation of an equivalent pathway is implemented in all experimental schemes [57,58]. In particular, two different data sets are recorded with an inverted sign of encoding gradients $g6$, $g5$ and $g1$ and inverted phase $\phi4$, $\phi3$ and $\phi6$ in R_1, R_2 and NOE experiments, respectively. Before the acquisition the proton magnetisation in these two sets is given by $\pm I_y \cos(\Omega_s t_1) + I_x \sin(\Omega_s t_1)$. Sine and cosine amplitude modulated signals, required for purely absorptive line-shapes, are then generated by adding and subtracting the recorded data sets.

1.4.2.1. R_1 measurements. In ^{15}N R_1 experiments (Fig. 2a) the magnetisation at the beginning of the relaxation period T corresponds to $\pm S_z$. During the relaxation delay T the ^{15}N magnetisation approaches its steady-state value, i.e. the time dependence of magnetisation is given by a three-parameter exponential decay $\langle I_z\rangle(t) = \langle I_z\rangle(\infty) + \langle I_z\rangle(0)\exp(-R_1T)$. The contribution of steady-state ^{15}N magnetisation is cancelled by alternation of the direction of the ^{15}N magnetisation at the beginning of the relaxation period T (alternation of phase $\phi1$) with simultaneous inversion of the receiver phase (see [65]). The dependence of the resulting peak intensity in spectra with different values of T is thus given by $A = A_1\exp(-R_1T)$.

The unwanted cross-relaxation $S_z \rightarrow 2I_zS_z$ caused by cross-correlation between the DD and CSA relaxation mechanisms during relaxation period T is suppressed either by repeating 180° ^1H pulses or by broadband ^1H decoupling [66].

1.4.2.2. R_2 measurements R_2 (CPMG) and $R_{1\rho}$ experiments. Transverse relaxation rates R_2 can be measured using the CPMG technique [37,38]. In the R_2 (CPMG) experiment (Fig. 2b), at the beginning of the relaxation period T, the magnetisation is of the form $\pm S_x$. During the relaxation period T the effects of heteronuclear scalar coupling, field inhomogeneity and micro-millisecond conformational exchange are suppressed by the CPMG sequence, comprising the repeating ^{15}N $180°_{(x)}$ pulses separated by a delay 2δ. Because of the scalar coupling between **I** and **S** the apparent transverse relaxation rate R_2 of spin **S**, measured in the CPMG experiments, is a superposition of the relaxation rates of inphase S_x and anti–phase $2I_zS_x$ coherences [67]:

$$R_2 = \frac{1}{2}\left(R_{S_x}\left(1 + \frac{\sin\alpha}{\alpha}\right) + R_{2I_zS_x}\left(1 - \frac{\sin\alpha}{\alpha}\right)\right) \tag{1.47}$$

where $\alpha = 2\pi J\delta$, J is the scalar coupling constant ($J \approx 90$ Hz for amide NHs), the relaxation rates R_{S_x} and $R_{2I_zS_x}$ are given by Eqs. (1.30a)–(1.30e). Thus, in R_2 (CPMG) experiments the condition $2\pi J\delta \ll 1$ should hold (i.e. $\delta < 0.5 - 0.7$ ms should be used). The unwanted cross-relaxation $S_{x,y} \rightarrow 2I_zS_{x,y}$ due to cross-correlation between the DD and CSA **S** relaxation mechanisms during the relaxation period T is suppressed by 180° ^1H pulses corresponding to even CPMG echoes [67]. Since the transverse magnetisation approaches zero at $T \rightarrow \infty$, the dependence of peak intensities in the spectra with different values of T is given by a two-parameter exponential decay $A = A_1\exp(-R_2T)$.

It has been reported recently [68,69] that off-resonance effects stemming from the finite length of the 180° pulses in a CPMG pulse train affect the measured R_2 (CPMG) rates. These effects can be neglected only if the RF pulse field strength ω_1 (in frequency units) substantially exceeds the spectral width. In practice this condition holds neither for ^{15}N nor for ^{13}C R_2 measurements. Substantial errors in R_2 are expected if the spectral width is of the same order as ω_1. It was shown [68] that after $2n$ repetitions

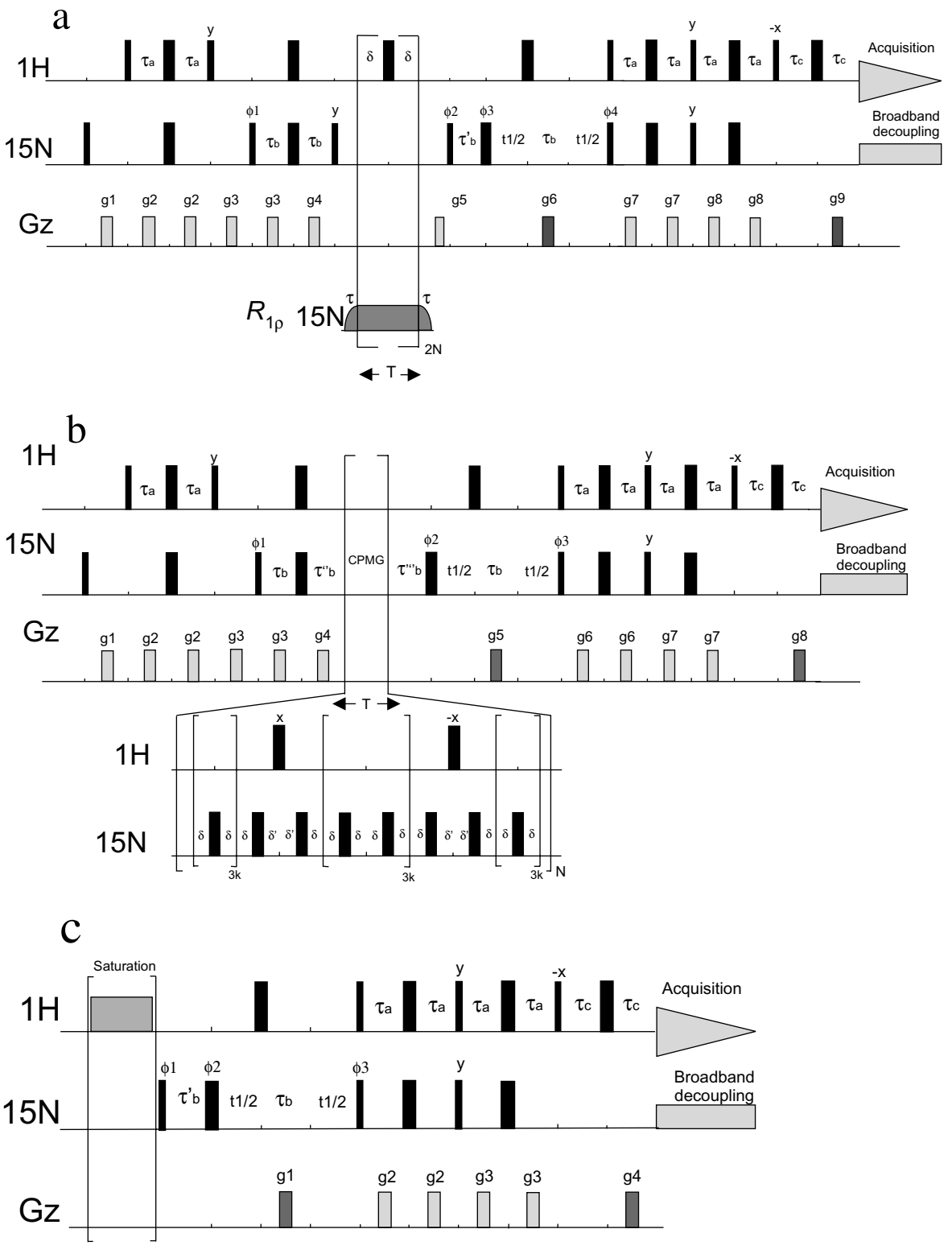
a
1H
15N
Gz
Acquisition
Broadband decoupling
$R_{1\rho}$ 15N
2N
T
b
CPMG
3k
N
c
Saturation

of the δ-180°$_{(x)}$-δ CPMG block the magnetisation is not aligned along the x-axis of the rotating frame, but rotates by an angle $2n\Phi$ about an effective axis in the xz-plane of the rotating frame tilted versus the x-axis by an angle Θ (Fig. 3). The angles Φ and Θ depend on the resonance offset from the carrier $-\Delta\omega$, the inter-pulse delay -2δ, and the field strength of the pulse $-\omega_1$:

$$\tan(\Theta) = \cos(\lambda)\cot(\theta) + \sin(\lambda)\sin^{-1}(\theta)\cot(\phi/2) \quad (1.48)$$

$$\cos(\Phi/2) = \cos(\lambda)\cos(\phi/2) - \sin(\lambda)\cos(\theta)\sin(\phi/2),$$

where $\lambda = \Delta\omega\delta$, $\theta = \arctan(\omega_1/\Delta\omega)$, $\phi = k\pi\sqrt{1 + (\omega_1/\Delta\omega)^2}$, k is the factor accounting for pulse imperfection ($k = 1$ for a perfectly calibrated pulse). Offset-dependent oscillations with the amplitude of $\sin^2(\Theta)$ are superimposed on the exponential decay of experimentally observed x-components of magnetisation. These oscillations may result in a bias of the R_2 values measured by the CPMG technique from the actual ones. Fortunately, for ^{15}N spectral widths typical for proteins the effect of oscillations can be safely neglected [69]. However, the fact that magnetisation processes out of the xy-plane during the CPMG sequence causes a contribution of R_1 to the apparent R_2 relaxation rates measured in the CPMG experiments. Korzhnev et al. [69] showed

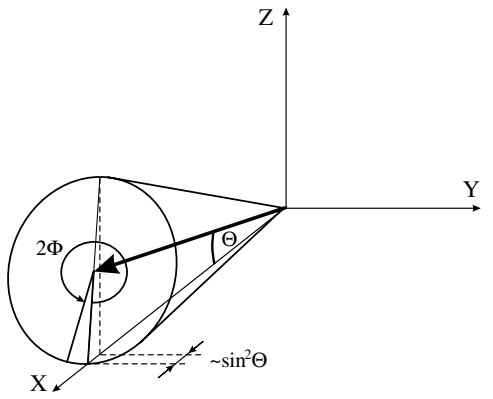

Fig. 3. Schematic representation of the effective rotation of magnetization during the CPMG sequence. The angles Θ and Φ are given by Eq. (1.48). Reproduced from [69] with kind permission from Kluwer Academic Press.

that for typical CPMG settings this effect leads to systematic (up to 10%) offset dependent underestimations of ^{15}N R_2 for proteins of intermediate and large size (Fig. 4). In some cases, the off-resonance effects yield a dependence of the apparent ^{15}N R_2 (CPMG) on the CPMG pulse repetition rate, which might be erroneously interpreted as a consequence of conformational exchange in the millisecond time-scale (see Fig. 4).

A reasonable alternative to the R_2 (CPMG) measurements is provided by relaxation measurements

Fig. 2. Enhanced sensitivity pulse sequences [51] employing pulse field gradients for the measurements of (a) ^{15}N R_1 (modification allowing $R_{1\rho}$ measurements is also shown), (**b**) ^{15}N R_2 and (**c**) ^{1}H{^{15}N} NOE with minimal saturation of water resonance. Narrow and wide bars in all sequences indicate 90 and 180° pulses, respectively. Unless indicated otherwise, all pulses are given along the x-direction. Darker gradient pulses are used for selection of a coherence transfer pathway. In all experiments $\tau_a = 2.25$ ms ($<1/(4J_{NH})$), $\tau_b = 2.75$ ms ($1/4J_{NH}$)). Delays τ_b', τ_b'' and τ_b''' are given by $\tau_B + 2pw$, $\tau_B + (2/\pi)pwn$ and $\tau_B + 2pw + (2/\pi)pwn$, respectively, where pw — ^{1}H 90° pulse length, pwn — 90° ^{15}N pulse length. (a) The phase cycling used in the R_1 experiment is $\phi1 = x, -x$; $\phi2 = y$; $\phi3 = 2(x), 2(y), 2(-x), 2(-y)$; $\phi4 = x$; receiver $x, -x, -x, x$. During the relaxation period T an even number of ^{1}H 180° pulses are applied with the delay $\delta = 2.5$ ms. For each increment of $t1$ two one-dimensional spectra scans are collected with the inverted phase $\phi4$ and inverted sign of gradient $g6$. For $R_{1\rho}$ measurements [63] ^{15}N magnetisation before the relaxation period is rotated from the z-direction to the direction of the effective field using amplitude- and phase-modulated tanh/tan adiabatic pulses with the modulation functions $\omega_1(t) = \omega_1\tanh(10t/\tau)$ and $\Delta\omega(t) = \Delta\omega_0(\tan(\tan^{-1}(50)(1 - t/\tau)))/50$ for amplitude and frequency, respectively (recommended adiabatic pulse length τ is 6 and 4 ms for spin-lock field ω_1 of 1.0 and 2.0 kHz, respectively, at 14.1 T (600 MHz ^{1}H) spectrometer; $\Delta\omega_0 = 30$ kHz; sign of $\Delta\omega_0$ is selected according to resonance offset from spin-lock carrier). The continuous wave RF irradiation period T, the pulse for rotation of magnetisation to the effective field and the pulse for returning of magnetisation to the z-direction are implemented as one adiabatic pulse with the particular carrier frequency (see Ref. [63]). (b) The phase cycling used in the R_2 experiment is $\phi1 = x, -x$; $\phi2 = 2(x), 2(y), 2(-x), 2(-y)$; $\phi3 = x$; receiver $x, -x, -x, x$. Delays δ in CPMG can be varied from ~0.2 to 0.5–0.7 ms, $\delta = \delta' - pw$. For each increment of $t1$ two spectra are collected with inverted phase $\phi3$ and inverted sign of gradient $g5$. (**c**) The phase cycling used in the NOE experiment is $\phi1 = y$; $\phi2 = x, y, -x, -y$; $\phi3 = x$; receiver $x, -x$. For each increment of $t1$ two spectra are collected with inverted phase $\phi3$ and inverted sign of gradient $g1$. ^{1}H saturation is achieved by the application of ^{1}H 120° pulses spaced at 5 ms intervals for 3–5 s prior to the first ^{15}N pulse. Two data sets are recorded, one with and one without proton saturation.

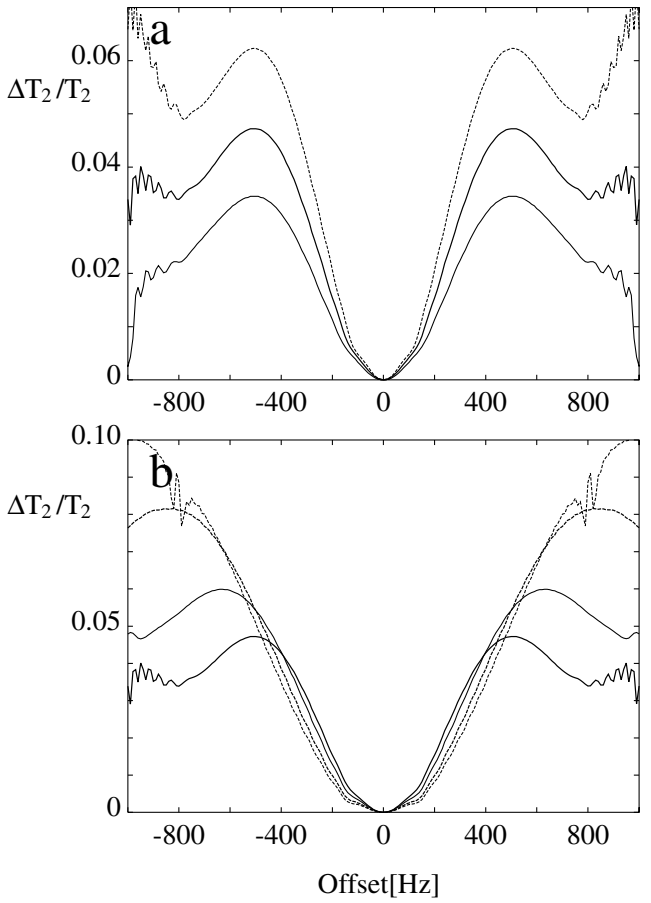

Fig. 4. Relative difference for transverse relaxation times $\Delta T_2/T_2 \approx -\Delta R_2/R_2 (\Delta T_2 = T_{2app} - T_2; \Delta R_2 = R_{2app} - R_2)$, characterising the deviation of the apparent relaxation rate R_{2app} (CPMG) from the actual R_2 value, versus the resonance offset from the carrier frequency of ^{15}N 180° pulses of the CPMG sequence (Hz). The apparent transverse relaxation rates R_{2app} (CPMG) for the ^{15}N nucleus with actual $R_1 =$ 1.66 Hz and $R_2 = 10.0$ Hz were calculated using numerical modelling of the CPMG sequence [69]. Different CPMG settings were used: (**a**) ^{15}N 90° pulse length — 70, 54 and 40 μs (curves from top to bottom), delay δ of δ-180°$_{(x)}$-δ CPMG block — 500 μs. (**b**) ^{15}N 90° pulse length — 54 μs, $\delta = 250$, 300, 400 and 500 μs from top to bottom (e.g. at 1000 Hz offset). Reproduced from [69] with kind permission from Kluwer Academic Press.

in the presence of a transverse spin-locking field (off-resonance $R_{1\rho}$ measurements) (for a recent review see Ref. [27]). The R_2 value may be obtained from $R_{1\rho}$ and R_1 data using Eq. (1.36b). A modification of the ^{15}N R_1 pulse sequence allowing off-resonance $R_{1\rho}$ measurements is shown in (Fig. 2a). Before the relaxation period the ^{15}N magnetisation can be aligned along the effective field using adiabatic rotations [63,70]. In the case of a small chemical shift dispersion the method of chemical shift precession [71] may also be used. It should be noted that the outcome of a $R_{1\rho}$ experiment may be affected by inaccurate calibration of the spin-lock field strength, the spin-lock field inhomogeneity and by power losses residing in a drop of the amplifier output after long RF irradiation [72].

1.4.2.3. ^{15}N{^{1}H} NOE measurements. The heteronuclear NOE experiment starts from the magnetisation of the heteronucleus **S** (Fig. 2c). Two different spectra are recorded starting from: (i) equilibrium magnetisation

of **S** at $\langle I_z \rangle = I_{z0}$; and (ii) from steady-state magnetisation of **S** under the condition of saturation of **I**: $\langle I_z \rangle = 0$. The value of the heteronuclear NOE (Eq. (1.29b)) is then obtained as a ratio of the peak intensities in these two spectra. The saturation of proton **I** is reached, e.g. by a sequence of repeated 120° ^{1}H pulses [73]. The saturation period in spectra with initial $\langle I_z \rangle = 0$ and a delay between scans in spectra with initial $\langle I_z \rangle = I_{z0}$ should ideally exceed the transverse relaxation time T_1 of spin **S** by 4–5 times.

Complications in the backbone ^{15}N{^{1}H} NOE measurements are mainly associated with the saturation transfer from solvent protons to amide protons occurring through chemical exchange, spin diffusion or direct NOE with the solvent protons (see Ref. [74,75]). These effects can substantially reduce the signal intensities in ^{15}N{^{1}H} NOE spectra obtained without prior saturation of the amide protons. Subsequently, this leads to overestimation of the absolute value of the ^{15}N{^{1}H} NOE Eq. (1.29b). Since T_1 of the solvent protons is relatively long (for water at 30°C it is ∽4 s, i.e. of the order of the delay between the scans) it is desirable to use sequences with minimal perturbation of the solvent magnetisation. In particular, one needs to avoid a gradient de-phasing of the solvent magnetisation and to return the solvent magnetisation to the positive z direction at the end the pulse sequence (see Ref. [74]).

1.4.3. Temperature control in the relaxation experiments

Special precautions should be taken to keep the temperature constant throughout relaxation experiments. It is known that radio-frequency irradiation during NMR experiments can cause substantial heating of the sample, resulting in different effective temperatures of the sample for different experiments [76–78]. The temperature dependent drifts of the longitudinal and transverse relaxation rates are of about 3% per K due to changes in the overall rotation rate of the molecule affected by the changes in the solvent viscosity. The effect of sample heating may introduce a significant bias in the extracted relaxation data and subsequently in parameters of molecular motions. First, the extracted relaxation data are affected by the temperature variations between the data points of the individual relaxation experiments (e.g. R_1 and R_2 data points recorded with different relaxation delays T or ^{1}H{^{15}N} NOE recorded with or without proton saturation). Second, a different mean temperature in different types of relaxation experiments results in inconsistency between experimental relaxation data.

The mean temperature in different relaxation experiments might be adjusted by an appropriate setting of the temperature control unit. Several approaches may be considered to keep the temperature constant for different data points of individual relaxation experiments: (i) All spectra with different relaxation delays can be recorded separately with individual temperature corrections; however, this approach can result in artefacts due to the spectrometer and sample instabilities during long experiments. (ii) Additional delays and/or off-resonance irradiation can be introduced into the pulse sequences in order to equalise the heat dissipation for different relaxation delays (as has been done in the ^{15}N{^{1}H} NOE measurements [79,80]). (iii) Temperature fluctuations can be averaged by using interleaved acquisition [78]. The latter method uses the fact that the time constant for temperature equilibration exceeds the duration of single scan. Thus, when the equilibrium conditions in a NMR experiment are reached, the temporary changes in the sample heating due to irradiation in the different experiments are efficiently averaged out and do not lead to significant temperature fluctuations provided these occur fast enough and periodically. These requirements can be met by interleaved acquisition where relaxation delays are alternated after each scan such that the long and short delays are grouped pairwise. Since the duration of a single scan is ca. 2–4 s, the frequency of alternation is sufficiently high to achieve good averaging of the temperature fluctuations.

1.5. Parameters governing relaxation

The relaxation rates in a two-spin 1/2 system depend, among other things, on the parameters of the physical interactions governing the relaxation. The DD relaxation rates depend on the dipolar constant A_D (Eq. (1.22b)) which is connected with the distance between the two nuclei. The relaxation rates due to CSA mechanism are determined by the constants $A_{CSA(I)}$, $A_{CSA(S)}$ (Eq. (1.24d)), which depend on eigenvalues of the shielding anisotropy tensors of

the nuclei.[2] A dynamic analysis is greatly facilitated by the fact that the bond distances and shielding anisotropy tensors are approximately constant, and are known within a reasonable precision for particular spin systems in proteins. However, at least two assumptions, intrinsic consequences of the previous statement, should be emphasised. It is assumed that the interaction parameters are constant in time and are not significantly different for the different sites in the protein. Though reasonable and productive, neither of the two assumptions holds rigorously. In this section we address some practical aspects: What are the limitations of these assumptions? What values of the parameters should one use? And what reservations on the results of the dynamic analysis should one make due to the parameter uncertainties?

1.5.1. Chemical shift anisotropy

The relaxation rates due to the CSA mechanism depend on the symmetric traceless tensor of the shielding anisotropy, which in general can be parameterised by two constants: δ_z and $\eta = (\delta_x - \delta_y)/\delta_z$ (see Section 1.2.2). For an axially symmetric shielding ($\eta = 0$) the relaxation due to the CSA mechanism depends on the single value $\Delta\delta = \delta_{\|} - \delta_{\perp} = (3/2)\delta_z$, where $\delta_{\|} = \delta_z$ and $\delta_{\perp} = \delta_{x,y}$ are shielding constants corresponding to the directions along and perpendicular to the symmetry axis of the shielding tensor. The value of $\Delta\delta$ is usually referred to as the CSA value.

The CSA values for $^{13}C^{\alpha}$ nuclei are in the range 0–40 ppm [81–84]. Though these values are detectable for a protein in solution and carry valuable structural information [83], the relaxation due to the CSA mechanism is usually negligible in a regular dynamics analysis employing $^{13}C^{\alpha}$ R_1, R_2, and ^1H–^{13}C NOE measurements. Omission of the CSA relaxation in the analysis of $^{13}C^{\alpha}$ data is motivated not only by the small values of CSA, but also by the complications arising from their strong dependence on the structure and from the lack of axial symmetry of the $^{13}C^{\alpha}$ shielding tensor.

For the amide ^{15}N, the CSA relaxation pathway is comparable in efficiency with that due to the ^1H–^{15}N DD interaction. The analysis of the relaxation data in terms of the HN bond dynamics is significantly facilitated by the facts that the amide nitrogen shielding tensor is almost axially symmetric with the symmetry axis nearly parallel to the HN bond. For the amide ^{15}N, the value $\delta_{\|}$ corresponds to the least shielded (most high-field) component of the chemical shielding tensor, which results in a negative sign for CSA. Solid-state NMR experiments provide a relatively narrow distribution for the amide ^{15}N CSA with a mean value of -156.0 ppm and a standard deviation of ca. 5.7 ppm (Table 2). The symmetry axis of the shielding tensor is tilted 15–25° from the direction of the HN bond. Based on these data, the uniform CSA values of -160 ppm were commonly employed in early backbone relaxation studies on proteins in solution [49]. However, it was noted later that the use of uniform ^{15}N CSA values of -170 ppm provide a better fit to the relaxation data [17,85]. Similar CSA values were inferred from measurements of small changes of chemical shifts induced by a weak protein alignment in a strong magnetic field [86] or in liquid crystalline systems [87]. It has been suggested [85] that the difference of ca. 10 ppm between this value and values derived in solid-state experiments can be alleviated by properly taking into consideration thermal and zero-point quantum liberations, which are often neglected in the analysis of solid-state data.

Chemical shielding tensors, having their origin in the molecular electronic configuration, are quite sensitive to changes in molecular geometry. The CSA tensors of a flexible polypeptide molecule are thus time- and site-dependent regarding their principal values and the orientations of the principal axes. The effect of the CSA relaxation increases as the square of the magnetic field. For the amide ^{15}N at the fields higher than ca. 18.0 T one needs to take into account not only the CSA relaxation mechanism per se but also the variability of the CSA values [88] at different sites of the protein. CSA calculations employing density functional theory on the snapshots from the

[2] For a ^{15}N–^1H nuclear pair of the protein backbone the value of the dipolar constant A_D (Eq. (1.22b)) calculated assuming a constant N–H distance of 1.02 Å is -1.973×10^4 s^{-1}. The value of A_{CSA} (Eq. (1.24d)) for ^{15}N nucleus, calculated assuming an axially symmetric shielding tensor with $\delta_{\|} - \delta_{\perp} = (3/2)\delta_z = -160$ ppm is -7.916×10^2s^{-1} T^{-1}. The value of A_{CSA} (Eq. (1.24d)) for ^1H nucleus, calculated assuming an axially symmetric shielding tensor with $\delta_{\|} - \delta_{\perp} = (3/2)\delta_z = 10$ ppm is -4.884×10^2T^{-1} s^{-1}. The constants A_D and A_{CSA} were calculated using the values 1.054×10^{34} J s for the Planck constant $\hbar$, $4\pi \times 10^7$ T mA^{-1} for the permeability of free space μ_0, 2.675×10^8 T^{-1} s^{-1} for γ_H and -2.71×10^7 T^{-1}·s^{-1} for γ_N.

Table 2
Summary of the ^{15}N chemical shift tensors (ppm) from different peptides obtained by solid-state NMR (Here δ_{11}, δ_{22}, and δ_{33} are the frequency ordered ($\delta_{11} > \delta_{22} > \delta_{33}$, and δ_{11} is the most high field) principal values of the chemical shift tensor [14]; α is the angle between the direction of δ_{11} component and amide H–N bond; $\delta_{iso} = (\delta_{11} + \delta_{22} + \delta_{33})/3$; $\Delta\delta$ are CSA values defined as $\Delta\delta = (\delta_{33} + \delta_{22})/2 - \delta_{11}$; CSA values are distributed with the mean of −156.0 ppm and standard deviation of 5.7 ppm. All ^{15}N chemical shifts are referenced relative to liquid (25°C) NH_3 (27.3 ppm for saturated aqueous NH_4Cl) [256]. An asterisk notes the residues labelled by ^{15}N)

Sample	δ_{33}	δ_{22}	δ_{11}	δ_{iso}	α	$\Delta\delta$	Reference
Ala*Ala	65.3	78.1	215.5	119.6	12.6°	−144	[243]
AcGly*AlaNH$_2$	44.6	85.1	229.4	119.7	17.6 ± 2°	−164.55	[244]
(*Ala)$_n$ α-helix	47.7	64.1	213.7	108.5		−157.8	[245]
(*Ala)$_n$-5 β-sheet	53.7	71.4	210.7	111.9		−148.2	[245]
(*Ala,Leu)$_n$ α-helix	44.7	66.6	213.7	108.3		−158.1	[245]
(*Ala,Asp (OBzl))$_n$ α-helix	47.7	68.4	217.7	111.3		−159.7	[245]
(*Ala,Glu (OBzl))$_n$ α-helix	48.7	66.4	215.7	110.3		−158.2	[245]
(*Ala,Glu (OMe))$_n$ α-helix	46.7	67.8	214.7	109.7		−157.5	[245]
(*Ala, Val)$_n$ β-sheet	44.7	72.1	211.7	109.5		−153.3	[245]
(*Ala,I1e)$_n$ β-sheet	49.7	72.7	209.7	110.7		−148.5	[245]
(*Asp (OBzl))$_n$-1 α_R-helix	48.7	62.5	214.7	108.6		−159.1	[246]
(*Asp (OBzl))$_n$-2 α_L-helix	50.7	58	210.7	106.5		−156.35	[246]
(*Asp (OBzl))$_n$-3 ω_L-helix	49.7	57.1	211.7	106		−158.3	[246]
(*Asp (OBzl))$_n$-4 β-sheet	50.7	66.1	212.7	109.7		−154.3	[246]
N-Ac*Gly	37.0	82.8	220.4	113.4	25.5 ± 1°	−160.50	[247]
(*Gly) collagen powder	42.3	67.0	223.4	110.9	24.5 ± 1°	−168.75	[247]
(*Gly) collagen oriented	42.3	67.0	223.4	110.9	24.5 ± 2°	−168.75	[247]
(*Gly) collagen	45.6	67.6	216.8	110.0	23°	−160.20	[248]
(*Gly) maganine	42.0	73.2	215.0	110.1	22 ± 2°	−157.40	[249]
Boc-(Gly)$_2$ *Gly-OBzl	55.1	62.1	223.0	113.4	22 ± 1°	−164.40	[250]
Boc-(Gly)$_2$ *Gly-OBzl	36.4	83.4	220.4	113.4	24 ± 1°	−160.50	[250]
Gly *Gly	46.8	79.7	220.8	115.8		−157.55	[251]
Gly *Gly·HCL	57.3	59.8	210.0	109.0	18.6 ± 2°	−151.45	[244]
AcGly *GlyNH$_2$	40.7	64.2	210.0	105.0	17.6 ± 2°	−157.55	[244]
Gly *Gly· HCl·H$_2$O (powder)	58.5	64.1	209.5	110.7	25 ± 5°	−148.20	[99,252]
Gly *Gly· HCl·H$_2$O (crystal)	60.3	70.9	215.9	115.7	21.3°	−150.30	[253]
(*Gly)$_n$ β-sheet	45.7	61.4	205.7	104.3		−152.15	[254]
(*Gly)$_n$ 3$_{10}$-helix	49.7	62.8	214.7	109.1		−158.45	[254]
(*Gly,Ala)$_n$ α-helix	44.7	57.6	212.7	105.0		−161.55	[254]
(*Gly,Ala)$_n$ β-sheet	39.7	66.0	206.7	104.1		−153.85	[254]
(*Gly,Leu)$_n$ α-helix	45.7	61.7	210.7	106.0		−157.00	[254]
(*Gly,Leu)$_n$ β-sheet	40.7	66.2	206.7	104.5		−153.25	[254]
(*Gly,Val)$_n$ β-sheet	39.7	74.6	203.7	106.0		−146.55	[254]
(*Gly,Ile)$_n$ β-sheet	45.8	68.3	209.7	108.6		−152.65	[254]
(*Gly,Lys(Z))$_n$ α-helix	40.7	69.2	208.7	106.2		−153.75	[254]
(*Gly,Glu(OBzl))$_n$ α-helix	47.7	61.2	210.7	106.5		−156.25	[254]
(*Gly,Sar)$_n$	38.7	65.8	204.7	103.1		−152.45	[254]
(*Phe) maganine	55.0	80.0	220.0	118.3	22 ± 3°	−152.5	[255]
AcGly *TyrNH$_2$	52.1	77.1	209.3	112.8	19.6 ± 2°	−144.70	[244]

molecular dynamic simulation on ubiquitin were recently reported [89]. It was shown that the CSA values exhibit substantial fluctuations in the picosecond–nanosecond time-scale, which could have a significant effect on the measured relaxation rates. Recently several new methods were introduced allowing measurements on amide ^{15}N CSA for proteins in solution [17,22,88,90]. These measurements resulted in a rather broad distribution of ^{15}N CSA with a mean value of −172 ppm [88] for ribonuclease H and −159 ppm [90] for human ubiquitin, and standard deviations of about 13 ppm and 16 ppm respectively.

Similar mean values and variances were obtained in a dynamic study of a peptide (1–36) from bacteriorhodopsin, where CSAs or H–N distances were adjusted along with the parameters of the dynamic models [78] using relaxation data measured at three magnetic fields. Ab initio calculations reveal substantial dependence of the CSA values both from the backbone conformation and the parameters of the hydrogen bonding. Thus, CSA values of −158, −135, and −124.5 ppm were obtained in density functional calculations [91] for a glycine amide nitrogen in extended, β-sheet, and α-helix conformations, respectively. In these and other studies somewhat less prominent changes of the CSA values (ca. 3–9 ppm) upon the formation of a hydrogen bond were also reported [84,91,92].

Recent reports present interesting data on the CSA of amide protons [54,84,93–96]. Solid-state NMR measurements [95,96] on model compounds showed that the shielding tensor of an amide proton is not axially symmetric. The most shielded component of the tensor is aligned parallel to the H–N bond. Studies on amide CSA for proteins in solutions using cross-correlated cross-relaxation measurements were characterised mostly by its pronounced dependence on the parameters of hydrogen bonding. The CSA values obtained for ubiquitin, HIV-1 protease, HU protein, and savinase assuming an axially symmetric shielding tensor are distributed in the range 0–25 ppm [54,93,94], with the lowest and highest values corresponding to the non hydrogen bonded amides and amides with the shortest hydrogen bonds, respectively. An empirical dependence for the CSA was proposed [94]:

$$\Delta\delta = 4.9 + 1.96/(r_{H\ldots O} - 1.3)^2, \qquad (1.49)$$

where $\Delta\delta$ is given in ppm and the length of the hydrogen bond $r_{H\ldots O}$ in Å. The residual root mean square deviation between the CSA values predicted by Eq. (1.49) and those measured for ubiquitin is as small as 1.8 ppm. Eq. (1.49) is in qualitative agreement with the results of ab initio calculations on *N*-methylacetamide [84], which also indicates a steep dependence of the amide CSA on the length of the hydrogen bond. Since the hydrogen bonds are usually slightly shorter in β-sheets than in α-helices, the amide CSA are sensitive to the type of secondary structure, with mean values of 9 ± 4 ppm and 16 ± 6 ppm for α-helixes and β-sheets, respectively [54]. For amides exposed to the water the CSA values are only slightly (ca. 1 ppm) smaller than those in β-sheets [94].

1.5.2. Length of $^1H–^{15}N$ and $^1H–^{13}C^\alpha$ bonds

The length of the amide HN bond to be used in ^{15}N relaxation studies is the subject of an ongoing debate, with solid-state NMR yielding values ca. 0.04 Å larger than the neutron diffraction and ab initio calculations [97]. The bond length obtained from the neutron diffraction ranges from 1.02 to 1.04 Å. Ab initio calculations on *N*-methylacetamide resulted in an even shorter value of 1.000–1.008 Å for the energy minimum of the H–N amide bond [98]. Solid-state NMR on model peptides yields distances of 1.06–1.07 Å [95,99]. A typical ab initio value for the $^1H–^{13}C^\alpha$ bonds is 1.085 Å with a little variation for different arrangements. Neutron diffraction yields 1.09–1.10 Å [98,100] for the $^1H–^{13}C^\alpha$ bonds. The NMR experiment, again, provides a higher value of 1.17 Å [101].

It is accepted now [98,99] that the discrepancies between the distances inferred from the measurements of the dipolar interaction in NMR and those obtained using scattering amplitudes in neutron diffraction are mostly due to the anharmonicity of the bonding potential and to the different averaging of zero-point vibrational motion. Both experimental methods provide apparent effective distances, which are biased from their values anticipated from the position of the bond energy minimum. It should be emphasised that vibrations are mostly defined by the local structure. These vibrations are present even at zero temperature. In this regard, the selection of a particular value for the H–N or $H–C^\alpha$ distance can be related to the selection of a reference dynamic behaviour [98], or, in other words, a reference amplitude of molecular fluctuations. In some circumstances, the choice of this reference is a matter of convenience. Changing from an unphysical rigid reference system, where all intramolecular motions are ‘frozen’, to a system accounting for local stretching and bending vibrations will just scale the order parameters or density functional values by a constant factor. For example, one can use a traditional value [49] of 1.02 Å for the length of the amide H–N bond to consider the difference in order parameters between difference amides in a protein,

but only those S^2 values, which are below ca. 0.9 can be thought as reasonable and might be interpreted in terms of relevant thermal motions of an H–N bond. Alternatively, a *quantum* reference was proposed [98], which allows for vibrations by employing an effective distance between the nuclei (1.04 Å and 1.17 Å for H–N and H–C^{α}, respectively). This of course leads to order parameters that are much closer to unity. Complications with the reference frame arise, however, if relaxation data (or residual dipolar coupling measurements [101]) are analysed simultaneously for different pairs of nuclei, e.g. for $^{1}H-^{15}N$ and $^{1}H-^{13}C^{\alpha}$. Vibrational corrections must also be considered if dynamic parameters are used for a quantitative interpretation in terms of simple classical models (e.g. diffusion in a cone), calculation of the residual entropy, or comparison with results of a molecular dynamics simulation [102].

Lack of high-resolution neutron diffraction data on proteins and inability of ab initio calculations to deal with big systems leave the question open to what extent the HN distance variations observed in neutron diffraction and NMR experiments are connected with the structural environment of the protein and can change in the course of conformational transformations. It is notable in this respect that an H–N distance depends on the parameters of a hydrogen bond. Ab initio calculations [81,98,100,103] on *N*-methylacetamide have shown that the HN distance increases by 0.001–0.018 Å upon dimerisation accompanied by formation of a hydrogen bond. Even larger elongations of up to 0.04 Å were suggested [100] for the transition from gas to a crystalline environment, where the hydrogen bonds became arranged into a network with π-bond cooperativity [97]. In the dynamics study of (1–36) bacteriorhodopsin under hydrostatic pressure of 2000 bar [104], it was suggested that both ^{15}N CSA and H–N distances could be slightly modified relative to their values at ambient pressure. Namely, an elongation by ca. 0.01 Å was proposed for the amides in the α-helical part of the peptide.

From the above one can anticipate that, as it concerns NMR relaxation, H–N distances and amide ^{15}N CSA values can be subjected to significant site-to-site variations depending on the structural and dynamic properties of the corresponding hydrogen bonds. For the relaxation of the C^{α} nuclei, however, much smaller variations induced by different molecular configurations are expected due to variations in both CSA and H–C^{α} distances.

2. Brownian overall molecular motion

A comprehensive theory connecting different mechanisms of spin relaxation with values of the spectral density function at characteristic frequencies has been described in the previous sections. A further analysis of the NMR relaxation data relies on the particular form of the spectral density functions characteristic for molecular dynamic processes. For relatively rigid macromolecules, such as proteins, two types of molecular motion should be considered in solution: (i) overall Brownian diffusion; and (ii) intramolecular mobility. The assumption of independence of these motions allows one to consider them separately, which substantially simplifies the data analysis. Typically intramolecular motion affects NMR relaxation to a much lesser extent than the Brownian diffusion. Thus, the effect of internal motion is always masked by the overall molecular motion. In some cases improper assumptions about molecular diffusion result in erroneous parameters for intramolecular dynamics extracted from the NMR relaxation data [105,106]. Therefore, a correct characterisation of the overall molecular motion plays a key role in NMR relaxation studies of internal dynamics of macromolecules.

In this section we consider the effect of Brownian diffusion of the molecule on NMR relaxation. Derivation of the NMR correlation functions (see Refs. [107,108]) based on Green's function for rigid body diffusion [109,110] is presented in Section 2.1. Some of these results have been already reviewed [16,111,112]. In Sections 2.2 and 2.3 we review the properties of the diffusion tensors characterising the molecular Brownian diffusion, the computational methods for their calculation and applications of these methods to proteins.

2.1. Diffusion of a rigid particle. NMR correlation functions

2.1.1. Separation of overall and internal motions

The spectral density function $J(\omega)$ in the

Table 3
The eigenvalues and eigenfunctions for the rotational diffusion of a rigid molecule (Here the eigenfunctions of the asymmetric rotator are written in a form used by Huntress [111]. The expansion coefficients a_{Lnk} are given explicitly in the expressions for eigenfunctions of the asymmetric rotator ψ_{Lnm})

Eigenvalues E_{Ln}	Eigenfunctions ψ_{Lmn}
Isotropic molecule	
$DL(L+1)$	$\phi_{Lkm} = \sqrt{\frac{2L+1}{8\pi^2}} D^{L^*}_{mk}(\Theta)$
where $D = D_x = D_y = D_z$ are eigenvalues of the rotational diffusion tensor of the molecule	ϕ_{Lkm} — eigenfunctions for symmetric rotator
	$D^L_{mk}(\Theta)$ — Wigner functions (Appendix A)
Axially symmetric molecule	
$E_{lk} = D_\perp L(L+1) + (D_\parallel - D_\perp)k^2$ where $D_\perp = D_x = D_y$; $D_\parallel = D_z$ are eigenvalues of the rotational diffusion tensor of the molecule	$\phi_{Lkm} = \sqrt{\frac{2L+1}{8\pi^2}} D^{L^*}_{mk}(\Theta)$ ϕ_{Lkm} — eigenfunctions for symmetric rotator
Asymmetric molecule (*for* $L = 2$)	
$E_{2,2} = 6(D + \sqrt{D^2 - D'^2})$	$\psi_{Lnm} = \sum_k a_{Lnk}\phi_{Lkm} = \sqrt{\frac{2L+1}{8\pi^2}} \sum_k a_{Lnk} D^{L^*}_{mk}(\Theta)$
$E_{2,-2} = D_x + D_y + 4D_z$	where $\sum_k a_{Lnk} a^*_{Lnk} = 1$,
$E_{2,-1} = D_x + 4D_y + D_z$	ψ_{Lnm} — eigenfunctions for asymmetric rotator — linear combinations of eigenfunctions of symmetric rotator
$E_{2,1} = 4D_x + D_y + D_z$	$\psi_{2,2,m} = \frac{1}{N}\left[u\phi_{2,0,m} + \frac{w}{\sqrt{2}}(\phi_{2,2,m} + \phi_{2,-2,m})\right]$
$E_{2,0} = 6(D - \sqrt{D^2 - D'^2})$	$\psi_{2,-2,m} = \frac{1}{\sqrt{2}}[\phi_{2,2,m} - \phi_{2,-2,m}]$
where $D = \frac{D_x + D_y + D_z}{3}$	$\psi_{2,-1,m} = \frac{1}{\sqrt{2}}[\phi_{2,1,m} - \phi_{2,-1,m}]$
$D' = \sqrt{\frac{D_xD_y + D_yD_z + D_xD_z}{3}}$	$\psi_{2,1,m} = \frac{1}{\sqrt{2}}[\phi_{2,1,m} - \phi_{2,-1,m}]$
	$\psi_{2,0,m} = \frac{1}{N}\left[w\phi_{2,0,m} - \frac{u}{\sqrt{2}}(\phi_{2,2,m} + \phi_{2,-2,m})\right]$
	where $N = 2\sqrt{\Delta w}$, $u = \sqrt{3}(D_x - D_y)$,
	$w = 2D_z - D_x - D_y + 2\Delta$, $\Delta = 3\sqrt{D^2 - D'^2}$

expressions for relaxation rates (see Section 1.2) is the Fourier transform of the correlation function $C(t)$ (Eqs. (1.13a), (1.13b)). The correlation functions for DD and CSA relaxation mechanisms (see Eqs. (1.19b) and (1.24e)) are given by:

$$C_{mm'}(t) = 4\pi\langle Y^*_{2m}(\Phi^{\mathrm{L}}(0))Y_{2m'}(\Phi^{\mathrm{L}}(t))\rangle, \tag{2.1}$$

where Φ^{L} denote the polar angles θ and φ that determine the orientation of the relaxation relevant vector in the laboratory co-ordinate frame. If the overall and internal molecular motions are independent it is convenient to consider them separately:

$$C_{mm'}(t) = 4\pi \sum_{n,n'=-2}^{2} \langle D^{2^*}_{mn}(\Theta(0))D^2_{m'n'}(\Theta(t))\rangle \times \langle Y^*_{2n}(\Phi^{\mathrm{M}}(0))Y_{2n'}(\Phi^{\mathrm{M}}(t))\rangle, \tag{2.2}$$

where Θ denote the Euler angles α, β and γ defining the orientation of the molecular co-ordinate frame with respect to the laboratory, Φ^{M} the polar angles defining the orientation of the relaxation relevant vector in the molecular frame, D^2_{mn} are Wigner functions of rank 2 (see Appendix A). Here the molecular

co-ordinate frame means the frame where the rotational diffusion tensor of the molecule (see below) has a diagonal form. The first averaging in Eq. (2.2) corresponds to the overall molecular diffusion and is given by:

$$\langle D^{2^*}_{mn}(\Theta(0))D^{2}_{m'n'}(\Theta(t))\rangle = \int \mathrm{d}\Theta_0 \int \mathrm{d}\Theta P(\Theta_0)G(\mathbf{r},\Theta,t|\mathbf{r}_0,\Theta_0,0) \times D^{2^*}_{mn}(\Theta_0)D^{2}_{m'n'}(\Theta)\,\mathrm{d}\mathbf{r}\,\mathrm{d}\mathbf{r}_0, \quad (2.3)$$

where $P(\Theta_0)$ denotes the probability density for initial orientation Θ_0 of the molecular frame at zero moment of time ($P(\Theta_0)$ is equal to $1/(8\pi^2)$ for the isotropic media), $G(\mathbf{r},\Theta,t|\mathbf{r}_0,\Theta_0,0)$ is the *Green function for rigid body diffusion*, defining the probability to find a rigid body at the point $\mathbf{r}$ with the orientation Θ at time t, if at zero time it was in the point $\mathbf{r}_0$ with the orientation Θ_0. The second averaging in Eq. (2.2) represents intramolecular motions.

2.1.2. Green function for rigid body diffusion

For the consideration of DD and CSA relaxation in macromolecules the translational diffusion is not important and only Brownian rotation of the molecule should be taken into account. It is clear, however, that a body of irregular shape undergoes a coupled translational and rotational diffusion. For example, translation of a screw-shaped particle would lead to a rotation and vice versa. Therefore, we consider the more general case of coupled translational and rotational diffusion [110] instead of pure rotational diffusion of the molecule [109].

The Green function for the coupled translational and rotational diffusion of a rigid body obeys the following relationship [110]:

$$\frac{\partial}{\partial t}G(\mathbf{r},\Theta,t|\mathbf{r}_0,\Theta_0,0) = \hat{H}G(\mathbf{r},\Theta,t|\mathbf{r}_0,\Theta_0,0) \quad (2.4a)$$

with the initial condition

$$G(\mathbf{r},\Theta,0|\mathbf{r}_0,\Theta_0,0) = \delta(\mathbf{r}-\mathbf{r}_0)\delta(\Theta-\Theta_0), \quad (2.4b)$$

where

$$\hat{H} = -\hat{\mathbf{P}}\cdot\mathbf{D}_{\mathrm{t}}\cdot\hat{\mathbf{P}} - \hat{\mathbf{P}}\cdot\mathbf{D}_{\mathrm{tr}}\cdot\hat{\mathbf{L}} - \hat{\mathbf{L}}\cdot\mathbf{D}_{\mathrm{rt}}\cdot\hat{\mathbf{P}} - \hat{\mathbf{L}}\cdot\mathbf{D}_{\mathrm{r}}\cdot\hat{\mathbf{L}}, \quad (2.4c)$$

$\hat{\mathbf{P}}$ and $\hat{\mathbf{L}}$ are molecular momentum and angular momentum operators, respectively; $\mathbf{D}_{\mathrm{t}}$, $\mathbf{D}_{\mathrm{r}}$ and $\mathbf{D}_{\mathrm{rt}} = \mathbf{D}_{\mathrm{tr}}^{\mathrm{T}}$ are 3×3 diffusion tensors accounting for molecular translation, rotation and coupling between translation and rotation, respectively. Tensors $\mathbf{D}_{\mathrm{t}}$, $\mathbf{D}_{\mathrm{tr}}$, $\mathbf{D}_{\mathrm{rt}}$ and $\mathbf{D}_{\mathrm{r}}$ comprise the generalised 6×6 diffusion tensor describing the diffusion of rigid body [113]. Goldstein [110] showed that a Green function (Eq. (2.4a)) that rigorously accounts for the rigid body translation, rotation and coupling between them is given by:

$$G(\mathbf{r},\Theta,t|\mathbf{r}_0,\Theta_0,0) = \sum_{L,n,L',n',m}\int \frac{\mathrm{d}p_z}{2\pi}\,\mathrm{e}^{\mathrm{i}p_z(r_z-r_{z0})}\psi_{Lnm}(\Theta)\psi^*_{L'n'm}(\Theta_0) \times \exp[-(p_z^2D_0 + E_{Ln} + p_z^2\hat{V}^{(2)}_{Ln})t] \times \langle 0|\hat{T}s_{Lnm}\exp\left[\int_0^t \hat{H}^I(t')\,\mathrm{d}t'\right]s^+_{L'n'm}|0\rangle, \quad (2.5)$$

where p_z is the z-projection of the molecular momentum in the laboratory co-ordinate frame; $\mathbf{r}$ is the origin of the molecular co-ordinate frame; the $\psi_{Lnm}(\Theta)$ constitute a complete orthonormal set of eigenfunctions of the anisotropic rotator with the eigenvalues E_{Ln} (see Table 3); $D_0 = \mathrm{Tr}(\mathbf{D}_{\mathrm{t}})/3$; $V^{(2)}_{Ln} = \langle\psi_{Lnm}|\hat{V}^{(2)}|\psi_{Lnm}\rangle$ is the matrix element of $\hat{V}^{(2)}$ operator in Goldstein's notation [110, Eq. (25)]; $\hat{T}$ is the operator of chronological order; $\hat{H}^I$ is the off-diagonal part of the Green function evolution operator (Eq. (2.4c)) in the interaction representation and representation of the secondary quantisation [110, Eq. (31)]; the raising and destroying operators s^+ and s obey the following rules: $s_{Lnm}|\psi_{Lnm}(\Theta)\rangle = |0\rangle$ and $s^+_{Lnm}|0\rangle = |\psi_{Lnm}(\Theta)\rangle$. The matrix element $\langle 0|\cdots|0\rangle$ on the right-hand side of Eq. (2.5) is responsible for the coupling between the translation and rotation.

Calculation of the correlation function (Eq. (2.2)) requires an estimation of the integral on the right-hand side of Eq. (2.3). From Eqs. (2.3) and (2.5), after integration over the co-ordinates $\mathbf{r}$ and $\mathbf{r}_0$, one can get (see Ref. [114]):

$$\langle D^{2^*}_{ql}(\Theta(0))D^{2}_{q'l'}(\Theta(t))\rangle = \frac{1}{8\pi^2}\int D^{2^*}_{ql}(\Theta)D^{2}_{q'l'}(\Theta_0)\,\mathrm{d}\Theta\,\mathrm{d}\Theta_0 \sum_{L,n,L',n',m}\int \mathrm{d}p_z\delta(p_z) \times \psi_{Lnm}(\Theta)\psi^*_{L'n'm}(\Theta_0)\exp[-(p_z^2D_0+E_{Ln}+p_z^2\hat{V}^{(2)}_{Ln})t] \times \langle 0|\hat{T}s_{Lnm}\exp\left[\int_0^t \hat{H}^I(t')\,\mathrm{d}t'\right]s^+_{L'n'm}|0\rangle. \quad (2.6)$$

The right-hand side of Eq. (2.6) contains the factor $\delta(p_z)$. However, if $p_z = 0$, $\hat{H}^I$ is also zero [110, Eq. (31)]. Thus, the matrix element $\langle 0|\cdots|0\rangle$ responsible for the coupling between translation and rotation in Eq. (2.6) reduces to $\delta_{LL'}\delta_{nn'}$. Finally, the integration over p_z in Eq. (2.6) results in:

$$\langle D^{2^*}_{ql}(\Theta(0))D^{2}_{q'l'}(\Theta(t))\rangle = \frac{1}{8\pi^2}\int G_R(\Theta,t|\Theta_0,0)D^{2^*}_{ql}(\Theta_0)D^{2}_{q'l'}(\Theta)\,\mathrm{d}\Theta_0\,\mathrm{d}\Theta, \tag{2.7}$$

where $G_R(\Theta,t|\Theta_0,0)$ is the Green function for the pure rotational diffusion without coupling with translation:

$$G(\Theta,t|\Theta_0,0) = \sum_{L,n,m}\psi_{Lnm}(\Theta)\psi^*_{Lnm}(\Theta_0)\,\mathrm{e}^{-E_{Ln}t} \tag{2.8}$$

The same form of the Green function for pure rotational diffusion was initially obtained by Favro [109]. Therefore, the coupling between molecular translation and rotation can be disregarded in the calculation of NMR correlation functions and does not affect NMR relaxation.

2.1.3. NMR correlation functions

Let us now derive the expressions for the correlation function (Eq. (2.2)) of a vector, attached to a particle of arbitrary shape, with rotational diffusion described by Favro's Green function (Eq. (2.8)). Special cases of asymmetric, axially symmetric and isotropic molecules are considered.

Asymmetric molecule. To derive the expression for the correlation function one needs to perform averaging on the right-hand side of Eq. (2.3). Using Favro's Green function (Eq. (2.8)), eigenfunctions and eigenvalues for an asymmetric rotator (Table 3) one can write Eq. (2.3) in the following form:

$$\begin{aligned}\langle D^{2^*}_{mn}(\Theta(0))D^{2}_{m'n'}(\Theta(t))\rangle &= \frac{1}{8\pi^2}\int \mathrm{d}\Theta_0\int \mathrm{d}\Theta D^{2^*}_{mn}(\Theta_0)D^{2}_{m'n'}(\Theta)\\ &\quad\times\sum_{L\eta\mu}\psi^*_{L\eta\mu}(\Theta_0)\psi_{L\eta\mu}(\Theta)\,\mathrm{e}^{-E_{L\eta}t}\\ &= \frac{1}{8\pi^2}\sum_{L}\frac{2L+1}{8\pi^2}\sum_{\mu\eta}\mathrm{e}^{-E_{L\eta}t}\\ &\quad\times\left[\sum_k a^*_{Lk\eta}\int D^{2^*}_{mn}(\Theta_0)D^{\mathrm{L}}_{\mu k}(\Theta_0)\,\mathrm{d}\Theta_0\right]\\ &\quad\times\left[\sum_k a_{Lk'\eta}\int D^{2}_{m'n'}(\Theta)D^{\mathrm{L}^*}_{\mu k'}(\Theta)\,\mathrm{d}\Theta\right]\\ &= \frac{1}{5}\sum_{\eta}a^*_{2n\eta}a_{2n'\eta}\,\mathrm{e}^{-E_{2\eta}t}.\end{aligned} \tag{2.9}$$

Here we used the orthogonality of the Wigner functions, i.e. the delta-functions $\delta_{L,2}$, $\delta_{mm'\mu}$, δ_{kn} and $\delta_{k'n'}$ arising upon integration allows us to avoid the summation over the indexes L, μ, k and k'. Substituting Eq. (2.9) into Eq. (2.2) one can write the expression for the correlation function in a form:

$$C_{mm'}(t) = \frac{4\pi}{5}\sum_{\eta}\mathrm{e}^{-E_{2\eta}t}\sum_{n,n'}a^*_{2n\eta}a_{2n'\eta} \times\langle Y^*_{2n}(\Phi^{\mathrm{M}}(0))Y_{2n'}(\Phi^{\mathrm{M}}(t))\rangle, \tag{2.10a}$$

or, under the condition that a vector is *rigidly* attached to an asymmetric molecule and its orientation in the molecular frame is given by the polar angles Φ^{M}:

$$C_{mm'}(t) = \sum_{\eta=-2}^{2}c_\eta\,\mathrm{e}^{-t/\tau_\eta}, \tag{2.10b}$$

where

$$c_\eta = \frac{4\pi}{5}\sum_{n,n'}a^*_{2n\eta}a_{2n'\eta}Y^*_{2n}(\Phi^{\mathrm{M}})Y_{2n'}(\Phi^{\mathrm{M}})$$

$$\text{and}\quad \tau_\eta = \frac{1}{E_{2\eta}}. \tag{2.10c}$$

The expressions for $E_{2\eta}$, corresponding to the inverse of the correlation times τ_η, are listed in Table 3. The coefficients in c_η in the correlation function (Eqs. (2.10b) and (2.10c)) are calculated using the expansion coefficients $a_{2n\eta}$ for the eigenfunctions of the asymmetric rotator (see Table 3):

$$c_2 = \frac{u^2}{4N^2}(3\cos^2\theta-1)^2 + \frac{3w^2}{4N^2}\sin^4\theta\cos^2 2\varphi + \frac{\sqrt{3}u}{8\Delta}(3\cos^2\theta-1)\sin^2\theta\cos 2\varphi = d - e \tag{2.10d}$$

$$c_{-2} = \tfrac{3}{4}\sin^4\theta\sin^2 2\varphi = 3l^2m^2$$

$$c_{-1} = \tfrac{3}{4}\sin^2 2\theta\cos^2\varphi = 3l^2n^2$$

$$c_1 = \tfrac{3}{4}\sin^2 2\theta\sin^2\varphi = 3m^2n^2$$

$$c_0 = \frac{w^2}{4N^2}(3\cos^2\theta - 1)^2 + \frac{3u^2}{4N^2}\sin^4\theta\cos^2 2\varphi - \frac{\sqrt{3}u}{8\Delta}(3\cos^2\theta - 1)\sin^2\theta\cos 2\varphi = d + e,$$

where

$$d = \frac{3(l^4 + m^4 + n^4) - 1}{4}$$

$$e = \frac{\epsilon_x(3l^4 + 6m^2n^2 - 1) + \epsilon_y(3m^4 + 6l^2n^2 - 1) + \epsilon_z(3n^4 + 6l^2m^2 - 1)}{12}$$

$$\epsilon_i = \frac{D_i - D}{\sqrt{D^2 - D'^2}} \quad (i = x, y, z).$$

The coefficients u, w and N are listed in Table 3; the coefficients c_η in the correlation function (Eqs. (2.10b) and (2.10c)) are written: (i) in terms of the polar angles θ, φ determining the vector direction in the molecular co-ordinate frame, where the rotational diffusion tensor has diagonal form; and (ii) in terms of directional cosines l, m and n for the vector with respect to the x-, y- and z-axes of the molecular frame. From Eqs. (2.10b)–(2.10d) it is seen that the correlation function $C_{mm'}(t) = C(t)$ for a vector in a rigid asymmetric molecule has a five-exponential form. The correlation times in the exponents depend on the components of the rotational diffusion tensor. The weights of the exponential terms depend on the components of the rotational diffusion tensor and on the direction of the relaxation-relevant vector in the molecular co-ordinate frame. The same result was obtained by Woessner [107] without implementation of the Green function formalism.

Axially symmetric molecule. The correlation function for a vector *rigidly* attached to an axially symmetric molecule is calculated analogously to that for the asymmetric molecule, i.e. using eigenvalues and eigenfunctions of the symmetric rotator (Table 3). Assuming that $D_{x,y} = D_\perp$ and $D_z = D_\parallel$ one can write the correlation function in a form:

$$C(t) = A\,\mathrm{e}^{-t/\tau_A} + B\,\mathrm{e}^{-t/\tau_B} + C\,\mathrm{e}^{-t/\tau_C}, \tag{2.11a}$$

where

$$A = \tfrac{1}{4}(3\cos^2\theta - 1)^2 = c_0$$
$$B = \tfrac{3}{4}\sin^2 2\theta = c_1 + c_{-1} \tag{2.11b}$$
$$C = \tfrac{3}{4}\sin^4\theta = c_2 + c_{-2}$$

$$(\tau_A)^{-1} = 6D_\perp = E_{2,0} \quad (\tau_B)^{-1} = 5D_\perp + D_\parallel = E_{2,\pm1}$$
$$(\tau_C)^{-1} = 2D_\perp + 4D_\parallel = E_{2,\pm2}, \tag{2.11c}$$

the values of $E_{2\eta}$ are listed in Table 3, the coefficients c_η are given by Eq. (2.10d). From Eqs. (2.11a)–(2.11c) it is seen that the correlation function for the vector in the axially symmetric rigid molecule reduces to a three-exponential form. The weights of exponential terms in the correlation function (Eq. (2.11a)) depend only on the direction of the vector with respect to the symmetry axis of the rotational diffusion tensor.

Spherical molecule. For a vector rigidly attached to a rigid isotropic molecule ($D_x = D_y = D_z = D$) the correlation function reduces to the mono-exponential form:

$$C(t) = \mathrm{e}^{-t/\tau_R}, \tag{2.12}$$

where $\tau_R = 1/(6D)$ (see Table 3). In the case of an isotropic molecule with intramolecular motions the correlation function (Eqs. (2.2) and (2.10a)) can be written as:

$$C(t) = \mathrm{e}^{-6Dt}\left(\frac{4\pi}{5}\sum_{n=-2}^{2}\langle Y_{2n}^*(\Phi^M(0))Y_{2n}(\Phi^M(t))\rangle\right) = \underbrace{\mathrm{e}^{-6Dt}}_{C_O(t)}\,\underbrace{\langle P_2(\boldsymbol{\mu}^M(0)\boldsymbol{\mu}^M(t))\rangle}_{C_I(t)} = C_O(t)C_I(t), \tag{2.13}$$

where $P_2(x) = (3x^2 - 1)/2$ is the Legendre

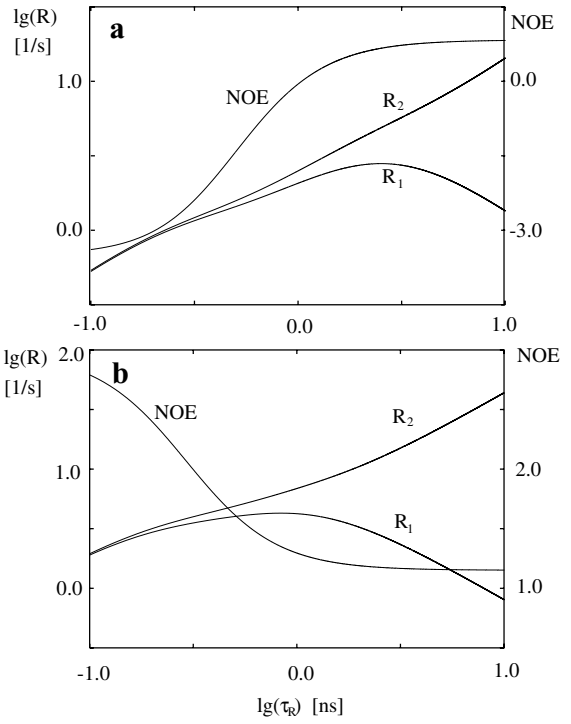

Fig. 5. R_1, R_2, and heteronuclear NOEs for (a) amide ^{15}N and (b) $^{13}C^{\alpha}$ nuclei versus the overall rotation correlation time of rigid isotropic molecule — τ_R, calculated using Eqs. (1.28a)–(1.28c), (1.29b), (1.30a)–(1.30c) and (2.12).

polynomial of rank 2 (here we used the addition theorem for spherical harmonics, see Appendix A), $\boldsymbol{\mu}^M$ is the unit vector pointed along the relaxation-relevant direction, i.e. along the **IS** vector for DD relaxation or along the symmetry axis of the shielding anisotropy tensor for CSA relaxation. From the Eq. (2.13) it is seen that for an isotropic molecule the correlation function can be represented as a product of the correlation functions of overall $C_O(t)$ and internal $C_I(t)$ motions. The only condition required for such a separation is independence of the internal and overall motions. As is clear from Eq. (2.10a), for the axially symmetric and asymmetric molecule the separation $C(t) = C_O(t)C_I(t)$ is *not rigorous*, but is often used as an approximation. In this case the correlation functions given by Eq. (2.10b)–(2.10d) and Eqs. (2.11a)–(2.11c) are used as $C_O(t)$ and polar angles θ, φ or direction cosines l, m, n in Eqs. (2.10d) and (2.11b) refer to the averaged orientation of the relaxation-relevant vector.

The spectral density functions required for calculation of the relaxation rates in a rigid asymmetric, axially symmetric or isotropic molecule are given by cosine Fourier transforms of the correlation functions Eqs. (2.10b), (2.11a) and (2.12), respectively. As an example, the longitudinal and transverse relaxation rates and heteronuclear NOEs for ^{15}N and $^{13}C^{\alpha}$ nuclei of $^{15}N-^{1}H$ and $^{13}C^{\alpha}-^{1}H$ pairs, calculated using the isotropic spectral density, are shown in Fig. 5.

2.2. Calculations of the diffusion tensors

The correlation function of a vector rigidly attached to an anisotropic molecule (Eqs. (2.10b), (2.11c)) depends on, $\mathbf{D}_r$, the rotational diffusion tensor of the molecule. In principle, $\mathbf{D}_r$ for an anisotropic molecule can be obtained directly from relaxation data for a set of $^{15}N-^{1}H$ vectors (see below). However, the analysis of the relaxation data is significantly facilitated if $\mathbf{D}_r$ is known from another experimental or computational method. Several computational approaches such as finite elements methods (see, e.g. [115]) or methods based on beads modelling [116–118] have been applied to predict hydrodynamic properties of proteins with known spatial structure. Here we briefly reviewed the beads model approximation for calculation of molecular diffusion tensors [116–118].

2.2.1. Properties of the diffusion tensors

The properties of the friction and diffusion tensors, characterising coupled translational and rotational Brownian motions of a rigid molecule of an arbitrary shape, were formulated by Brenner [113,119]. The hydrodynamic behaviour of the molecule is described by the generalised friction tensor $\mathbf{R}_P$ (6×6) comprising rotational $\Xi_{P,r}$ (3×3), translational Ξ_t (3×3) and coupling $\Xi_{P,c}$ (3×3) parts. The index P in the rotational $\Xi_{P,r}$ and the coupling $\Xi_{P,c}$ friction tensors means that these tensors depend on the origin P of the molecular co-ordinate frame. In contrast, the translational friction tensor Ξ_t does not depend on the origin of the molecular frame. The friction tensor $\mathbf{R}_P$ connects the frictional force $\mathbf{F}$ and torque $\mathbf{M}_P$ with the fluid velocity $\mathbf{U}_P$ at the point P and the angular

velocity $\boldsymbol{\omega}$ of the molecule:

$$\begin{bmatrix} \mathbf{F} \\ \mathbf{M}_P \end{bmatrix} = \underbrace{\begin{bmatrix} \Xi_{\mathrm{t}} & \Xi_{P,\mathrm{c}}^{\mathrm{T}} \\ \Xi_{P,\mathrm{c}} & \Xi_{P,\mathrm{r}} \end{bmatrix}}_{\mathbf{R}_P} \begin{bmatrix} \mathbf{U}_P \\ \boldsymbol{\omega} \end{bmatrix}. \tag{2.14}$$

The friction tensor $\mathbf{R}_P$ is connected with the generalised diffusion tensor $\mathbf{D}_P$ through the generalised Stokes–Einstein relationship:

$$\underbrace{\begin{bmatrix} \mathbf{D}_{P,\mathrm{t}} & \mathbf{D}_{P,\mathrm{c}}^{\mathrm{T}} \\ \mathbf{D}_{P,\mathrm{c}} & \mathbf{D}_{\mathrm{r}} \end{bmatrix}}_{\mathbf{D}_P} = k_{\mathrm{B}}T \underbrace{\begin{bmatrix} \Xi_{\mathrm{t}} & \Xi_{P,\mathrm{c}}^{\mathrm{T}} \\ \Xi_{P,\mathrm{c}} & \Xi_{P,\mathrm{r}} \end{bmatrix}^{-1}}_{\mathbf{R}_P}, \tag{2.15}$$

where k_{B} is the Boltzmann constant, T is the temperature, $\mathbf{D}_{P,\mathrm{t}}$, $\mathbf{D}_{\mathrm{r}}$ and $\mathbf{D}_{P,\mathrm{c}}$ are translational, rotational and coupling diffusion tensors, respectively. Brenner has shown, that unlike the friction tensors, the rotational diffusion tensor $\mathbf{D}_{\mathrm{r}}$ does not depend on the origin, but translational $\mathbf{D}_{P,\mathrm{t}}$ and coupling $\mathbf{D}_{P,\mathrm{c}}$ diffusion tensors do.

The most important properties of the friction and diffusion tensors are summarised below:

$$\Xi_{P,\mathrm{c}} = \Xi_{O,\mathrm{c}} - \mathbf{r}_{OP} \bullet \Xi_{\mathrm{t}} \tag{2.16a}$$

$$\Xi_{P,\mathrm{r}} = \Xi_{O,\mathbf{r}} - \mathbf{r}_{OP} \bullet \Xi_{\mathrm{t}} \bullet \mathbf{r}_{OP} + \Xi_{O,\mathrm{c}} \bullet \mathbf{r}_{OP} - \mathbf{r}_{OP} \bullet \Xi_{O,\mathrm{c}}^{\mathrm{T}}$$

$$\mathbf{D}_{P,\mathrm{c}} = \mathbf{D}_{O,\mathrm{c}} + \mathbf{D}_{\mathrm{r}} \bullet \mathbf{r}_{OP} \tag{2.16b}$$

$$\mathbf{D}_{P,t} = \mathbf{D}_{O,t} - \mathbf{r}_{OP} \bullet \mathbf{D}_{\mathrm{r}} \bullet \mathbf{r}_{OP} + \mathbf{D}_{O,\mathrm{c}}^{\mathrm{T}} \bullet \mathbf{r}_{OP} - \mathbf{r}_{OP} \bullet D_{O,\mathrm{c}},$$

where O and P denote the origins of two arbitrary molecular frames, $\mathbf{r}_{OP}$ is the vector that goes from O to P, $\bullet$ means the dyadic product. The dyadic products of 3×3 tensor $\mathbf{R}$ and vector $\mathbf{v}$ of dimension 3 — $\mathbf{v} \bullet \mathbf{R}$ and $\mathbf{R} \bullet \mathbf{v}$ are defined as:

$$(\mathbf{v} \bullet \mathbf{R})^{k,l} = R^{k-1,l} v^{k+1} - R^{k+1,l} v^{k-1} \tag{2.16c}$$

$$(\mathbf{R} \bullet \mathbf{v})^{k,l} = R^{k,l+1} v^{l-1} - R^{k,l-1} v^{l+1},$$

where and k and l are cyclic indexes running from 1 to 3 (e.g. $k - 1 = 3$ if $k = 1$, $k + 1 = 1$ if $k = 3$).

The rotational and translational friction tensors $\Xi_{P,\mathrm{r}}$ and Ξ_{t} are symmetric in any co-ordinate frame. The coupling tensor $\Xi_{P,\mathrm{c}}$ is symmetric only in a unique co-ordinate frame. The origin of this co-ordinate frame is called the centre of resistance:

$$\Xi_{R,\mathrm{c}} = \Xi_{R,\mathrm{c}}^{\mathrm{T}}. \tag{2.17a}$$

The position of the centre of resistance in an arbitrary co-ordinate frame, with the origin O is given by:

$$\mathbf{r}_{OR} = \begin{pmatrix} x_{OR}^1 \\ x_{OR}^2 \\ x_{OR}^3 \end{pmatrix} = \begin{pmatrix} \Xi_{\mathrm{t}}^{22} + \Xi_{\mathrm{t}}^{33} & -\Xi_{\mathrm{t}}^{12} & -\Xi_{\mathrm{t}}^{13} \\ -\Xi_{\mathrm{t}}^{12} & \Xi_{\mathrm{t}}^{11} + \Xi_{\mathrm{t}}^{33} & -\Xi_{\mathrm{t}}^{23} \\ -\Xi_{\mathrm{t}}^{13} & -\Xi_{\mathrm{t}}^{23} & \Xi_{\mathrm{t}}^{22} + \Xi_{\mathrm{t}}^{11} \end{pmatrix}^{-1} \times \begin{pmatrix} \Xi_{O,\mathrm{c}}^{32} & -\Xi_{O,\mathrm{c}}^{23} \\ \Xi_{O,\mathrm{c}}^{13} & -\Xi_{O,\mathrm{c}}^{31} \\ \Xi_{O,\mathrm{c}}^{21} & -\Xi_{O,\mathrm{c}}^{12} \end{pmatrix}. \tag{2.17b}$$

By analogy with the friction tensors $\mathbf{D}_{P,\mathrm{t}}$ and $\mathbf{D}_{\mathrm{r}}$ are always symmetric, but $\mathbf{D}_{P,\mathrm{c}}$ becomes symmetric only in the unique co-ordinate frame with the origin referred to as the centre of diffusion:

$$\mathbf{D}_{R,\mathrm{c}} = \mathbf{D}_{R,\mathrm{c}}^{\mathrm{T}}. \tag{2.17c}$$

The position of the centre of diffusion with respect to an arbitrary origin O can be obtained from an equation similar to Eq. (2.17b) in which Ξ_{t} and $\Xi_{O,\mathrm{c}}$ are replaced by $\mathbf{D}_{O,\mathrm{t}}$ and $\mathbf{D}_{O,\mathrm{c}}$, respectively. In general, the centre of resistance and the centre of diffusion do not coincide (see, e.g. Ref. [120]).

2.2.2. Calculation of diffusion tensors using the beads model approximation

Here we consider the beads model approximation for calculation of the protein friction and diffusion tensors [116–118]. In this method the rigid molecule is modelled as a set of N spherical sources of scalar friction otherwise called beads, characterised by the friction constants $\zeta_i (i = 1 \ldots N)$. The motion of the system of beads is described by a system of linear equations:

$$\mathbf{F}_i + \zeta_i \sum_{j=1,\, j \neq i}^{N} \mathbf{T}_{ij} \cdot \mathbf{F}_i = \zeta_i \mathbf{v}_i, \tag{2.18}$$

where $\mathbf{F}_i$ is the vector of force, acting on the ith bead, $\mathbf{v}_i$ is the velocity of the ith bead with respect to the solvent. The second term in the left-hand side of Eq. (2.18) refers to hydrodynamic interactions between the beads, which are characterised by the Oseen tensor $\mathbf{T}$ of dimensionality $3N \times 3N$, composed of 3×3 blocks $\mathbf{T}_{ij}$. Owing to the hydrodynamic interactions, the internal velocity field, created at the position of a friction element by the motion of other elements, has to be added to the external velocity field. The hydrodynamic interaction (Oseen) tensor was originally written as [119]:

$$\mathbf{T}_{ij} = \frac{1}{8\pi\eta R_{ij}}\left(\mathbf{I} + \frac{\mathbf{R}_{ij}\cdot\mathbf{R}_{ij}}{R_{ij}^2}\right), \tag{2.19a}$$

where η is the solvent viscosity, $\mathbf{R}_{ij}$ is distance vector between ith and jth beads, '$\cdot$' denotes the direct product of 3×1 to 1×3 matrices, $\mathbf{I}$ is the diagonal unit 3×3 matrix. Eq. (2.19a) implicitly assumes that the bead radii are much smaller than the distance between them. The Oseen tensor (Eq. (2.19a)) was modified for the case of equal [121,122] and different [116] beads of non-vanishing radii:

$$\mathbf{T}_{ij} = \frac{1}{8\pi\eta R_{ij}}\left(\mathbf{I} + \frac{\mathbf{R}_{ij}\cdot\mathbf{R}_{ij}}{R_{ij}^2} + \frac{\sigma_i^2 + \sigma_j^2}{R_{ij}^2}\left(\tfrac{1}{3}\mathbf{I} - \frac{\mathbf{R}_{ij}\cdot\mathbf{R}_{ij}}{R_{ij}^2}\right)\right), \tag{2.19b}$$

where $\sigma_i + \sigma_j$ are radii of ith and jth beads respectively. It is notable that Eq. (2.19b) is only valid in the case of $\sigma_i + \sigma_j < R_{ij}$. For overlapped beads of *equal* radii σ, corresponding off-diagonal elements of the Oseen tensor should be replaced by [121]:

$$\mathbf{T}_{ij} = \frac{1}{6\pi\eta\sigma}\left(\left(1 - \frac{9R_{ij}}{32\sigma}\right)\mathbf{I} + \frac{3\mathbf{R}_{ij}\cdot\mathbf{R}_{ij}}{32\sigma R_{ij}}\right). \tag{2.19c}$$

In Eqs. (2.19a)–(2.19c) all vectoral and tensoral quantities are written for an arbitrary co-ordinate frame, centred at point P.

Eq. (2.18) can be solved for the forces:

$$\mathbf{F}_i = \sum_{j=1}^{N} (\zeta_i\zeta_j)^{1/2}\mathbf{S}_{ij}\cdot\mathbf{v}_j, \tag{2.20a}$$

where

$$\mathbf{S} = (\mathbf{Q}^{\mathrm{s}})^{-1} \tag{2.20b}$$

$$\mathbf{Q}^{\mathrm{s}}_{ij} = \zeta_i^{-1/2}\mathbf{Q}_{ij}\zeta_j^{1/2}, \quad \mathbf{Q}_{ij} = \delta_{ij}\mathbf{I} + (1 - \delta_{ij})\zeta_i\mathbf{T}_{ij},$$

here $\mathbf{I}$ is the unit tensor and δ_{ij} is the Kronecker's delta. Since $\mathbf{Q}$ is not symmetric when the beads have different friction constants it is numerically convenient to form the symmetric matrix $\mathbf{Q}^{\mathrm{s}}$ [123]. The torques $\mathbf{M}_i$ with respect to the origin P of the co-ordinate frame, in which $\boldsymbol{\Xi}_{P,\mathrm{c}}$ and $\boldsymbol{\Xi}_{P,\mathrm{r}}$ have been calculated, are given by:

$$\mathbf{M}_i = \mathbf{R}_i \times \mathbf{F}_i = \sum_{j=1}^{N} (\zeta_i\zeta_j)^{1/2}\mathbf{R}_i \times (\mathbf{S}_{ij}\cdot\mathbf{v}_j), \tag{2.20c}$$

where $\mathbf{R}_i$ is the position vector of the ith friction point with respect to P, $\times$ means the vector product.

Using Eqs. (2.14) and (2.20a)–(2.20c) one can derive the expressions for translational, rotational and coupling friction tensors. Let us consider first the case of uniform translation of the particle. Assuming that for all beads $\mathbf{v}_i = \mathbf{v} = \mathbf{U}_P$ and $\boldsymbol{\omega} = 0$ one can write Eq. (2.14) in the form: $\mathbf{F} = \boldsymbol{\Xi}_i\cdot\mathbf{v}$ and $\mathbf{M}_P = \boldsymbol{\Xi}_{P,\mathrm{c}}\cdot\mathbf{v}$. The translational $\boldsymbol{\Xi}_{\mathrm{t}}$ and coupling $\boldsymbol{\Xi}_{P,\mathrm{c}}$ friction tensors are then obtained by summing over the index i in Eqs. (2.20a) and (2.20c), respectively:

$$\boldsymbol{\Xi}_{\mathrm{t}} = \sum_{i=1}^{N}\sum_{j=1}^{N} (\zeta_i\zeta_j)^{1/2}\mathbf{S}_{ij} \tag{2.21a}$$

$$\boldsymbol{\Xi}_{P,\mathrm{c}} = \sum_{i=1}^{N}\sum_{j=1}^{N} (\zeta_i\zeta_j)^{1/2}\mathbf{R}_i \times \mathbf{S}_{ij}. \tag{2.21b}$$

To derive an expression for the rotational friction tensor $\boldsymbol{\Xi}_{P,\mathrm{r}}$ it is convenient to consider pure rotational motion about the origin P with angular velocity ω i.e. for all beads $\mathbf{v}_i = \boldsymbol{\omega} \times \mathbf{R}_i$. It can be shown that in this case Eq. (2.14) reduces to $\mathbf{F} = \boldsymbol{\Xi}^{\mathrm{T}}_{P,\mathrm{c}}\cdot\boldsymbol{\omega}$ and $\mathbf{M}_P = \boldsymbol{\Xi}_{P,\mathrm{r}}\cdot\boldsymbol{\omega}$. By summing over i in Eq. (2.20c) one can get:

$$\boldsymbol{\Xi}_{P,\mathrm{r}} = -\sum_{i=1}^{N}\sum_{j=1}^{N} (\zeta_i\zeta_j)^{1/2}\mathbf{R}_i \times \mathbf{S}_{ij} \times \mathbf{R}_j \tag{2.21c}$$

The diffusion tensors are calculated from corresponding friction tensors using the generalised Stokes–Einstein relationship (Eq. (2.15)). To obtain reliable values of the translational diffusion rates all calculations have to be carried out in the centre of resistance (Eq. (2.17a) and (2.17b)) co-ordinate frame [120].

2.2.3. Representation of the molecule as an array of beads. Boundary conditions

For calculations of molecular diffusion tensors using the beads model approximation one needs: (i) to represent the molecule as an array of spherical friction elements; and (ii) to assign them friction constants. Several methods can be considered for representation of the molecule by a set of beads (reviewed in Ref. [124]). In relatively large molecules the beads might correspond to the molecular domains or sub-domains. The beads, corresponding to the residues or atoms of the molecule, may be selected for a more detailed description of the molecular shape. Within a filling model the volume enclosed by the molecular surface is filled by beads located, e.g. in the cells of a cubic grid superimposed onto the protein. Since hydrodynamic friction takes place at the surface of the molecule, it was also proposed to arrange the small beads in a shell that describes as closely as possible the molecular surface.

The friction constants for beads are assigned using Stokes law. For the beads corresponding to large regions of the protein such as domains, sub-domains or possibly residues, the Stokes law with *stick* boundary conditions is used. Stick boundary conditions mean that the tangential velocity of the solvent is zero at the surface of the diffusing object. The translational friction coefficients for 'stick spheres' is given by:

$$\zeta = 6\pi\eta\sigma, \tag{2.22a}$$

where σ is the sphere radius and η is the solvent viscosity.

It was shown that to a good approximation the translational and rotational diffusion of small molecules obey *slip* boundary conditions (see Refs. [125,126] and references cited therein). 'Slip spheres' possess translational friction coefficients equal to:

$$\zeta = 4\pi\eta\sigma. \tag{2.22b}$$

The atoms of molecules are also expected to obey slip boundary conditions [125]. The friction constants for the beads corresponding to the atoms of the molecule may be assigned, e.g. using the accessible surface area (ASA) model [125,127].

2.3. Practical aspects of applying hydrodynamic calculations in NMR relaxation studies

The details and the current state of hydrodynamic calculations using the beads model have been recently reviewed [124]. Thus, instead of describing details of the calculations, we focus on major complications arising in practical applications of the beads model for studies of protein hydrodynamics. First, the beads model cannot account for concentration effects due to molecular crowding (i.e. self-obstruction) and aggregation [128,129]. Even at the limit of an infinite dilution, where the effects of protein–protein interaction can be neglected, the results of the calculations might be offset anyway due to ambiguity in the protein hydration shell [124] and to electrolyte friction effects [129–132]. It became evident a long ago that one could expect a significant improvement in the prediction of the molecular hydrodynamic properties if the calculations are complemented by measurements of some relevant parameters [124]. For the analysis of NMR relaxation data, one usually needs independent estimates of overall rotation correlation times and the anisotropy of the rotational diffusion. In this case supplementary measurements of translational self-diffusion coefficients can be performed [133–136]. These measurements could be helpful both for a characterisation of the protein aggregation and for the selection of proper parameters for hydrodynamic calculations.

2.3.1. Water shell in hydrodynamic calculations

Significant experimental and theoretical efforts have been aimed at understanding the solvation of macromolecules (for recent reviews see, e.g. [137–140]). Usually only a small number of specific water binding sites with water residence times longer than one nanosecond can be identified by X-ray and NMR protein structural studies. The residence times of water molecules at all other sites of the protein surface are below 0.1 ns. The properties of the solvent in the vicinity of the protein differ, however, from those of the bulk solvent. Calorimetric and specific volume measurements provide a hydration level of 0.2–0.5 g of water per gram of protein [141,142], which corresponds approximately to one mono-layer of solvent for globular proteins. Solvent distribution functions obtained from X-ray diffraction [143] also indicate a

well-defined first solvation shell. In hydrodynamic calculations using either beads or finite elements methods it was found that usually 20–70% of water mono-layer occupation is appropriate for reproduction of the experimental data on translational and rotational diffusion, sedimentation, intrinsic viscosity, and radius of gyration [124,127,144,145].

The parameters of the diffusion anisotropy for globular proteins obtained from hydrodynamic calculations are almost insensitive to the choice of the shell parameters, provided the protein has a nearly spherical shape. In our experience, any reasonable representation of the protein molecule by an array of spherical frictional elements, reproducing the molecular shape (e.g. 1.0 Å beads corresponding to all protein heavy atoms or 3.5 Å beads corresponding to C^{α} atoms [146]), allows one to predict the direction of principal axes and the ratios of eigenvalues of the rotational diffusion tensor with good accuracy.

The thickness of the solvation shell, however, has a dramatic effect on the absolute rates of translational and rotational diffusion. Owing to ambiguities in the solvation shell and in the friction constants of the beads one cannot, usually, predict the absolute values of diffusion coefficients with the precision required for the analysis of the relaxation data. As indicated in the next sections, even a single adjustable parameter of the molecular overall rotation can lead to an unaffordable ambiguity in the analysis of protein internal dynamics (see [106]). In this case it is desirable to have completely independent estimates of the rotational diffusion tensor. Unfortunately, the level of hydration varies significantly for different proteins, which is probably the main source of uncertainty in the prediction of protein hydrodynamics [124].

To alleviate the problem, several procedures based on similar ideas have been proposed, which use one or several experimentally measured values to adjust the level of hydration [124,127,144,145,147,148]. The essence of this approach can be illustrated by the example of a spherical particle. In this case the translational (D_t) and rotational (D_r) diffusion coefficients are given by Stokes formulas:

$$D_t = \frac{k_B T}{6\pi\eta\sigma} \qquad D_r = \frac{k_B T}{8\pi\eta\sigma^3}, \tag{2.23}$$

where k_B and T are the Boltzman constant and temperature, η and σ are the solvent viscosity and the radius of the particle. Provided that D_t is obtained experimentally, the hydrodynamic radius of the molecule, including unknown hydration shell, can be excluded from the expression for the rotational diffusion coefficient:

$$D_r = \frac{27\pi^2\eta^2 D_t^3}{k_B^2 T^2}. \tag{2.24}$$

Similar reasoning is applicable to more sophisticated models describing the hydrodynamics of particles of an arbitrary shape (see, e.g. [148]). Commonly, in the latter case the hydration level is described by a single parameter, which is adjusted to match experimental value(s). Recently de la Torre et al. [124] presented results of hydrodynamic calculations for 13 globular proteins. The authors found that using the beads method with hydration adjustment allows one to predict the rotational diffusion coefficients with an accuracy of 5–10%. In the same paper it was noted that the residual discrepancy might be due to the obvious fact that the experimental values used for the hydration shell adjustment and for the evaluation of the results of the calculations are themselves not free from artifacts. If one puts aside instrumental problems and assumptions inherent in a particular experimental method (see, e.g. [106]), this statement might address the effects of non-ideal solutions, which are not considered in the hydrodynamic theory described above.

2.3.2. Non-ideal solutions. Effect on the translational and rotational diffusion

A comprehensive theory of multi-component electrolytes containing interacting macromolecules, which should be applied to a quantitative description of protein diffusion, is not yet completely established, though one can see considerable advances in this field (see, e.g. Refs. [130,131,149]). However, as it concerns NMR relaxation for proteins, several important findings can be formulated.

At millimolar concentrations typical for protein NMR studies, the distances between adjacent protein molecules are of the order of the size of the molecule, which results in so-called crowding effects on the Brownian translational and rotational diffusion. For non-interacting hard spheres or for charged spheres at high ionic strength the theoretical calculations

yield a linear attenuation of the translational diffusion rate [150,151]:

$$D_t(\varphi) = D_t(0)(1 - a\varphi), \tag{2.25}$$

where φ is the volume fraction of the protein and $a = 2.0 - 3.0$ is a crowding coefficient. In a study of self-diffusion of globular proteins Le Bon et al. [152] observed a linear concentration dependence of D_t up to the protein volume fraction of 10% with $a \approx 5.5$ for all five proteins considered. A higher value of a, in comparison with those predicted for hard spheres, was partly attributed to protein hydration, which leads to a larger effective volume fraction. It is notable that these data were obtained at solutions with high ionic strength. Protein molecules with a significant net charge at low ionic strength interact through a balance of electrostatic repulsion and attractive dispersion forces. With increasing ionic strength, the macromolecular Coulombic interactions are essentially screened, and an overall attraction between species is expected. Thus, it was shown that lysozyme exhibits highest diffusion rates at a moderate concentration of salt. This corresponds to a compromise between strong self-obstruction effects due to the electrostatic repulsion at low ionic strength and the protein aggregation at NaCl concentration exceeding 0.5 M.

Electrolyte friction refers to additional friction on a charged colloidal particle due to its interaction with its counter shell of ions and water molecules (see, e.g. Ref. [130]). The effect of electrolyte friction can contribute up to 10% of the translational diffusion rates [130]. The effect of electrolyte friction increases with the increase of the net protein charge and at low ionic strength, where the Debye screening length is high. Since the electrolyte friction does not necessarily imply interaction between protein molecules, it does not vanish at infinite dilution. It has been shown that the self-diffusion coefficient D_t of lysozyme extrapolated to an infinite dilution at low salt is ca. 10% smaller than that measured at 0.15 M NaCl [129]. Fortunately, both the interaction among the protein molecules, i.e. those due to long-range molecular interactions and volume exclusion, and the electrolyte friction, are known to be negligible for the rotational diffusion of globular proteins (see, e.g. Ref. [131] and references therein), provided that the protein volume fraction does not exceed ca. 5% (see Ref. [153]).

As the attraction between the species increases, one faces protein aggregation, which results in a wide dispersion of species in solution with different molecular weights and, consequently, with different overall rotation correlation times. This is obvious and the most important hindrance for relaxation data analysis in terms of a particular dynamic model [105,154–156]. Certainly, the results of hydrodynamic calculations based on a single defined spatial structure would be completely irrelevant in this case.

Taking into account the above mentioned complications due to non-ideal protein solutions, several conclusions regarding the application of hydrodynamic calculations in NMR relaxation studies of proteins can be formulated: (i) The beads model provides quite accurate parameters of the rotational diffusion anisotropy, suitable for the analysis of relaxation data in anisotropic molecules. (ii) The beads model cannot provide accurate absolute values of overall rotation correlation times without reference to additional experimental data (e.g. the protein self-diffusion coefficient D_t). If D_t is used for estimating the rotational correlation times (Eq. (2.24)), one should use the values extrapolated to infinite dilution, which is commonly assumed in hydrodynamic calculations. Self-diffusion should be measured at moderate ionic strengths and, if possible, at the pH values corresponding to a small net charge of the protein in order to decrease the electrolyte friction effects. One should also check for protein aggregation, which can be done by measuring the relaxation rates and/or self-diffusion coefficient at several protein concentrations. Even with these precautions, the contributions from the non-ideal solution effects to the derived rotational correlation times can be significant.

3. Analysis of relaxation data in terms of molecular motions

NMR relaxation data contain information about overall rotational diffusion and internal motions in macromolecules. Extraction of this information is usually based on a particular form of the correlation function (Eq. (1.13a)) characteristic for molecular

dynamic processes. As has been shown in previous sections, overall Brownian diffusion of a rigid molecule obeys well established relationships and corresponding correlation functions (Eqs. (2.10b)–(2.12)) are parameterised by the eigenvectors and eigenvalues of the rotational diffusion tensor $\mathbf{D}_r$. The parameters of $\mathbf{D}_r$ can be inferred from the relaxation data analysis as well as from computations (see Sections 2.2 and 2.3).

Parameterisation of the correlation function of intramolecular motions is a much more elaborate procedure. Intramolecular dynamics of biological macromolecules, such as proteins, is very complex consisting of motions of different types, time-scales and amplitudes (see [157]). Two different approaches should be considered when constructing a correlation function for internal motions. First, a particular model can be assumed for a molecular motion and the correlation function for this type of motion is used. Alternatively, within the framework of 'model-free' approaches one can assume a particular type of correlation (or spectral density) function instead of a particular type of molecular motion.

The analyses of relaxation data using different models of molecular motions have been recently reviewed [158]. In this type of data analysis one a priori assumes a model of molecular motion and uses the correlation function for this model of motion. Examples of such motional models are wobbling in a cone [159] and multiple site jump models [12,160]. The particular form of a correlation function may be also derived from a computer modelling of protein motions using molecular dynamics simulations or normal mode analysis (see, e.g. Refs. [161,162]). The use of motional models suffers, however, from the possibility of over-interpretation of the relaxation data. Indeed, the limited amount of relaxation data and their information content often do not allow one to distinguish between different models.

Within the framework of model-free approaches one can construct a hierarchical set of correlation functions depending on different numbers of parameters (see Ref. [163] or Refs. [164–166]), which could eliminate the ambiguity in the selection of the model used for relaxation data analysis. Being extracted from the relaxation data, the parameters of the correlation function can be interpreted assuming different types of intramolecular motion. The drawback of model-free approaches is that the extracted parameters of the correlation (or spectral density) function are not, in general, unambiguously related to the spatial and temporal characteristics of the actual protein internal motions.

In flexible, partially unfolded or aggregated molecules it is convenient to analyse the relaxation data using the 'spectral density function mapping' approach [29,167]. This method requires minimal assumptions about the protein dynamics. The approach is based on the fact that the relaxation rates are linear combinations of the values of the spectral density function $J(\omega)$ at several characteristic frequencies. Consequently, the values of $J(\omega)$ at these frequencies can be extracted by solving the system of linear equations for relaxation rates. The extracted $J(\omega)$ values may be interpreted qualitatively or used for further analysis in terms of a particular model of molecular motions.

In this section we consider the methods for the analysis of backbone ^{15}N relaxation data in proteins used for the characterisation of protein overall tumbling, picosecond–nanosecond and microsecond–millisecond intramolecular motions. In Section 3.1 we review a general method for back-calculation of the model parameters and their uncertainties. Section 3.2 is devoted to the strategies and problems of model-free relaxation data analysis. In Section 3.3 we briefly review $J(\omega)$ mapping. In Section 3.4 we consider the methods for characterisation of microsecond–millisecond time-scale motions in proteins. The last Section 3.5 is devoted to interpretation of NMR relaxation data using molecular dynamics simulations and normal mode analysis.

3.1. Calculation of model parameters based on experimental data

3.1.1. Back-calculation of model parameters and estimation of their uncertainties

Typically, analysis of experimental data implies back-calculation of the parameters of a particular model from N experimental data values V_i^{exp} determined with uncertainties ΔV_i^{exp}. Here, *model* means the theoretical dependence $V_i^{th}(\zeta)$ of the data on the set of $k(k < N)$ model parameters ζ. An example of back-calculation of the model parameters is the approximation of peak intensities in ^{15}N R_1 or R_2

spectra recorded with different delays for relaxation (see Section 1.4) by two-parameter exponential functions, depending on relaxation rate and initial peak amplitude. Another example is the calculation of the order parameters and correlation times from the experimental relaxation rates in a model-free analysis.

If the uncertainties of the experimental data follow a normal distribution, maximum likelihood estimates of the model parameters can be obtained by minimisation of the following target function:

$$\Gamma(\zeta) = \sum_{i=1}^{N} \frac{(V_i^{\text{th}}(\zeta) - V_i^{\text{exp}})^2}{(\Delta V_i^{\text{exp}})^2}, \tag{3.1}$$

where ζ denotes the set of adjustable parameters (see [168]). Minimisation may be performed, e.g. using the Levenburg–Marquardt algorithm [168]. Additional restraints of the form:

$$\begin{cases} K \min^2(\zeta_i - a, \zeta_i - b) & \text{if} \quad \zeta_i \notin (a, b) \\ 0 & \text{if} \quad \zeta_i \in (a, b) \end{cases} \tag{3.2}$$

may be introduced in Eq. (3.1) to ensure that all parameters fall into allowed ranges (here (a,b) is the allowed range for the parameter ζ_i, and K is a penalty factor for violation of the allowed region). Often, one needs to calculate maximum likelihood estimates for other parameters $\phi(\zeta)$ with known relationship to ζ, which can be obtained directly from the optimised values of ζ.

Uncertainties in model parameters can be estimated using Monte Carlo simulation of the distributions of the optimised parameters [168]. For this purpose one generates multiple pseudo-experimental data sets, obeying normal distributions with means calculated from optimised model parameters and standard deviations equal to ΔV_i^{exp}. The uncertainties of the parameters are given by the standard deviations of the distributions of the optimised model parameters, resulting from fitting to the simulated data. In the case of small data errors with normal distribution, the uncertainties of the optimised parameters can also be obtained from the covariance matrix of the optimised model [168]. Using the optimised model parameters ζ and the covariance matrix one can estimate the uncertainty for other parameters $\phi(\zeta)$ with a known relationship to ζ:

$$\sigma^2(\phi) = \sum_{i=1}^{N} \sum_{j=1}^{N} \left[\frac{\partial}{\partial \zeta_i} \frac{\partial}{\partial \zeta_j} \phi(\zeta) \right] \text{cov}(\zeta_i, \zeta_j), \tag{3.3}$$

where $\text{cov}(\zeta_i, \zeta_j)$ are the elements of the covariance matrix.

In some cases (e.g. when the number of experimental data and model parameters is small), it is useful to apply simple graphical procedures to determine and visualise the permissible regions of the parameter space [169,170]. For this purposes one draws the confidence regions for the experimental data in parameter space. The overlap of the permissible regions for all experimental data will correspond to legitimate values of the model parameters. It is also helpful to generate various likelihood/confidence contour plots, which give direct information on the likelihood that a particular set of model parameters is consistent with the experimental data, using Bayesian statistics approaches (see Ref. [171]).

3.1.2. Goodness of fit. Model selection

During the data analysis the following questions often arise: (i) is the particular model appropriate for the analysis of the experimental data; and (ii) which of the alternative models would account better for the experimental data?

The goodness of fit of the experimental data to a particular model may be evaluated on the basis of $\Gamma(\zeta)$ (Eq. (3.1)) in its minimum [168]. In particular, one can simulate pseudo-experimental data with a normal distribution with the means calculated from the optimised model parameters and standard deviations of the original experimental data ΔV_i^{exp}. The distribution of the optimised $\Gamma(\zeta)$ values, resulting from the simulated pseudo-experimental data, is then used to estimate the probability of getting by chance the target function (Eq. (3.1)) higher than those obtained from least-square fitting of the original experimental data. This probability characterises the confidence for rejecting the model under consideration.

If the experimental data errors are small, normally distributed, and uncorrelated with each other, $\Gamma(\zeta)$ in its minimum should correspond to a χ^2 distribution with $\nu = N - k$ degrees of freedom, where N is the number of experimental values, k is the number of

adjustable model parameters. In principle, χ^2 statistics (see Ref. [172]) is not applicable to the non-linear regression analysis. However, for most of the problems considered here the critical values of $\Gamma(\zeta)$ distribution calculated using Monte Carlo simulations almost coincide with those predicted by χ^2 statistics, provided that the model parameters do not approach their extreme values.

Commonly, the model is considered inappropriate, if the probability of getting the target function higher than those obtained from least-square fitting of the experimental data is less than 5–10%, i.e. if the obtained target function is higher than a corresponding critical value. For a large number of degrees of freedom, i.e. greater than ca. 20–30, this critical value is almost equal to the number of degrees of freedom.

If a set of hierarchical nested models is considered (i.e. if the parameters of a simple model form a subset of the parameters of a more complex model), the use of F-statistics for the selection of an appropriated model is very helpful (see [172]). These statistics address the question of whether or not a reduction of the target function obtained for the model with the greater number of parameters is statistically significant. For the comparison of two alternative models one can generate a normally distributed pseudo-experimental data set with mean values calculated from optimised parameters of a simple model and analyse this set with the same model and with a more complex model. The resulting optimised values of $\Gamma(\zeta_1)$ and $\Gamma(\zeta_2)$ are used to generate the distribution of the value $F(\zeta_1,\zeta_2)$:

$$F(\zeta_1,\zeta_2) = \frac{\nu_2(\Gamma(\zeta_1) - \Gamma(\zeta_2))}{(\nu_1 - \nu_2)\Gamma(\zeta_2)}, \tag{3.4}$$

where ζ_1 and ζ_2 denote the parameter sets for a simple and a more complex model, respectively; ν_1 and ν_2 ($\nu_1 > \nu_2$) are the number of degrees of freedom of the models. The generated distribution of $F(\zeta_1,\zeta_2)$ is used to estimate the probability of obtaining by chance a given reduction of the minimised target function (Eq. (3.1)) upon the transition to a more complex model. This probability characterises the confidence for the introduction of the model with additional parameters compared to the simpler model. For most of the problems considered here the critical values of the $F(\zeta_1,\zeta_2)$ distributions, calculated using Monte Carlo simulations, almost coincide with those provided by F-statistics with ν_2 and $\nu_1 - \nu_2$ degrees of freedom.

Commonly, the selection between hierarchical nested models is based both on χ^2 and F-statistics criteria (see, e.g. Refs. [173,174]). In particular, a more complex model is accepted, e.g. if the simpler model is rejected based on the χ^2 criterion with 90% probability and the F-statistics criterion shows with at least 80% confidence that the observed reduction of the target function cannot be obtained by chance.

3.1.3. Bayesian statistics approach for estimation of parameters and their uncertainties

In the case of non-linear estimation problems with a high number of parameters and experimental data (say N, $k > 20$–30; $N > k$) it is often not possible to estimate the uncertainties of the optimised model parameters using conventional Monte Carlo simulations. Indeed, one would have to generate multiple data sets corresponding to all experimental data and perform non-linear optimisation for all data sets. One of the possibilities in this case is to obtain some estimates of the parameter uncertainties from the covariance matrix of the optimised model. Another possibility is to use a Bayesian statistics approach (see [175] and references cited therein), allowing Monte Carlo sampling to be performed in the parameter space instead of the data space. This strategy is computationally efficient since it allows one to avoid repeated multiple non-linear optimisation. The approach uses the fact that the joint probability density $P(\zeta|V^{\exp})$ of getting model parameters ζ at a given $V^{\exp}$ is proportional to the product of likelihood of the data $P(V^{\exp}|\zeta)$ and the prior probability of the parameters $P(\zeta)$ (Bayes theorem):

$$P(\zeta|V^{\exp}) \sim P(V^{\exp}|\zeta)P(\zeta), \tag{3.5}$$

where ζ and $V^{\exp}$ denote the parameter and data sets, respectively. The likelihood of observing the data set $V^{\exp}$ given the particular values of model parameters ζ is given by:

$$P(V^{\exp}|\zeta) = \prod_{i=1}^{N} \frac{1}{\sqrt{2\pi(\Delta V_i^{\exp})^2}} \exp\left[-\frac{(V_i^{\text{th}}(\zeta) - V_i^{\exp})^2}{2(\Delta V_i^{\exp})^2} \right]. \tag{3.6}$$

The prior probability of the parameters $P(\zeta)$ is assumed to be equal to 1 if the model parameters lie

in the allowed ranges and 0 otherwise. Based on Monte Carlo sampling of the parameter space and using Eqs. (3.5) and (3.6) one can estimate the joint probability density for any subset of the parameter set ζ, comprising $l(l < k)$ parameters $\zeta_1, ..., \zeta_l$:

$$P(\zeta_1 ... \zeta_l | V^{\exp}) = \int P(\zeta | V^{\exp})\, \mathrm{d}\zeta_{l+1} ... \mathrm{d}\zeta_k. \tag{3.7}$$

This probability density may then be used for the estimation of parameter uncertainties as well as for the generation of various likelihood/confidence maps.

The Bayesian statistics approach is especially helpful if the experimental data and the model parameters can be grouped in such a manner that the data in each group depend only on a corresponding group of parameters except for a small number of global parameters [175]. The example of such a problem is fitting of the relaxation data for multiple nuclei in a protein by simultaneous optimisation of the parameters of molecular overall rotation (common for all nuclei) and the parameters of intramolecular motions (assumed to be different for different nuclei). In this case the likelihood (Eq. (3.6)) is calculated for each group of data separately, using Monte Carlo simulations for the parameters of the corresponding group. The resulting likelihood for the complete data set is then obtained as a product of likelihoods for all data groups. This procedure saves a considerable amount of computational time.

It is worthwhile to note that the Bayesian statistics approach is also expected to be useful for the problem of selection between hierarchical nested models [175].

3.2. Model-free analysis of relaxation data

3.2.1. Original formulation of the model-free approach

The most popular method for the analysis of backbone ^{15}N relaxation data in proteins is the model-free approach proposed originally by Lipari and Szabo [164,165] and extended by Clore et al. [166]. The model-free approach implicitly uses the assumption that the overall and internal molecular motions are independent and that the correlation function $C(t)$ can be represented as a product of internal and overall parts (see Eq. (2.13)) even in the case of anisotropic molecular reorientation. An exact form of the correlation function of molecular overall rotation $C_O(t)$, corresponding to either isotropic (Eq. (2.12)) or anisotropic (Eqs. (2.10b)–(2.11c)) diffusion, is used. The approach does not contain any assumption concerning the physical nature (model) of the intramolecular motion. Instead, it postulates a particular form of the correlation function of the internal motions $C_I(t)$. The parameters of $C_I(t)$, extracted using least squares fitting of relaxation data (see Section 3.1), are assumed to be the quantities of model-independent significance, which may later be related with spatial and temporal measures of intramolecular motions within the frame of different physical models.

Lipari and Szabo [164,165] proposed to use a single-exponential approximation for $C_I(t)$:

$$C_I(t) = S^2 + (1 - S^2)\, \mathrm{e}^{-t/\tau_\mathrm{e}}, \tag{3.8a}$$

where S is the quantity known as the *generalised order parameter*, τ_e is the effective correlation time. The corresponding spectral density function $J(\omega)$ is given by the cosine Fourier transform of the correlation function $C(t) = C_O(t)C_I(t)$ (Eq. (1.13b)). In the case of isotropic overall rotation $J(\omega)$ is given by:

$$J(\omega) = \frac{S^2 \tau_R}{1 + (\omega\tau_R)^2} + \frac{(1 - S^2)\tau'_\mathrm{e}}{1 + (\omega\tau'_\mathrm{e})^2}, \tag{3.8b}$$

where $\tau_\mathrm{e}'^{-1} = \tau_R^{-1} + \tau_\mathrm{e}^{-1}$. In the more general case of anisotropic overall rotation $J(\omega)$ is given by:

$$J(\omega) = \sum_{\eta=-2}^{2} c_\eta \left[\frac{S^2 \tau_\eta}{1 + (\omega\tau_\eta)^2} + \frac{(1 - S^2)\tau_{\mathrm{e},\eta}}{1 + (\omega\tau_{\mathrm{e},\eta})^2} \right], \tag{3.8c}$$

where $\tau_{\mathrm{e},\eta}^{-1} = \tau_\eta^{-1} + \tau_\mathrm{e}^{-1}$, τ_η are given by Eq. (2.10c) (see also Table 3), c_η are given by Eq. (2.10d). For a wide range of intramolecular dynamic processes one can use Eq. (3.8a) as an approximation for the actual correlation function $C_I^m(t)$ if S^2 and τ_e are given by:

$$S^2 = C_I^m(\infty) = \int \mathrm{d}\Phi_1 \int \mathrm{d}\Phi_2 P(\Phi_1) P(\Phi_2) P_2(\boldsymbol{\mu}^\mathrm{M}(\Phi_1)\boldsymbol{\mu}^\mathrm{M}(\Phi_2)) \tag{3.9a}$$

$$\tau_\mathrm{e}(1 - S^2) = \int_0^\infty (C_I^m(t) - S^2)\, \mathrm{d}t, \tag{3.9b}$$

where Φ_1 and Φ_2 are the polar angles describing the

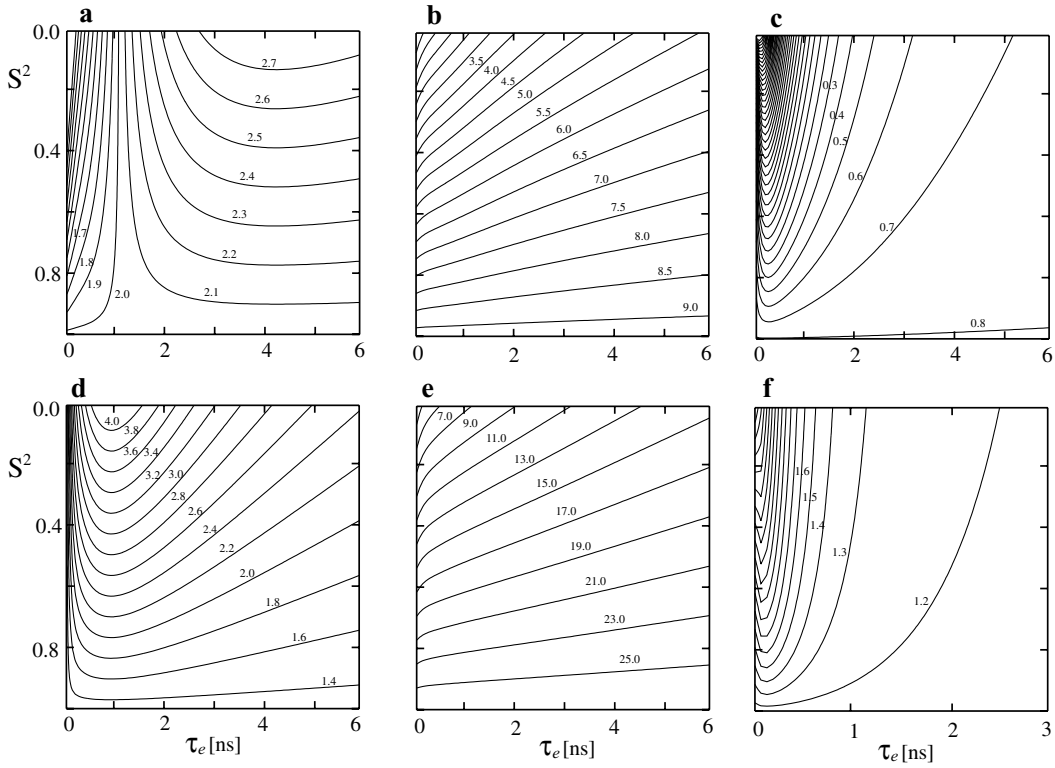

Fig. 6. Dependencies of R_1, R_2 and NOE of protein backbone ^{15}N and ^{13}C$^{\alpha}$ nuclei on S^2 and τ_e at 14.1 T spectrometer. R_1, R_2 and NOE are generated using Eqs. (1.28a)–(1.30e) and a model-free spectral density for isotropic molecules (Eq. (3.8b)) with $\tau_R = 6$ ns. (a) ^{15}N R_1, (b) ^{15}N R_2 (c) ^{15}N{^{1}H} NOE, (d) ^{13}C R_1, (e) ^{13}C R_2, (f) ^{13}C{^{1}H} NOE.

orientation of the relaxation relevant unit vector $\boldsymbol{\mu}^{M}$ in the molecular co-ordinate frame (see Eq. (2.13)), $P(\Phi_1)$ and $P(\Phi_2)$ are equilibrium probability densities for Φ_1 and Φ_2. From Eq. (3.9a) it is seen that the order parameter S^2 contains no information about the time-scale of dynamics; it is rather a measure of the spatial restriction of the internal motions. The allowed range for the order parameter is $0 \leq S^2 \leq 1; S^2 = 1$ for completely restricted internal motions; $S^2 = 0$ for unrestricted isotropic internal motion.[3] The effective correlation time τ_e (Eq. (3.9b)), however, depends both on the rates of intramolecular motions and on the spatial nature of the motions. The dependencies of ^{15}N and ^{13}C R_1, R_2 and NOE on S^2 and τ_e, calculated using the model-free spectral density function for an isotropic molecule (Eq. (3.8b)) are shown in Fig. 6.

Lipari and Szabo [164,165] showed that for different models of the internal motions, a single-exponential approximation for $C_l(t)$ (Eq. (3.8a)) with S^2 and τ_e given by Eqs. (3.8a) and (3.8b) provides almost exact relaxation rates if: (i) the internal motions are much faster than the molecular overall rotation ($\tau_e \ll \tau_R$); and (ii) the internal (but not overall) motions are in the extreme narrowing limit ($\omega\tau_e \ll 1$). For ^{15}N nuclei at 9.4–18.8 T this holds if $\tau_e < 50$–100 ps and $\tau_R > 1$ ns.

In the limiting case of infinitely fast internal motions ($\tau_e \to 0$) the second term in Eqs. (3.8b) and (3.8c) for $J(\omega)$ may be neglected. The resulting expressions for $J(\omega)$ do not depend on τ_e. Thus, the relaxation rates contain information only about spatial restriction of the fast internal motions without detailed

[3] Note that $S^2 = 0$ not only for unrestricted isotropic motion. For example, $S^2 = 0$ for diffusion in a cone with semi-angle $\pi/2$ [159] or for unrestricted rotation about a single axis if the angle between the relaxation relevant vector and the axis is 54.7° (see [176]).

information about their time-dependence. In the limiting case of slow internal motions ($\tau_e \gg \tau_R$) Eqs. (3.8b) and (3.8c) for $J(\omega)$ is reduced to $J(\omega)$ for pure rotational motion, obtained by substituting of $S^2 = 1$ in Eqs. (3.8b) and (3.8c). Thus, slow motions do not affect the relaxation rates and cannot be detected by relaxation measurements (if these motions do not modulate the isotropic chemical shift of the nucleus).

If the internal motions are not in the extreme narrowing limit one can construct successively better approximations for the correlation function of intramolecular motions, consisting of a growing number of exponential terms. In particular, Clore et al. [166] proposed a two-exponential correlation function $C_I(t) = S^2 + A_f\, e^{-t/\tau_f} + A_s\, e^{-t/\tau_s}$ with $S^2 + A_f + A_s = 1$, where τ_f and τ_s are correlation times for fast and slow components, respectively. When τ_f and τ_s differ by at least one order of magnitude ($\tau_f \ll \tau_s$), $C_I(t)$ reaches an intermediate plateau value $S_f^2 = 1 - A_f$. In this case the correlation function $C_I(t)$ is given by:

$$C_I(t) = S^2 + (1 - S_f^2)\, e^{-t/\tau_f} + (S_f^2 - S^2)\, e^{-t/\tau_s}. \tag{3.10a}$$

The value of S_f may be regarded as an order parameter of fast internal motions. If it is assumed that fast motions are axially symmetric and independent of slow motions, the generalised order parameter S^2 is given by $S^2 = S_f^2 S_s^2$, where the value of S_s may be regarded as the order parameter of the slow motion. In terms of S_f^2 and S_s^2 the correlation function (Eq. (3.10a)) is written as:

$$C_I(t) = S_f^2 S_s^2 + (1 - S_f^2)\, e^{-t/\tau_f} + S_f^2(1 - S_s^2)\, e^{-t/\tau_s}. \tag{3.10b}$$

In the case of isotropic overall rotation the corresponding spectral density function is given by:

$$J(\omega) = \frac{S_f^2 S_s^2 \tau_R}{1 + (\omega\tau_R)^2} + \frac{(1 - S_f^2)\tau_f'}{1 + (\omega\tau_f')^2} + \frac{S_f^2(1 - S_s^2)\tau_s'}{1 + (\omega\tau_s')^2}, \tag{3.10c}$$

where $\tau_f'^{-1} = \tau_R^{-1} + \tau_f^{-1}$ and $\tau_s'^{-1} = \tau_R^{-1} + \tau_s^{-1}$.

For anisotropic overall rotation $J(\omega)$ has the form:

$$J(\omega) = \sum_{\eta=-2}^{2} c_\eta \left[\frac{S_f^2 S_s^2 \tau_\eta}{1 + (\omega\tau_\eta)^2} + \frac{(1 - S_f^2)\tau_{f,\eta}}{1 + (\omega\tau_{f,\eta})^2} + \frac{S_f^2(1 - S_s^2)\tau_{s,\eta}}{1 + (\omega\tau_{s,\eta})^2} \right], \tag{3.10d}$$

where $\tau_{f,\eta}^{-1} = \tau_\eta^{-1} + \tau_f^{-1}$, $\tau_{s,\eta}^{-1} = \tau_\eta^{-1} + \tau_s^{-1}$, τ_η are given by Eq. (2.10c) (see also Table 3), c_η are given by Eq. (2.10d). The 'extended' form of $C_I(t)$ (Eq. (3.10b)) is often required to analyse R_1, R_2 and NOE data when slow internal motions are not in the extreme narrowing limit. An example of such a situation is shown in Fig. 7. In the limiting case of $\tau_f \to 0$ the second term in Eqs. (3.10c) and (3.10d) for $J(\omega)$ can be neglected. The resulting form of the spectral density function depends on three parameters characterising intramolecular motions: S_f^2, S_s^2 and τ_s.

3.2.2. Conventional model-free data analysis

A typical set of ^{15}N relaxation data consists of longitudinal R_1 and transverse R_2 relaxation rates and $^{15}N\{^1H\}$ NOE measured at one or several magnetic fields (Section 1.4). For the analysis of these data the theoretical expressions for relaxation rates (or *models* for data analysis) are constructed based on the different spectral density functions $J(\omega)$ corresponding to the different forms of $C_O(t)$ (Eqs. (2.10b)–(2.12)) and $C_I(t)$ (Eqs. (3.8a) and (3.10a)). Commonly used forms of $C_O(t)$ and $C_I(t)$ are summarised in Table 4. The models for the relaxation data analysis should also account for the contribution of the conformational exchange in the microsecond–millisecond time-scale to transverse relaxation rates. Usually this is done by addition of an adjustable term R_{ex} to the predicted transverse relaxation rates. For relaxation data recorded at one magnetic field strength the use of an adjustable exchange term corresponds to the exclusion of R_2 data from the data analysis. If the data are measured at several magnetic fields and the exchange is fast [177] the R_{ex} term can be parameterised by a single parameter, since the exchange line broadening is proportional to the square of the magnetic field (see Section 1.3). Usually relaxation data are interpreted with the increasing complexity of

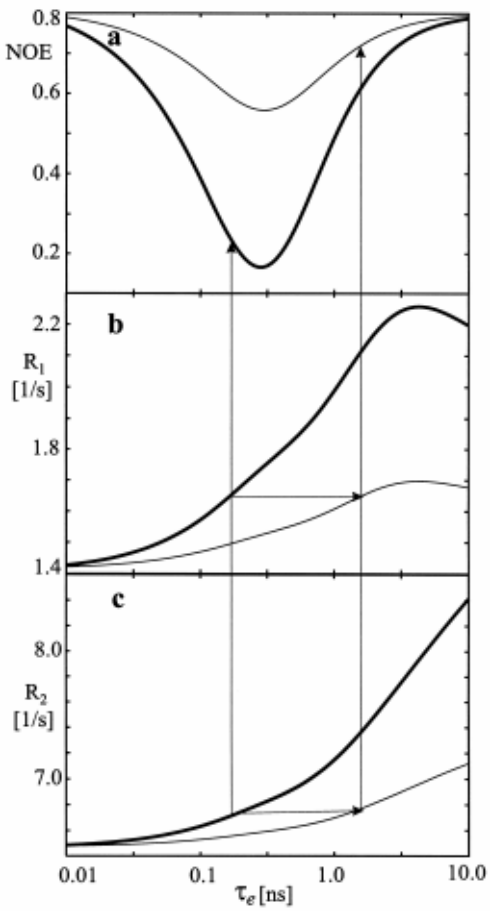

Fig. 7. Dependence of (a) $^{15}N\{^1H\}$ NOE, (b) ^{15}N R_1, (c) ^{15}N R_2 on the effective correlation time τ_e for internal motions calculated using a 'simple' (Eqs. (3.8a)–(3.8c)) and an 'extended' (Eqs. (3.10a)–(3.10d)) form of $C_I(t)$. Bold curves correspond to the single internal motion: $S^2 = 0.7$, thin curves correspond to the motions in two distinct time-scales: $S_f^2 = 0.8$, $\tau_f = 0$ and $S_s^2 = 0.875$, $\tau_s = \tau_e$ ($S^2 = S_f^2 S_s^2 = 0.7$). The curves were calculated for 14.1 T field assuming isotropic molecule with $\tau_R = 6.0$ ns. It is seen that in the case of internal motions occurring in a two distinct time-scales the $^{15}N\{^1H\}$ NOEs may substantially exceed the values, expected from ^{15}N R_1 and R_2 assuming the simple model-free formula (Eq. (3.8a)–(3.8c)).

models of the spectral density functions. The hierarchy of models used for relaxation data analysis is shown in Fig. 8.

The conventional strategies for the model-free analysis of ^{15}N relaxation data are described in [50,173,178]. The analysis includes two main steps:

1. Selection of the model and determination of the parameters of molecular overall rotation.
2. Selection of the model and determination of the parameters of the correlation function of internal motions $C_I(t)$ for each ^{15}N nucleus.

Additionally, the analysis may include re-optimisation of the parameters of $C_O(t)$ and $C_I(t)$ (see, e.g. [50,51]). These main steps of the model-free relaxation data analysis are discussed below in detail.

3.2.2.1. Characterisation of molecular overall rotation. Most commonly, the simplest isotropic form of the overall rotation correlation function $C_O(t)$ (Eq. (2.12)), depending on the single parameter τ_R, is adopted. Several methods for estimating τ_R can be considered. Usually, it is assumed that intramolecular motions for most ^{15}N nuclei in a protein are in the extreme narrowing limit. In this case an initial guess of τ_R is obtained from the R_2/R_1 ratio [49,178]. Under the conditions $\tau_e < 100$ ps and $\tau_R > 1$ ns the R_2/R_1 ratio is a monotonic function of τ_R, essentially independent of the parameters of the internal motions. The τ_R value is usually determined either from the mean R_2/R_1 ratio for the set of ^{15}N nuclei [50,178], by averaging τ_R obtained from the individual R_2/R_1 ratios for a set of ^{15}N nuclei [51], or by simultaneous optimisation of the R_2/R_1 ratios for the set of ^{15}N nuclei [179]. The ^{15}N nuclei with R_2/R_1 ratios substantially higher or lower than the mean value (e.g. outside one standard deviation) are usually excluded from the set used for the τ_R calculation [178]. The nuclei with high R_2/R_1 ratios are presumably subjected to conformational exchange in the microsecond–millisecond time-scale. The residues with low R_2/R_1 are involved in slow sub-nanosecond–nanosecond motions. Low $^{15}N\{^1H\}$ NOEs (e.g. <0.6) can also be used to exclude ^{15}N nuclei involved in extensive sub-nanosecond motions from the set used for the τ_R calculation [50]. Alternatively, τ_R can be obtained as an adjustable parameter in simultaneous fitting of the relaxation data for the set of ^{15}N nuclei, assuming a particular form of $C_I(t)$ [78,148,180–183].

The isotropic approximation for the molecular overall rotation often appears to be inappropriate

Table 4
Correlation functions and their adjustable parameters. (S, S_f, S_s are the generalised order parameter and order parameters for fast and slow motions: τ_e, τ_f and τ_s are correlation times of fast and slow motions, respectively; D_i, $i = x, y, z$ are principal components of the rotational diffusion tensor $\mathbf{D}_r$; $D_\perp = D_x = D_y$ and $D_\parallel = D_z$; α, β, and γ are Euler angles defining the orientation of the molecular frame where $\mathbf{D}_r$ has diagonal form with respect to the reference molecular frame. The effective overall rotation correlation time for the anisotropic molecule is defined as $\tau_R = 1/(2\mathrm{Tr}(\mathbf{D}_r))$)

Type	Equation	Model parameters	Citation	Description
$C_I(t)$	3.8a	S^2, ($\tau_e \to 0$)	[164]	Very fast internal dynamics
$C_I(t)$	3.8a	S^2, τ_e	[164]	Picosecond internal dynamics
$C_I(t)$	3.10b	S_f^2, S_s^2, τ_s, ($\tau_f \to 0$)	[166]	Very fast internal dynamics and slow sub-nanosecond – nanosecond motions
$C_I(t)$	3.10b	S_f^2, S_s^2, τ_s, τ_f	[166]	Picosecond internal dynamics and slow sub-nanosecond – nanosecond motions
$C_O(t)$	2.12	τ_R	e.g. [164]	Isotropic overall tumbling
$C_O(t)$	2.11	τ_R, $D_\parallel/D_\perp$, α, β	[107, 108]	Tumbling of axially-symmetric anisotropic molecule
$C_O(t)$	2.10	τ_R, D_x/D_z, D_y/D_z, α, β, γ	[107, 108]	Tumbling of asymmetric anisotropic molecule

and results in a serious misinterpretation of the relaxation data [77,85,105] (see below). In this case one needs an anisotropic form of the overall rotation correlation function $C_O(t)$ (Eqs. (2.10b)–(2.11c)). The correlation function $C_O(t)$ for any vector in a molecule of arbitrary shape may be calculated if the rotational diffusion tensor $\mathbf{D}_r$ of the molecule is known. In general, $\mathbf{D}_r$ is characterised by six independent values (Table 4) — its principal components $D_i(i = x, y, z)$ and Euler angles α, β, γ characterising the directions of its principal axes in the reference molecular frame. In some cases it is convenient to use another set of values instead of $D_i(i = x, y, z)$, i.e. $\tau_R = 1/(2\mathrm{Tr}(\mathbf{D}_r))$, D_x/D_z, and D_y/D_z or τ_R, $2D_z/(D_x + D_y)$ (anisotropy parameter), and $3/4(D_y - D_x)/(2D_z - (D_y + D_x))$ (rhombicity parameter). In the case of an axially symmetric anisotropic molecule, $\mathbf{D}_r$ is characterised by four independent values (Table 4).

Several approaches can be used to derive $\mathbf{D}_r$ from the relaxation data. Under the condition that internal motions are in the extreme narrowing limit ($\tau_e < 100$ ps) and all the correlation times of the anisotropic correlation function $C_O(t)$ (Eqs. (2.10b)–(2.10d)) are relatively long ($\tau_\eta > 1.0$ ns), $\mathbf{D}_r$ can be estimated from the ^{15}N R_2/R_1 ratios for the set of ^{15}N–^{1}H vectors, representatively sampling

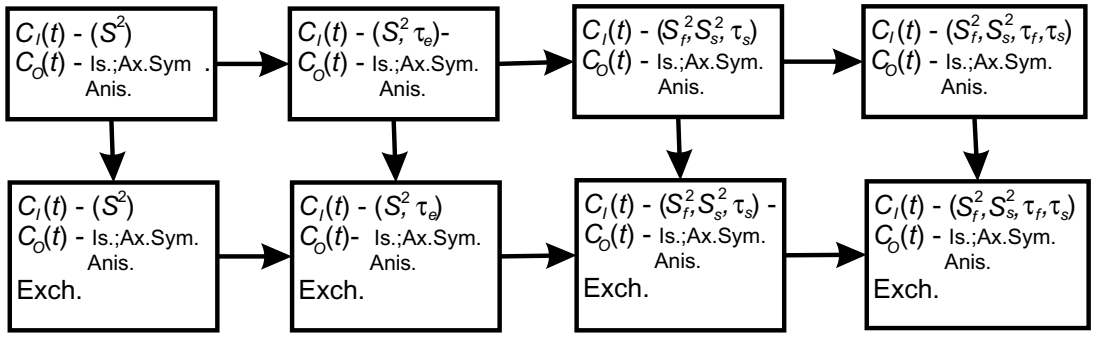

Fig. 8. Hierarchy of the models used for the analysis of the backbone ^{15}N relaxation data. Each *model* describes a theoretical dependence of the relaxation rates on the parameters of $C_O(t)$, $C_I(t)$ (see Table 4) and the adjustable exchange term R_{ex}. The arrows denote the transitions from simple to more complex models. Here and below the models are referred to by: (i) parameters of $C_I(t)$; (ii) type of overall rotation; and (iii) adjustable exchange term. The following abbreviations are used: Is. — isotropic; Ax. Sym. — axially symmetric; Anis. — anisotropic; Exch. — exchange. The models form a hierarchical nested set. Namely, the parameters of simpler models are a subset of the parameters of more complex models. The simpler models can be obtained from more complex model if the additional parameters of the complex model are set to their limiting values (i.e. 0 for R_{ex} and correlation times, 1.0 for order parameters).

all spatial directions. The parameters of the diffusion tensor are calculated by the least-square fitting of the R_2/R_1 ratios for the set of $^{15}N–^{1}H$ vectors [184,185] or by fitting local diffusion constants $(6\tau_{R,i})^{-1}$, where $\tau_{R,i}$ is obtained from R_2/R_1 ratio of ith ^{15}N nucleus [186,187]. In the latter method, referred to as the local diffusion approach, the diffusion tensor $\mathbf{D}_r$ is obtained as a least square solution of the equations:

$$(6\tau_{R,i})^{-1} = \boldsymbol{\mu}_i^T \mathbf{A}\mathbf{Q}\mathbf{A}^{-1}\boldsymbol{\mu}_i, \tag{3.11}$$

where $\boldsymbol{\mu}_i$ is the unit vector pointed along the ith NH in the reference molecular frame, $\mathbf{A}$ is the transformation matrix relating the reference molecular frame and the frame where $\mathbf{D}_r$ has diagonal form, and $\mathbf{Q}$ is a diagonal matrix with eigenvalues $(D_x + D_y)/2$, $(D_x + D_z)/2$, $(D_y + D_z)/2$. Using the above methods the parameters of $\mathbf{D}_r$ have been estimated in numerous ^{15}N relaxation studies of proteins (see, e.g. [77,85,184–192]). In principle, one can use models of different complexity for $\mathbf{D}_r$ — isotropic, axially symmetric and asymmetric (see, e.g. [77,85,190]). One can select between the models based on the values of the target function (Eq. (3.1)) obtained during fitting of $\mathbf{D}_r$ (see Section 3.1). It was noted, that if the molecule is essentially asymmetric, use of the axially symmetric model for $\mathbf{D}_r$ might result in two minima of the target function, corresponding to prolate and oblate representations of the system [190,193].

The calculation of $\mathbf{D}_r$ using R_2/R_1 ratios is valid only in the case of extremely fast intramolecular dynamics. Generally, R_2/R_1 ratios can be significantly biased by intramolecular motions. Thus, the most rigorous way for determination of $\mathbf{D}_r$ seems to be treatment of the parameters of anisotropic overall rotation as global adjustable parameters during simultaneous fitting of the relaxation data for multiple ^{15}N nuclei, assuming a particular form of $C_I(t)$ and the anisotropic $C_O(t)$ [78,148,182]. It is worth noting that even this procedure might fail if most of the molecule is involved in extensive nanosecond time-scale internal motions with characteristic times close to τ_R. In this case the parameters of rotational anisotropy become coupled with the parameters of the extended form of $C_I(t)$ [166] during fitting of the relaxation data.

Usually the ratios of principal components and

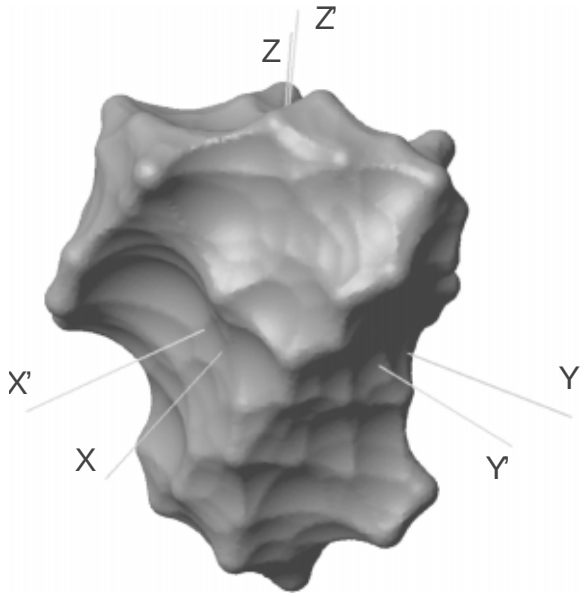

Fig. 9. Surface presentation of azurin (our unpublished results) with principal axes of two diffusion tensors $\mathbf{D}_r$ obtained from hydrodynamic calculations (x, y, z frame) and from the fitting of the relaxation data (x',y',z' frame). Both tensors are almost axially symmetric along their z-axes. The angle zz' is 18°.

directions of principal axes of $\mathbf{D}_r$, derived from ^{15}N relaxation data, correspond well to those obtained from the hydrodynamics calculations (Sections 2.2 and 2.3) (see Fig. 9). Therefore, it is convenient to fix some parameters of anisotropic overall molecular motion to the values obtained from hydrodynamic calculations.[4] In particular, one can fix up to five parameters including D_x/D_z, D_y/D_z, α, β, γ. As has been noted in the previous sections, hydrodynamic calculations do not provide correct estimates of τ_R. Thus, τ_R always has to be adjusted. Results of hydrodynamics calculations have been reported in several ^{15}N relaxation studies of proteins [78,146,148,184, 188–190,194].

3.2.2.2. Characterisation of intramolecular motions. Provided some reasonable approximation of the overall rotational diffusion has been chosen, one can

[4] Note that characterisation of the rotational anisotropy using the molecular inertia tensor is formally incorrect in the case of Brownian rotational diffusion.

proceed with the data analysis for individual ^{15}N nuclei. The data analysis is performed as described in Section 3.1 with a gradual increase of the complexity of the model (see Fig. 8; Table 4). The maximum likelihood estimates for the parameters of $C_l(t)$ and for the exchange term R_{ex} are obtained by minimisation of the target function (Eq. (3.1)), where the index i runs over the relaxation data for the particular ^{15}N nucleus. The uncertainties of the model parameters are estimated either using extensive Monte Carlo simulation or from the covariance matrix of an optimised model (Section 3.1). The simplest one-parameter (S^2) model is applied first. More complex two-parameter (S^2, τ_e) and (S^2, R_{ex}) models and, subsequently, three-parameter (S^2, τ_e, R_{ex}) and (S_f^2, S_s^2, τ_s) models (and so on) are used if the simpler models are rejected based on the χ^2 criterion and if the F-test confirms the significance of reduction of the target function under the transition to the more complex model. The analysis proceeds until a model providing a reasonable description of the relaxation data is found. This statistical protocol was first proposed for the analysis of the relaxation data in the studies [173,174].[5]

Numerous ^{15}N relaxation studies of proteins using the described strategy have shown that most of the globular proteins in native states are quite rigid, with relatively fast ($\tau_e < 100$ ps) and highly restricted ($S^2 = 0.7 - 0.9$) intramolecular motions of the backbone NH vectors (see, e.g. [195,196] and references cited therein). However, recent theoretical developments [106], confirmed by experimental work [78,148], reveal that the conventional model-free protocol does not provide an unambiguous description of protein dynamics due to the assumptions commonly adopted during the data analysis. Thus, one cannot exclude alternative interpretations of the relaxation data (see below).

3.2.3. Problems of model-free data analysis

The ambiguity of the conventional model-free data analysis mainly stems from various assumptions commonly made at the different stages of the analysis. If some of these assumptions are not valid, one can expect serious misinterpretations of the relaxation data. In particular, one should always account for the following potential sources of errors in the relaxation data analysis:

1. Commonly, it is assumed that molecular overall rotation is isotropic. Erroneously neglecting the anisotropy of molecular overall rotation can hamper the correct data analysis [85,105].
2. The conventional methods for characterisation of molecular overall rotation (either isotropic or anisotropic) a priori imply that intramolecular motions for most of protein $^{15}N–^{1}H$ groups are fast ($\tau_e < 100$ ps). This assumption is implicit if the τ_R or local correlation times $\tau_{R,i}$ (see Eq. (3.11)) are calculated from R_2/R_1 ratios or adjusted during fitting of relaxation data using the simple (S^2) or (S^2, τ_e) models of $C_l(t)$ (Table 4; Fig. 8). If this assumption does not hold, serious misinterpretations of the relaxation data are expected [106].
3. Usually the parameters governing relaxation of a ^{15}N nucleus (namely, ^{15}N CSA and $^{15}N–^{1}H$ distance) are kept fixed at predetermined values, assumed to be the same for all ^{15}N nuclei in the protein. Inconsistency between actual and assumed values of these parameters might result in errors in the subsequent data analysis (see, e.g. [78,85,197]).
4. From the very beginning, the model-free approach assumes that intramolecular motions are independent of molecular overall rotation. In the case of unfolded or partially unfolded states of proteins this assumption is unlikely to hold.
5. Conventional model-free protocols implicitly assume that the protein does not aggregate at concentrations typical for NMR relaxation studies. If the protein aggregates i.e. if considerable fractions of monomers, dimers and higher aggregates are present in the protein solution at the same time, the model-free analysis of relaxation data becomes impossible (or at least significantly more complicated) [105,156]. A strong indication of protein aggregation is the dependence of ^{15}N relaxation rates on protein concentration and apparently high values of order parameters obtained from regular data analysis.

Below we consider some of the mentioned problems in more details.

[5] In these works ^{15}N R_1, R_2, and $^{15}N\{^{1}H\}$ NOE were measured at one magnetic field. Therefore, the maximal number of adjustable model parameters was equal to 3.

3.2.3.1. Anisotropic molecular tumbling. The questions of what degree of rotation anisotropy can be neglected in $^{15}N-^{1}H$ NMR dynamic studies of proteins and what misinterpretations of the relaxation data are expected due to neglection of the rotation anisotropy were addressed by Schurr et al. [105]. We repeated some model calculations performed in this work and describe some recipes on how to cope with anisotropic molecules.

Model calculations (our unpublished results) for molecules with fast internal dynamics ($\tau_e < 100$ ps) show that a multi-exponential anisotropic rotation correlation function of an arbitrary $^{15}N-^{1}H$ vector (Eqs. (2.10b)–(2.11c)) can be well approximated by one exponent depending on the local correlation time $\tau_{R,i}$ obtained from the R_2/R_1 ratio of the ^{15}N nucleus (Fig. 10). Order parameters S^2 and correlation times τ_e originating from the use of an isotropic form of $C_O(t)$ (Eq. (2.12)) with a correlation time $\tau_{R,i}$ almost exactly reproduce the values obtained with the exact anisotropic expression for $C_O(t)$. Therefore, for moderately anisotropic molecules with fast internal dynamics one can analyse the relaxation data with the isotropic form of $C_O(t)$ (Eq. (2.12)) using local correlation time $\tau_{R,i}$ estimated from individual R_2/R_1 ratios. In this case each ^{15}N nucleus or subset of $^{15}N-^{1}H$ vectors having similar spatial orientations (e.g. NH's of an α-helix) are considered separately.

For molecules with fast internal dynamics the errors associated with neglect of the rotation anisotropy result from averaging of R_2/R_1 ratios or local $\tau_{R,i}$, commonly used for the refinement of overall rotation correlation time. For residues with the apparent $\tau_{R,i}$ smaller than the 'refined' τ_R, one should expect an underestimated S^2 and an overestimated τ_e (Fig. 10), or even wrong selection of the model for data analysis (Fig. 8; Table 4), favouring a (S_f^2, S_s^2, τ_s) model assuming sub-nanosecond – nanosecond motions [105]. For the residues with $\tau_{R,i}$ larger than the 'refined' τ_R, one should expect an overestimated S^2 and an underestimated τ_e (Fig. 10), or wrong selection of the model for data analysis, favouring models assuming conformational exchange in the micro millisecond time-scale [85]. The effects of motional anisotropy can be safely neglected for molecules with rotation anisotropy $0.8 < D_{\|}/D_{\perp} < 1.2$ [105].

3.2.3.2. Problem of τ_R selection. The conventional procedure for estimation of τ_R from R_2/R_1 ratios assumes that intramolecular motions for most of the protein ^{15}N nuclei are fast ($\tau_e < 100$ ps). However, if the major part of protein is involved in extensive nanosecond time-scale intramolecular motions the value of τ_R obtained in this way will be underestimated [106,183] (Fig. 11). The underestimated τ_R when used in further calculations leads to overestimated order parameters and underestimated correlation times of the internal motions and might result in apparent consistency of the relaxation data with the simplest models for data analysis (Fig. 8; Table 4), assuming fast intramolecular motions. An example of such a situation is shown in Fig. 12 [183]. The target function (Eq. (3.1)) obtained from fitting of the relaxation data for an ^{15}N nucleus involved in extensive nanosecond motions using a simple (S^2, τ_e) model of $C_l(t)$ exhibits two distinct minima, with depths depending on the τ_R value. The first artificial minimum at large S^2 and picosecond τ_e values becomes global when an

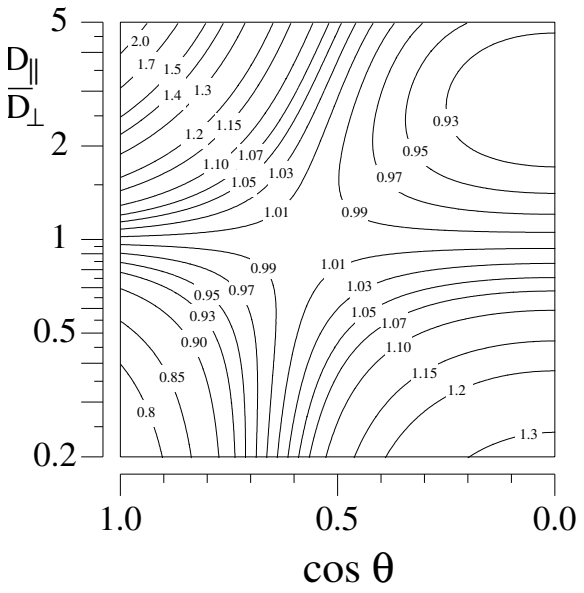

Fig. 10. Ratio of the local rotation correlation time $\tau_{R,i}$ and the effective $\tau_R = 1/(2\mathrm{Tr}(\mathbf{D}_r))$ of an axially symmetric molecule, $\tau_{R,i}/\tau_R$, versus the parameter of rotation anisotropy $D_{\|}/D_{\perp}$ and the angle θ between an NH vector and molecular symmetry axis. The local correlation time $\tau_{R,i}$ is calculated from R_2/R_1 for a particular ^{15}N nucleus assuming that the molecule is rigid.

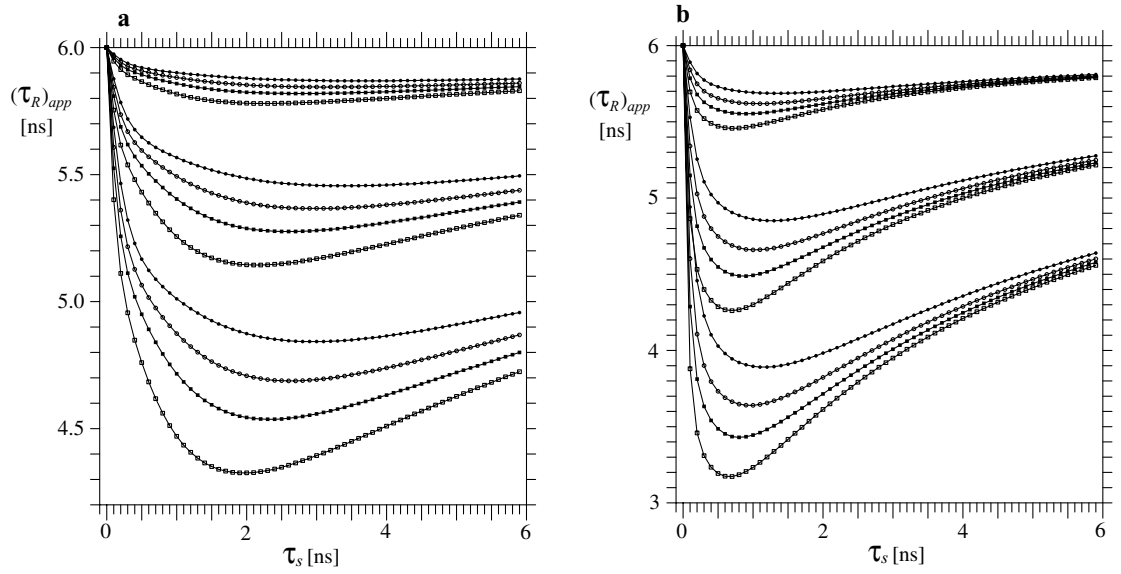

Fig. 11. Apparent overall rotation correlation time, $(\tau_R)_{app}$, calculated from the R_2/R_1 ratio as a function of the correlation time of the internal motions, τ_s. Relaxation rates R_1 and R_2 were simulated for a spherical molecule with $\tau_R = 6$ ns using (S_f^2, S_s^2, τ_s) model of $C_I(t)$ with $S_f^2 = 0.9$ (Fig. 8; Table 4). The three sets of curves from top to bottom correspond to three values of order parameters $S_s^2 = 0.95$, 0.8, and 0.6, respectively. In each set dependencies are shown for four magnetic fields: 9.4, 11.7, 14.1 and 17.6 T corresponding to filled circles, open circles, filled squares, and open squares respectively. (a) Data for the $^{15}N-^{1}H$ vector. (b) Data for the $^{13}C^{\alpha}-^{1}H$ vector. Reproduced from [106] with kind permission from Academic Press.

underestimated τ_R obtained from R_2/R_1 ratio is utilised. The second minimum at smaller S^2 and τ_e in the nanosecond range becomes global when the correct τ_R is used. Thus, the ambiguity of the τ_R selection is tightly coupled with the discrimination between the models of intramolecular motions and often has no straightforward solution.

Usually, the set of ^{15}N nuclei used for τ_R estimation is selected according to criteria of high $^{15}N\{^{1}H\}$ NOE and R_2/R_1 ratio close to a mean value. The additional criterion of involvement of a $^{15}N-^{1}H$ group in the hydrogen bonding network of a regular secondary structure may also be applied [198]. These criteria are expected to ensure that intramolecular motions for selected ^{15}N nuclei are fast and relatively restricted. However, neither these criteria nor statistical criteria implemented in the standard model selection protocol (see above) can detect the presence of collective nanosecond motions with correlation times τ_s longer than 1.5–2.0 ns, if the relaxation data are recorded at a *single* magnetic field strength. In the case of $\tau_s > 1.5$–2.0 ns the $^{15}N\{^{1}H\}$ NOEs have relatively high positive values and approach their upper theoretical limit with increasing τ_s (Fig. 13b). Deviation of the R_2/R_1 ratio from a mean value cannot help in the detection of nanosecond motions if most of the $^{15}N-^{1}H$ vectors are involved in these motions. Model calculations [106] show that in the case of $\tau_s >$ 1.5–2.0 ns the simplest (S^2) or (S^2, τ_e) models of $C_I(t)$ (Table 4), allowing estimation of τ_R from R_2/R_1 ratios, cannot be rejected based on the values of target functions $\Gamma(S^2)$ or $\Gamma(S^2, \tau_e)$ (Eq. (3.1)) (Fig. 13a). Relatively short $(\tau_e)_{app}$ obtained from data fitting with the (S^2, τ_e) model also does not contradict the choice in favour of models of fast internal motions (Fig. 13d). It follows that the regular protocol of the relaxation data analysis fails to detect the collective nanosecond time-scale internal motions with characteristic times longer than 1.5–2.0 ns. It is notable, however, that for relatively long τ_s the order parameters $(S^2)_{app}$ originating from erroneously chosen (S^2) or (S^2, τ_e) models of $C_I(t)$ might be regarded as rough estimates of actual order parameters of fast intramolecular motions – S_f^2 (Fig. 13c).

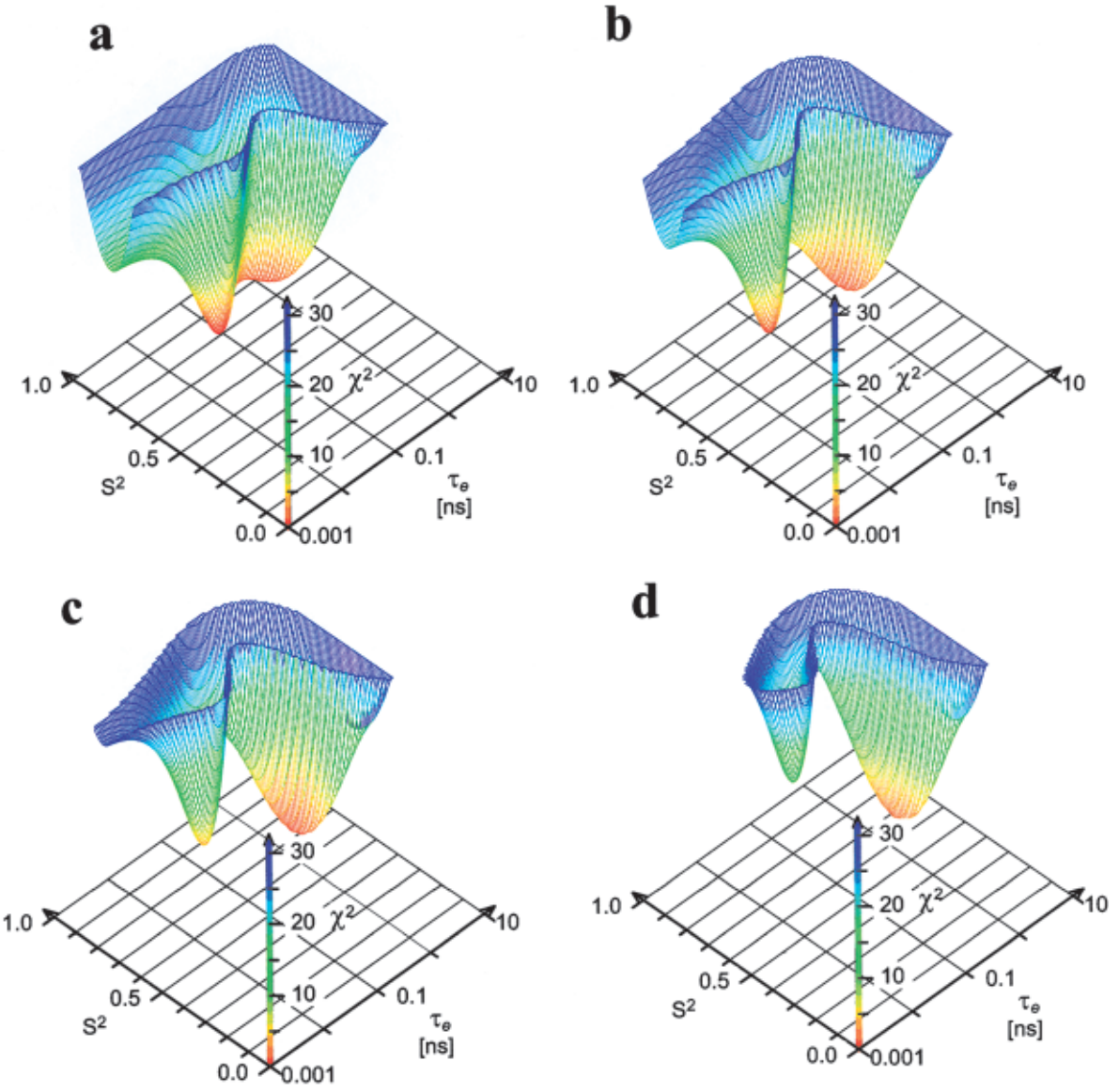

Fig. 12. Target function $\Gamma(S^2, \tau_e)$ (χ^2) versus S^2 and τ_e, reflecting the correspondence of simulated relaxation data to the simple (S^2, τ_e) model of $C_I(t)$ and isotropic $C_O(t)$ (Table 4) at different τ_R: 6.25, 7.0, 7.5, 8.0 ns (plots **a**, **b**, **c**, **d**, respectively). The relaxation data: ^{15}N R_1, R_2 and ^{15}N{^{1}H} NOE at 14.1 T magnetic field were simulated for a spherical molecule with actual $\tau_R = 7.0$ ns exhibiting motions in sub-nanosecond time-scale with $S_f^2 = 0.9$, $S_s^2 = 0.8$, $\tau_s = 0.8$ ns. Note, two distinct minima of the target function are present in all cases. Reproduced from [183] with kind permission from Kluwer Academic Press.

Again, if most of the protein ^{15}N nuclei are involved in a uniform conformational exchange process in the microsecond time-scale, the value of τ_R obtained from the R_2/R_1 ratio for the set of ^{15}N nuclei is expected to be overestimated. In principle, subsequent use of the overestimated τ_R might result in disappearance of the exchange term and the erroneous accepting of a simple model of fast intramolecular motions. As in the case of collective nanosecond time-scale motions detection of such cases based on

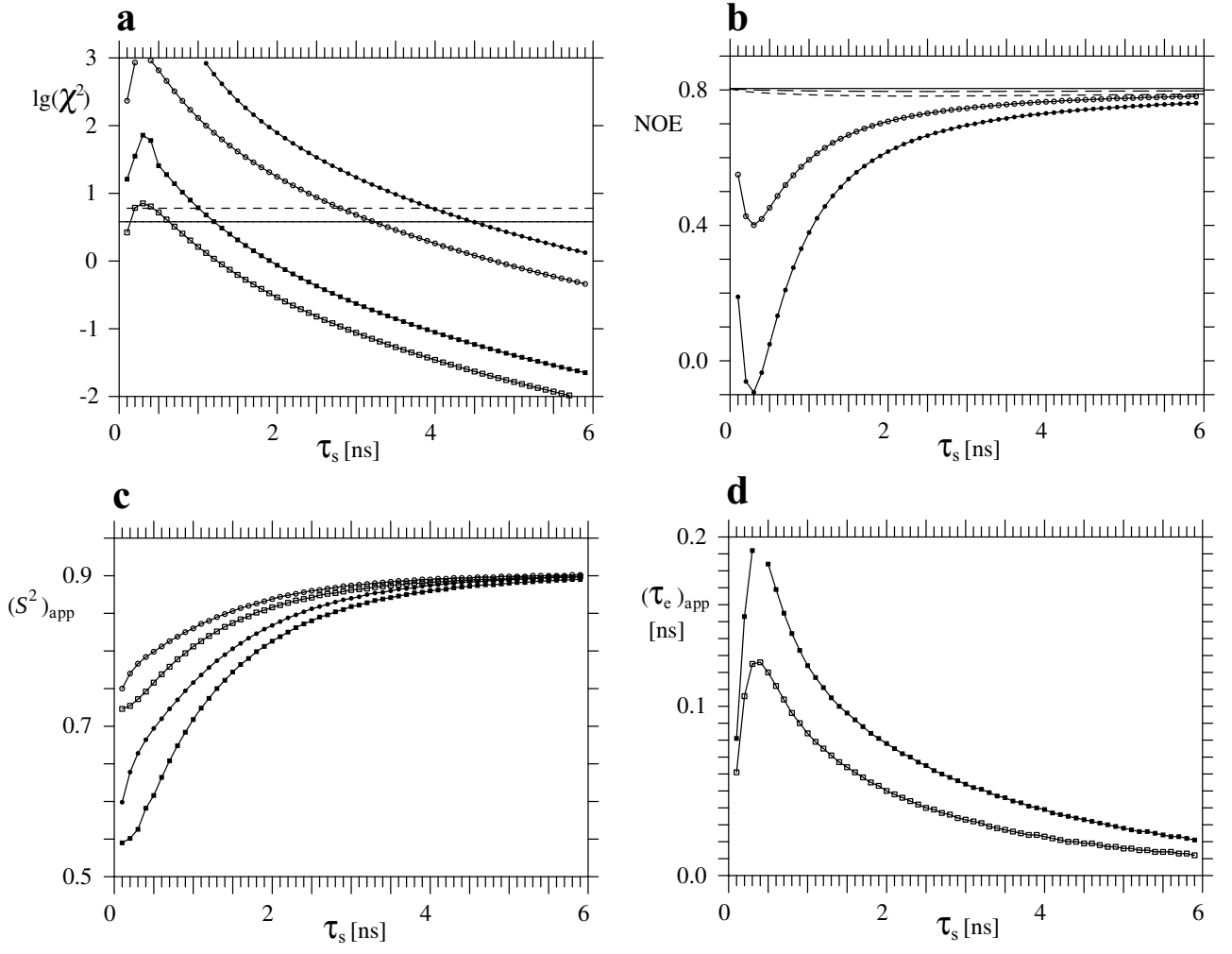

Fig. 13. Results of the formal model-free analysis of the relaxation data simulated for a molecule exhibiting internal motions in the nanosecond time-scale. Relaxation data (^{15}N R_1, R_2 and ^{15}N{^{1}H} NOE at 14.1 T magnetic field) were simulated for a spherical molecule with $\tau_R = 6$ ns using the (S_f^2, S_s^2, τ_s) model of $C_l(t)$ (Table 4) with $S_f^2 = 0.9$ and S_s^2 of 0.6 and 0.8 (filled and open signs in plots, respectively). The following uncertainties were assumed for simulated data − 2% for R_1, R_2 and 0.03% for NOE. Data were fitted using the (S^2, τ_e) and (S^2) models of $C_l(t)$ (squares and circles respectively) and isotropic $C_O(t)$. The apparent $(\tau_R)_{app}$ obtained from R_2/R_1 ratios were used in the fit. All values are plotted against the correlation time for nanosecond internal motions, τ_s. (a) Logarithm of $\Gamma(S^2, \tau_e)$ (χ^2) loss function (Eq. (3.1)). Five percent probability critical levels for the (S^2, τ_e) and (S^2) models are shown by horizontal dashed and solid lines respectively. (b) Simulated ^{15}N{^{1}H} NOE values (open and filled circles). Maximal NOE for exact τ_R and apparent $(\tau_R)_{app}$ are shown by solid dashed lines, respectively. (c) Apparent order parameters $(S^2)_{app}$. Note that for the long τ_s order parameters $(S^2)_{app}$ almost exactly reproduce the exact value of $S_f^2 = 0.9$. (d) Apparent correlation times of the internal motions $(\tau_e)_{app}$. Reproduced from [106] with kind permission from Academic Press.

Table 5
Apparent rotation correlation times τ_R (ns) obtained at several magnetic field strengths in ^{15}N NMR relaxation studies of proteins (all apparent rotation correlation times were calculated from mean R_2/R_1 ratios represented in the corresponding article)

Protein	Citation	Magnetic field strength (T)			
		7.0, 9.4	11.7	14.1	17.6
G(B1)	[179]		3.35	3.27	
Eglin c	[206]	4.35	4.12	4.04	
Fibronectin	[189]		5.3	5.0	4.9
P53	[257]		15.0	14.5	
4-OT	[258]		14.4	13.9	
434(1–63)	[194]	5.8			5.5

relaxation data recorded at one magnetic field strength is complicated.

Relaxation data measured at several magnetic fields provide a straightforward way for discriminating between models of intramolecular motions (Fig. 8; Table 4) and, therefore, for the selection of a correct τ_R value. In this case the models are well distinguished by the values of the target function (Eq. (3.1)) if τ_R is adjusted simultaneously with the parameters of internal motions [78,148,180,199]. Additionally, the field dependence of the apparent τ_R derived from R_2/R_1 ratios provides a strong indication on microsecond–millisecond conformational exchange or nanosecond time-scale motions [106]. In the former case the apparent τ_R increases with increasing field strength. In the case of nanosecond motions the apparent τ_R will be higher at lower field (Fig. 11). In fact, an increase of τ_R obtained from R_2/R_1 ratios with decreasing magnetic field strength was observed in several ^{15}N relaxation studies of proteins (Table 5).

3.2.3.3. Uncertainties in parameters governing ^{15}N relaxation. The interpretation of ^{15}N relaxation data requires the knowledge of ^{15}N CSA and the ^{15}N–^{1}H distance r_{NH}. During model-free analysis of relaxation data these values are usually kept fixed at predetermined values (e.g. −160 ppm for ^{15}N CSA and 1.02 Å for r_{NH}), assumed to be the same for all ^{15}N nuclei in protein, whereas the results of numerous works suggest that these parameters can vary for different positions in a protein molecule (see Section 1.5). In addition, one should keep in mind that the symmetry axis of the ^{15}N shielding anisotropy tensor is not collinear with the NH vector (this is important for strongly anisotropic molecules and at high magnetic fields [200]) and that the shielding anisotropy tensor, strictly speaking, is only approximately axially symmetric. The effects of uncertainties in ^{15}N CSA are of particular concern at very high field strengths, since the contribution of relaxation due to the CSA mechanism increases as the square of the field.

One can suggest that inconsistency between actual and assumed values of ^{15}N CSA and r_{NH} results in a substantial bias of the adjusted model parameters during fitting of the relaxation data [78,85,104,197]. In principle, one can avoid these errors by considering ^{15}N CSA and/or r_{NH} as an adjustable parameters for each ^{15}N nucleus in a protein, provided that an extensive set of relaxation data is measured at several magnetic fields [78,197]. It was noted that overestimation of ^{15}N CSA and/or underestimation of r_{NH} values lead to a decrease of the order parameters S^2.

3.2.3.4. Protein aggregation. To ensure high sensitivity, NMR experiments are performed at relatively high (typically millimolar) protein concentrations. At these concentrations specific or non-specific interactions between protein molecules might affect the overall rotation of a protein (see Section 2.3). If substantial fractions of different aggregate states of a protein are present in solution, the model-free approach can hardly provide a reasonable description of the relaxation data [105]. It was shown [105] that one could get an unphysical picture of almost ‘frozen’ internal dynamics, with the order parameters close to 1.0, if the protein aggregation is erroneously disregarded. Fushman et al. [156] proposed the method allowing model-free analysis of relaxation data in the case of non-specific protein dimerisation. In the general case, however, analysis of the relaxation data in aggregated molecules requires knowledge about the character of the association processes, the rate constants of these processes and the specificity of the protein–protein interactions. Therefore, probably the best recipe is to select the sample conditions were the protein is in a particular aggregate state (e.g. in pure monomer or dimer forms). If the aggregation is extremely strong, one could prefer the less assumption-demanding $J(\omega)$-mapping approach (Section 3.3) instead of the model-free analysis. In any case, one should check whether or

not the protein aggregates by measuring of ^{15}N R_1 or R_2 at several protein concentrations or by other methods. In fact, the dependence of ^{15}N relaxation rates on protein concentration has been reported in several relaxation studies of proteins [79,156,189,201].

3.2.4. Model-free analysis of relaxation data recorded at several magnetic fields

Conventional estimation of τ_R from R_2/R_1 ratios, assuming fast intramolecular dynamics, originates from the numerous relaxation studies of proteins performed at a single magnetic field. However, using τ_R obtained from R_2/R_1 ratios might result in an apparent inconsistency of the relaxation data recorded at several magnetic fields indicated, e.g. by the dependence of the τ_R obtained from R_2/R_1 ratios on the magnetic field (see above). Therefore, the analysis of relaxation data recorded at several magnetic fields requires a more general method for τ_R estimation and characterisation of molecular overall rotation.

Orekhov et al. [78,148] proposed a method for determination of τ_R and selection of a model for overall rotation using the relaxation data recorded at several magnetic fields. First, a representative set of protein ^{15}N nuclei possessing uniform R_1, R_2 and large uniform $^{15}N\{^1H\}$ NOE values is selected. This set can be restricted to ^{15}N–^1H groups involved in the hydrogen bonding network of a regular secondary structure. It is assumed that the relaxation data of all selected ^{15}N nuclei are accounted for by the same form of correlation function of internal motions $C_I(t)$. Additionally, adjustable exchange terms R_{ex} can be included for all selected ^{15}N nuclei. The relaxation data for all selected nuclei are fitted simultaneously for different combinations of $C_O(t)$ and $C_I(t)$ (Fig. 8) by minimisation of a 'cumulative' target function (Eq. (3.1)). Now the index i in Eq. (3.1) runs over all relaxation data of the set of ^{15}N nuclei. For given models of $C_I(t)$ and $C_O(t)$ the parameters of the overall rotation are adjusted simultaneously with the adjustment of the site-specific parameters of $C_I(t)$ and, possibly, R_{ex}. An appropriate model for the data analysis (Fig. 8) is selected according to the values of the optimised 'cumulative' target function using the statistical procedure described in Section 3.1. The final parameters of the overall rotation are taken from the most appropriate model. In short, the parameters of the overall rotation are adjusted along with the selection of the base model for the intramolecular dynamics. This is the main difference from the commonly used procedure, where fast dynamics (Eq. (3.8a)–(3.8c)) is implicitly accepted as the base model for the internal motions.

The subsequent analysis of the relaxation data is performed as in the conventional model-free protocol (see above). Namely, the model of $C_I(t)$ is selected and the model parameters with uncertainties are determined for each ^{15}N nucleus in the protein. Finally, in the frame of the chosen models of $C_O(t)$ and $C_I(t)$, one can re-adjust all the parameters of these models by simultaneous fitting.

Andrec et al. [175] noted that if the parameters of the overall rotation are fixed (as is done in the second stage of conventional model-free analysis) the uncertainties of the parameters of $C_I(t)$ will be underestimated. These authors proposed a Bayesian approach for estimation of the uncertainties of the model-free parameters. Reasonable estimates of the parameter uncertainties can also be obtained from the covariance matrix of the optimised model, calculated under simultaneous re-optimisation of the parameters of $C_I(t)$ for all ^{15}N nuclei with the adjustable parameters of overall rotation [182].

Below we consider two examples of the analysis of relaxation data recorded at several magnetic fields using the described strategy.

3.2.4.1. Repressor 434 (1–63). The above described strategy [148] was applied for the analysis of ^{15}N relaxation data of the DNA-binding domain (1–63) of 434 repressor measured at two magnetic fields — 9.4 and 17.6 T (400 and 750 MHz ^1H). The overall rotation correlation time τ_R of 434 (1–63) obtained from R_2/R_1 ratios at 9.4 T 5.80 ± 0.15 ns, exceeds the one for 17.6 T, 5.50 ± 0.15 ns. This difference as well as a systematic difference between local τ_R obtained from R_2/R_1 ratios of invidual backbone ^{15}N nuclei of 434 (1–63) at 9.4 and 17.6 T (Fig. 14) indicates non-local conformational changes in the protein occurring in the nanosecond time-scale (see above). Thus, τ_R derived from R_2/R_1 ratios is most probably underestimated and the original model-free protocol is not applicable for the analysis of ^{15}N relaxation data of 434 (1–63).

The τ_R for 434 (1–63) was selected by simultaneous fitting of the relaxation data for a selected set of the ^{15}N nuclei using different combinations of $C_I(t)$ and $C_O(t)$ (Fig. 8; Table 4). It was shown that neither the (S^2) nor the (S^2, τ_e) models of $C_I(t)$, implying fast intramolecular motions, can match the experimental data within the used uncertainties.

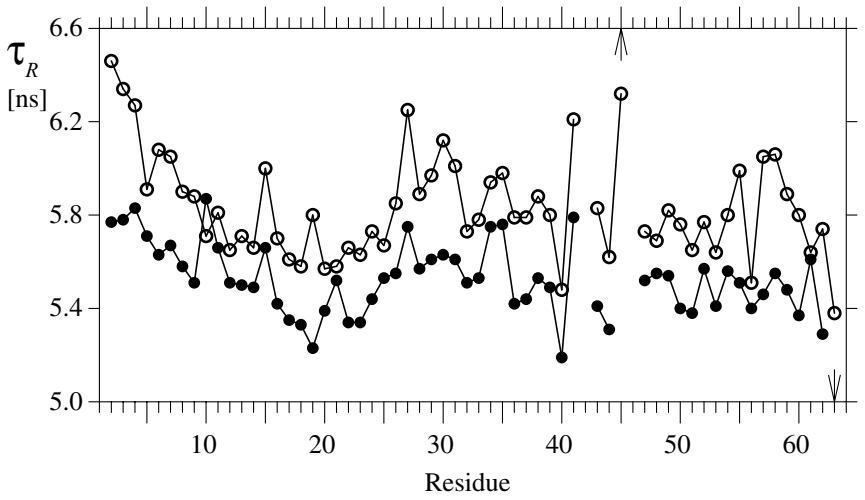

Fig. 14. Plot of local τ_R values for individual residues of the 434 repressor (1–63) obtained from experimental R_2/R_1 ratio at 9.4 T (blank circles) and 17.6 T (filled circles) magnetic fields. Apparent τ_R values for Leu45 and Thr63 for the 17.6 T spectrometer are 6.8 and 4.8 ns, respectively. Reproduced from [148] with kind permission from Adenine Press.

The model selection criteria (Section 3.1) results in a (S_f^2, S_s^2, τ_s) model of $C_I(t)$, implying nanosecond time-scale motions, and an isotropic model of $C_O(t)$ with τ_R ca. 30% higher than obtained from R_2/R_1 ratios.

The subsequent data analysis showed that the intramolecular motions of 434 (1–63) are characterised by mean order parameters S_f^2 and S_s^2 of 0.90 ± 0.03 and 0.59 ± 0.06, respectively, and correlation times τ_s of 5.1 ± 1.3 ns, suggesting collective intramolecular motions in the nanosecond time-scale for most backbone NH groups of 434 (1–63). These motions were tentatively attributed to rearrangement of the α-helix orientations in the molecular co-ordinate frame.

This study revealed an essential flexibility for 434 repressor (1–63), which can be regarded as being in contradiction with the common view on the protein internal dynamics. However, the common view is mostly based on the traditional model-free analysis of ^{15}N NMR relaxation data under assumptions posed by Lipari and Szabo [164], which never have been proved for the proteins. Moreover, there is no obvious reason to assume that certain time-diapason of intramolecular motions is absent in proteins. In fact, the question of whether proteins are floppier than is generally thought is the subject of ongoing debate [202,203].

3.2.4.2. Transmembrane segment (1–36) bacteriorhodopsin. The described strategy was also applied to study the backbone dynamics of the fragment (1–36) from bacteriorhodopsin (BR) solubilized in chloroform/methanol (1:1) mixture [78]. The peptide comprises a single transmembrane α-helix 8–32 and disordered N- and C-terminal parts. The heteronuclear ^{15}N R_1, R_2 and ^{15}N{^{1}H} NOE's for (1–36) BR were measured at three magnetic fields 11.7, 14.1 and 17.6 T (500, 600 and 750 MHz ^{1}H).

The overall rotation correlation time τ_R of (1–36) BR was obtained as an adjustable parameter in the minimisation of the 'cumulative' target function for the residues 9–31, which form the α-helix in (1–36) BR. Calculations for different models of $C_I(t)$ and $C_O(t)$ were performed. In addition, the models with adjustable exchange terms R_{ex}, adjustable ^{15}N CSA and adjustable r_{NH} included for all selected residues were tested. The statistical tests based on the values of a 'cumulative' target function strongly favour an isotropic form of the $C_O(t)$ and (S_f^2, S_s^2, τ_s) model of $C_I(t)$, implying nanosecond time-scale internal motions. Since all HN vectors in the α-helix are aligned in almost the same direction, it is not surprising that the isotropic form of $C_O(t)$ appears to be appropriate for relaxation data of the strongly anisotropic (1–36) BR, for which the D_x/D_z and D_y/D_z ratios are 0.296 and 0.297. The τ_R value of 5.8 ns

calculated for the isotropic $C_O(t)$ merely corresponds to the longest correlation time of the actual anisotropic $C_O(t)$ (Eqs. (2.10b)–(2.10d)).

In subsequent data analysis the (S_f^2, S_s^2, τ_s) model of $C_I(t)$ was selected for all ^{15}N nuclei from the α-helical 9–31 part and for most nuclei from the disordered N- and C-terminal parts of (1–36) BR. The intramolecular motions of amide NHs from the α-helical part are characterised by the mean order parameters of $S_f^2 = 0.84 \pm 0.02$, $S_s^2 = 0.60 \pm 0.05$ and correlation times $\tau_s = 3.0 \pm 1.0$ ns. The residues of N- and C-terminal parts exhibit high-amplitude motions with lower S_f^2 of 0.5–0.7 and S_s^2 of 0.2–0.4 and τ_s in the sub-nanosecond–nanosecond time-scale. For some of these residues more complex four-parameter. $(S_f^2, S_s^2, \tau_f, \tau_s)$ or $(S_f^2, S_s^2, \tau_s, R_{ex})$ models were found to be required to account for the experimental data.

Having a mean order parameter of nanosecond motions, S_s^2, as low as 0.6 indicates substantial conformational changes of most residues in the α-helix of (1–36) BR. It was suggested [78] that (1–36) BR exhibits transitions between folded and partially or completely unfolded states. Further support of these equilibrium helix–coil transitions arises from molecular dynamics simulation of (1–36) BR in a weakly polar medium [204], and from modelling of the dynamics of (1–36) BR using a statistical mechanics theory of helix-coil transitions [205].

3.3. $J(\omega)$ mapping

When the intrinsic assumptions of the model-free approach are violated the relaxation data still can be interpreted within the framework of the weaker assumptions that form the 'spectral density function mapping' approach, originally proposed by Peng and Wagner [29,167]. Below we briefly outline the essence of this method. The $J(\omega)$ mapping is based on the fact that the relaxation rates in a two-spin 1/2 system **IS** (Section 1.2) are given by linear combinations of the values of $J(\omega)$ at five frequencies: 0, ω_I, ω_S, $\omega_I \pm \omega_S$. These values may be obtained by solving the system of linear equations for relaxation rates measured at a particular magnetic field strength. The original approach includes measurements of six independent relaxation rates — $R_{1\mathbf{S}}$, $R_{1\mathbf{I}}$ and $R_{2I_zS_z}$ (Eqs. (1.28a)–(1.28f)), $R_{2\mathbf{S}}$ and $R_{2I_zS_x}$ (Eqs. (1.30a)–(1.30e)) and the dipolar cross-relaxation rate ρ_D (Eq. (1.28d)). These rates allow one to determine five values of $J(\omega)$ and the contribution to longitudinal relaxation of proton **I** due to its dipolar interactions with other protons in the protein, ρ_{IH}. The corresponding system of linear equations is given by:

$$\begin{bmatrix} R_{1\mathbf{S}} \\ R_{2\mathbf{S}} - R_{ex} \\ R_{2I_zS_x} - R_{ex} \\ R_{2I_zS_z} \\ R_{1\mathbf{I}} \\ \rho_D \end{bmatrix} = \begin{bmatrix} 0 & E & A & 0 & 6A & 0 \\ 2E/3 & E/2 & A/2 & 3A & 3A & 0 \\ 2E/3 & E/2 & A/2 & 0 & 3A & 1 \\ 0 & E & 0 & 3A & 0 & 1 \\ 0 & 0 & A & 3A & 6A & 1 \\ 0 & 0 & -A & 0 & 6A & 0 \end{bmatrix} \times \begin{bmatrix} J(0) \\ J(\omega_S) \\ J(\omega_I - \omega_S) \\ J(\omega_I) \\ J(\omega_I + \omega_S) \\ \rho_{IH} \end{bmatrix}, \quad (3.12a)$$

where $A = A_D^2/3$, $E = A_D^2 + 4A_{CSA(\mathbf{S})}^2 B_0^2$, A_D and $A_{CSA(\mathbf{S})}$ are given by Eqs. (1.22b) and (1.24d), B_0 is the magnetic field strength, R_{ex} is the contribution to $R_{2\mathbf{S}}$ due to the conformational exchange in the microsecond–millisecond time-scale (Section 1.3). In Eq. (3.12a) the relaxation of proton **I** due to the CSA mechanism is neglected. The solution of Eq. (3.12a) is given by:

$$\begin{bmatrix} J_{eff}(0) \\ J(\omega_S) \\ J(\omega_I - \omega_S) \\ J(\omega_I) \\ J(\omega_I + \omega_S) \\ \rho_{IH} \end{bmatrix} = \begin{bmatrix} -3/(8E) & 3/(4E) & 3/(4E) & -3(8E) & -3/(8E) & 0 \\ 1/(2E) & 0 & 0 & 1/(2E) & -1/(2E) & 0 \\ 1/(4A) & 0 & 0 & -1/(4A) & 1/(4A) & -1/(2A) \\ -1(12A) & 1/(6A) & -1(6A) & 1/(12A) & 1/(12A) & 0 \\ 1/(24A) & 0 & 0 & -1/(24A) & 1/(24A) & 1/(12A) \\ -1/4 & -1/2 & 1/2 & 1/4 & 1/4 & 0 \end{bmatrix} \begin{bmatrix} R_{1\mathbf{S}} \\ R_{2\mathbf{S}} \\ R_{2I_zS_x} \\ R_{2I_zS_z} \\ R_{1\mathbf{I}} \\ \rho_D \end{bmatrix}, \quad (3.12b)$$

where $J_{\rm eff}(0) = J(0) + \lambda R_{\rm ex}$, $\lambda = 3/(2E)$. The uncertainties of the $J(\omega)$ values and of ρ_{IH} are readily calculated from the uncertainties of the relaxation rates. From Eq. (3.12b) it is seen that conformational exchange in the microsecond–millisecond time scale affects only the value of $J(0)$. If the relaxation measurements are performed for N magnetic fields, one gets $4N$ values of $J(\omega)$ at non-zero frequencies and N values of $J_{\rm eff}(0)$. The dependence of $J_{\rm eff}(0)$ on the magnetic field can be used for identification of microsecond–millisecond conformational exchange even for residues with extensive sub-nanosecond nanosecond motions [206].

The values of $J_{\rm eff}(0)$ and $J(\omega_S)$ are less sensitive to the uncertainties of the experimental data and provide valuable information about the mobility of the relaxation relevant vector. Since the integral of $J(\omega)$ over the whole frequency range is constant, the intramolecular motions tend to increase the values of $J(\omega)$ at high frequencies and decrease $J(0)$. The values of $J(\omega)$ at high frequencies ω_I and $\omega_I \pm \omega_S$ are low and their estimates crucially depend on the uncertainties of the experimental data. Low precision of $J(\omega)$ at high frequencies might result in artificial apparent increases of $J(\omega)$ with increasing frequency, which is impossible for diffusive motions, or even in negative $J(\omega)$ values [29,167,206]. The conditions $J(\omega_I \pm \omega_S) > 0$ and $J(\omega_I + \omega_S) > J(\omega_I - \omega_S)$ (for an ^{15}N nucleus) result in the inequality $(14/5)\rho_{\rm D} > R_{1\mathbf{S}} + R_{1\mathbf{I}} - R_{2I_zS_z} > \rho_{\rm D}$, allowing one to estimate the precision of experimental relaxation rates, required for characterisation of $J(\omega)$ at high frequencies [206]. In particular, if the absolute uncertainties of the longitudinal relaxation rates exceed $(4/5)\rho_{\rm D}$ the values of $J(\omega)$ at high frequencies, obtained using the original $J(\omega)$ mapping, do not have much sense. It is noteworthy that the required precision of the relaxation rates increases with the increase of τ_R and B_0.

For large molecules it is convenient to use a reduced $J(\omega)$ mapping [206–210]. In the reduced $J(\omega)$ mapping one makes assumptions about the behaviour of $J(\omega)$ at high frequencies. In particular, if one accepts that $J(\omega_I) = J(\omega_I \pm \omega_S) = J(\omega_h)$, then values of $J(\omega)$ can be obtained from the system of linear equations for only three relaxation rates — $R_{1\mathbf{S}}$, $R_{2\mathbf{S}}$ and $\rho_{\rm D}$, which are obtained from conventional R_1, R_2 and NOE experiments (Section 1.4). In this case Eq. (3.12a) is reduced to:

$$\begin{bmatrix} R_{1\mathbf{S}} \\ R_{2\mathbf{S}} - R_{\rm ex} \\ \rho_{\rm D} \end{bmatrix} = \begin{bmatrix} 0 & E & 7A \\ 2E/3 & E/2 & 13A/2 \\ 0 & 0 & 5A \end{bmatrix} \begin{bmatrix} J(0) \\ J(\omega_S) \\ J(\omega_h) \end{bmatrix}. \tag{3.13a}$$

The solution of Eq. (3.13a) is given by

$$\begin{bmatrix} J_{\rm eff}(0) \\ J(\omega_S) \\ J(\omega_h) \end{bmatrix} = \begin{bmatrix} -3/(4E) & 3/(2E) & -9/(10E) \\ 1/E & 0 & -7/(5E) \\ 0 & 0 & 1/(5A) \end{bmatrix} \times \begin{bmatrix} R_{1\mathbf{S}} \\ R_{2\mathbf{S}} \\ \rho_{\rm D} \end{bmatrix}. \tag{3.13b}$$

Modifications in reduced $J(\omega)$ mapping for the case of $J(\omega)$ given by a sum of an arbitrary number of Lorentzians were also proposed [207].

Although the values of $J(\omega)$ provided by $J(\omega)$ mapping can be interpreted within the framework of different models of molecular motions or using the model-free approach, $J(\omega)$ mapping is mostly helpful in studies of unfolded or partially folded states of proteins where no specific assumptions about protein dynamics can be validated (see [207,210]). This approach should be recommended as well if very little is known about the overall rotation of the molecule, e.g. for strongly inhomogeneous aggregated proteins.

3.4. Conformational exchange as derived from relaxation data

Conformational exchange between states with different chemical shifts, occurring in the microsecond–millisecond time scale, provides an additional relaxation pathway for a ^{15}N nucleus (Section 1.3). Conformational exchange can be characterised using ^{15}N relaxation data in several possible ways. First, ^{15}N nuclei involved in microsecond–millisecond conformational exchange can be identified by their enhanced transverse relaxation rates or larger than average ^{15}N R_2/R_1 ratios. One can also

identify ^{15}N nuclei affected by the exchange by comparison of the R_2/R_1 ratios to the ratios of transverse and longitudinal DD–CSA ^{15}N cross-correlated cross-relaxation rates measured at a single magnetic field strength [55]. This method uses the fact that both $\eta_{DD,CSA(S)}$ (Eq. (1.30d)) and $\rho_{DD,CSA(S)}$ (Eq. (1.28e)) are independent of chemical exchange and their ratio is, to a good approximation, independent of the value of ^{15}N CSA and the direction of the principal axes of the ^{15}N shielding anisotropy tensor. More rigorously, the contribution R_{ex} of fast conformational exchange to R_2 can be extracted using model-free analysis of relaxation data recorded at several magnetic fields (Section 3.2.4). The conformational exchange characterised in such a way depends, however, on assumptions that are commonly made at different stages of the model-free data analysis (Section 3.2.3). Fast conformational exchange can also be described using $J(\omega)$ mapping (Section 3.3) from the dependence of $J_{eff}(0)$ on the magnetic field strength. It was also suggested that the contribution of fast conformational exchange to R_2 can be extracted from the field dependence of $R_2 - R_1/2$ [189,192]. However, the procedures mentioned above allow only an identification but not a detailed characterisation of conformational exchange.

A more detailed description of microsecond–millisecond conformational exchange is available on the basis of ^{15}N R_2 (CPMG) [44] and ^{15}N $R_{1\rho}$ measurements [70,71,80,211] (see Sections 1.3 and 1.4). Several R_2 (CPMG) experiments with a different pulse separation in the CPMG sequence and/or $R_{1\rho}$ experiments with different amplitudes ω_1 or resonance offsets $\Delta\omega$ of the applied spin-locking RF field are usually performed. Commonly, in the analysis of $R_{1\rho}$ and R_2 (CPMG) data it is assumed that the exchange occurs between two states A and B. In the case of fast two-state conformational exchange the dependence of $R_{1\rho}$ on ω_1 and $\Delta\omega$ is given by:

$$R_{1\rho} = R_1 \cos^2\theta + R_2 \sin^2\theta + p_A p_B \Delta\omega_{ex}^2 B_0^2 J_{ex}(\omega_e)\sin^2\theta, \tag{3.14}$$

where $\omega_e = \sqrt{\omega_1^2 + \Delta\omega^2}$, $J_{ex}(\omega) = k_{ex}/(k_{ex}^2 + \omega^2)$, $\theta = \arctan(\omega_1/\Delta\omega)$ (see Eqs. (1.36b), (1.38b), (1.41) and (1.43) in Sections 1.2 and 1.3). In the absence of conformational exchange, Eq. (3.14) can be used to extract R_1 and R_2 from $R_{1\rho}$ data measured with different $\Delta\omega$ and ω_1. If conformational exchange takes place one can also extract the exchange rate constant k_{ex} and the value of $p_A p_B \Delta\omega_{ex}^2$. The question whether a more complex model allowing for the exchange better fits the experimental $R_{1\rho}$ data may be addressed using statistical criteria (Section 3.1). Rotating-frame relaxation measurements are most efficient for studies of the conformational exchange occurring with rate constants k_{ex} on the order of the accessible effective field amplitudes ω_e. The contribution to $R_{1\rho}$ from extremely fast exchange with $k_{ex} \gg \omega_e$ is essentially independent of ω_e, which complicates the detection of such exchange by fitting of $R_{1\rho}$ data using Eq. (3.14). In practice, the amplitude ω_1 of the spin-locking RF field in the ^{15}N rotating frame relaxation experiments is selected to exceed the ^{15}N spectral width. The upper limit of ω_1 is, in turn, given by the amount of power that can be transmitted to the probe and the sample. Therefore, spin-locking RF fields of amplitudes $\omega_1/2\pi$ ranged from 1.0 to 2.0 kHz are usually applied. Since the exchange contribution to $R_{1\rho}$ is scaled as $\sin^2\theta$ it is useless to measure $R_{1\rho}$ far from on-resonance, i.e. at $\theta < 10°$, approximately corresponding to $\omega_e/2\pi > 10$ kHz. Thus, the values of ω_e sampled in ^{15}N $R_{1\rho}$ experiments lie in the range 1.0–10.0 kHz which allows one to study the microsecond–millisecond time-scale exchange starting from the processes occurring with characteristic times as fast as tens of microseconds [70,71,80,212].

The transverse relaxation rates R_2 measured with the CPMG sequence provide another possibility to obtain the exchange rate constant k_{ex} and information related to the chemical shift dispersion between the states (i.e. from the value of $p_A p_B \Delta\omega_{ex}^2$). For the fast exchange the equations for the exchange contributions R_{ex} to R_2 (CPMG) (Eqs. (1.44a)–(1.45c)) and $R_{\rho,ex}/\sin^2\theta$ to $R_{1\rho}$ (Eq. (1.43)) describe quite similar dependencies provided that they are plotted versus the CPMG frequency $\omega_{cp} = \pi/2\delta$ (2δ is the delay between the pulses in CPMG sequence) and ω_e, respectively (Fig. 15). In complete analogy to the $R_{1\rho}$ data the most pronounced dependence of R_2 (CPMG) on ω_{cp} is observed if the exchange occurs with rate constants k_{ex} of the order of ω_{cp}. The range of ω_{cp} accessible in ^{15}N R_2 (CPMG) experiment is somewhat different from those of ω_e in ^{15}N $R_{1\rho}$ measurements. The lower bound of $\omega_{cp}/2\pi$ in the ^{15}N R_2

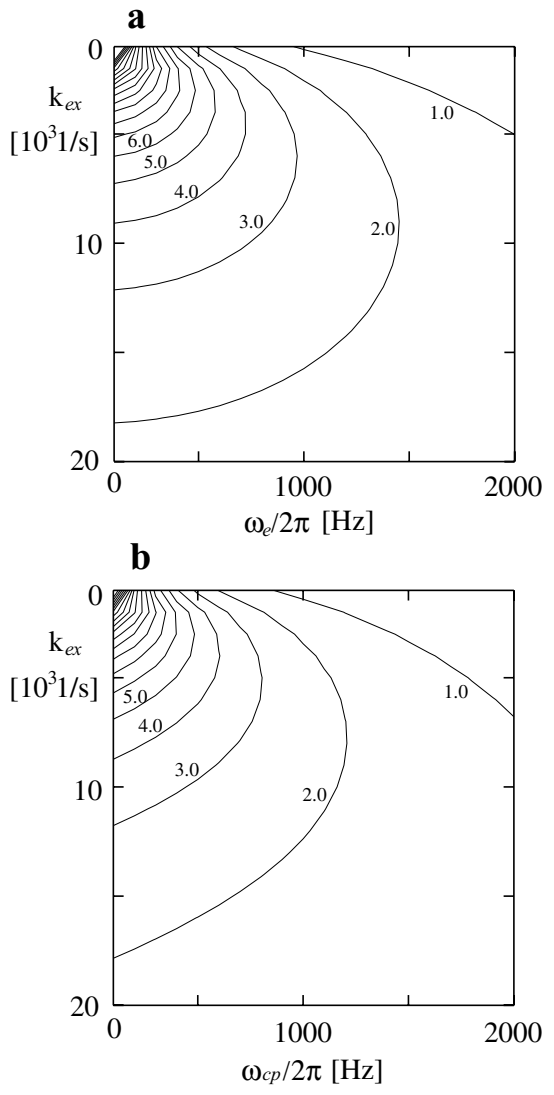

Fig. 15. (a) Exchange contribution $R_{\rho,ex}/\sin^2\theta$ of ^{15}N $R_{1\rho}$ (Eq. (1.43)) versus the exchange rate constant k_{ex} and the effective field amplitude $\omega_e/2\pi$. (b) Exchange contribution R_{ex} of ^{15}N R_2 (CPMG) (Eqs. (1.45a)–(1.45c)) versus the exchange rate constant k_{ex} and the CPMG frequency $\omega_{cp}/2\pi = 1/(4\delta)$ (2δ is the inter-pulse delay in CPMG sequence). The dependencies were calculated for 14.1 T spectrometer assuming the exchange between two equally populates states $p_A = p_B = 0.5$ with chemical shift difference $\Delta_{ex} = 1.0$ ppm.

(CPMG) experiment is about 400–500 Hz. This is required for effective suppression of mixing of in-phase and anti-phase components of ^{15}N magnetisation during the CPMG sequence (see Eq. (1.47)). To access pulse repetition rates $\omega_{cp}/2\pi$ comparable to one-bond scalar coupling constant $J_{NH} \approx 90$ Hz, a modified relaxation-compensated ^{15}N CPMG experiment was suggested [213]. The upper bound of $\omega_{cp}/2\pi$ is about 1200 Hz. This limit is imposed by the spectrometer hardware and the sample heating. Thus, in accordance with the accessible range of $\omega_{cp}/2\pi$, the ^{15}N CPMG experiment is most efficient for the description of the conformational exchange occurring in the hundred-of-microsecond–millisecond time-scale. Due to different accessible ranges of ω_e in $R_{1\rho}$ and ω_{cp} in CPMG, these two experiments effectively complement each other when considering the microsecond–millisecond time-scale motions [80].

To apply the equations listed in Section 1.3 for studies of conformational exchange one needs to ascertain whether the exchange is in the fast limit. In principle, one may distinguish between fast and slow exchange by the number of resonance lines present in the NMR spectra per exchanged spin. However, observation of single resonances in NMR spectra does not necessarily mean that the exchange is fast. This problem has been considered and recipes proposed on how to estimate the time-scale of an exchange process basing on CPMG data [177,214].

3.5. Analysis of relaxation data using computer simulations of molecular dynamics

NMR experiments provide relaxation data on ^{1}H, ^{13}C and ^{15}N nuclei and thus may describe most atoms in a protein molecule. However, even this extensive amount of relaxation data is insufficient for characterising the details of the complex conformational rearrangements that occur in proteins. Neither model-free parameters (see Section 3.2) nor the parameters of simple analytical motional models (reviewed by [158]) derived from the NMR relaxation data can reflect all modes of motions that affect varying subsets of atoms and occur at various frequencies. A complete characterisation of the internal motions in a protein, at the atomic level, can in principle be obtained from computer simulations, e.g. by integration of Newton's equation in MD (molecular dynamics) simulations or by separating 'essential' motions in normal mode analysis. In practice, these computational approaches suffer from a number of drawbacks, as will be summarised below.

Nonetheless, complementary information may be gained that allows for improvements in the models used to explain the NMR relaxation data; in return, experimental data from NMR may prove helpful for advancing the computer simulation approaches.

3.5.1. MD simulations: method and limitations

In MD simulations, the protein molecule and the surrounding solvent are represented by N atoms with co-ordinates $\mathbf{r}_i (i = 1 \ldots N)$, which interact with each other according to an energy potential $V(\mathbf{r}_i, \ldots \mathbf{r}_N)$ defined by a force-field (see, e.g. [215]). Typically, force fields include terms for deformations of the chemical structure (bond lengths, bond angles, torsion angles) and for long-range interactions (van der Waals and electrostatics potentials). From a carefully selected 'starting' structure, the time evolution can be obtained by integrating Newton's equation of motion in discrete, short time steps. Thus, MD simulations yield a very detailed description of the internal dynamics of proteins with very high resolution both in space and time.

The practice of MD simulations has been presented many times (e.g., [216]), and yet new developments such as the use of the particle mesh Ewald method [217] continue to provide improvements, sometimes at the risk of introducing new artefacts. Many MD simulations are recorded for macromolecules surrounded by explicit water molecules, and periodic boundary conditions are applied. They rely on protocols that remove fast vibrational modes for selected bonds, e.g. bonds with hydrogen atoms, with algorithms such as SHAKE [218], and they ensure constant temperature and pressure by frequent adaptation of the molecular co-ordinates and velocities [219].

This last statement leads to a discussion about the limitations of MD simulations. Besides the approximations implicit in classical force fields, 'non-physical' interference such as co-ordinate or velocity scaling in pressure or temperature control are applied. Other limitations result from the need for selecting a starting structure, the finite size of time steps in the simulations or the choice of a solvent model. Obviously, computer power sets limitations to the length of a simulation and to the number of independent trajectories (representing a molecular ensemble) that can be recorded for a given macromolecule. These shortcomings of MD simulations make it advisable to compare parameters extracted from a MD trajectory to similar parameters obtained from an experimental method. In a combined study using MD simulations and experimental data, the latter may increase the confidence in the simulation data, and the MD data provide better resolution in time and space for the dynamics experienced by a macromolecule.

3.5.2. Calculation of correlation functions and order parameters from MD trajectories

Similar model parameters as derived from NMR relaxation measurements can also be obtained from the analysis of MD trajectories. Measured heteronuclear NMR relaxation rates R_1 and R_2, and heteronuclear NOEs depend on the values of the spectral density function $J(\omega)$ at several characteristic frequencies. Values of the spectral density function $J(\omega)$, however, are usually not estimated from MD trajectories (although some authors have compared the results of $J(\omega)$ mapping and MD simulations; see, e.g. [220]). One reason is that the direct calculation of $J(\omega)$ values for ω_I, ω_S, $\omega_I \pm \omega_S$ frequencies requires trajectories with a length of hundreds of nanoseconds (see [221]). For short trajectories the correlation functions derived from MD simulations have to be approximated, e.g. by fitting a sum of exponents. Another reason is that the limited size of the systems in MD simulations does not allow the correct modelling of overall rotational diffusion of the molecule. Thus, only the correlation functions for intramolecular motions, $C_I(t)$, are usually calculated (molecular rotation and translation is usually eliminated during the MD simulation; in addition, the protein structures from a MD trajectory can be superimposed to remove the molecular rotation and translation). Correlation functions, for times not exceeding the length of the trajectory, can be calculated from the discrete snapshots of a MD simulation, e.g. as follows (see Eq. (2.13)):

$$C(k\tau) = \frac{1}{N-k} \sum_{i=1}^{N-k} P_2(\boldsymbol{\mu}_i \boldsymbol{\mu}_{i+k}), \tag{3.15}$$

where $\boldsymbol{\mu}$ is a unit relaxation relevant vector, N the number of snapshots in the trajectory, index i runs over $N-k$ snapshots, τ the time interval between the successive snapshots, $P_2(x) = (3x^2 - 1)/2$ is a

second-rank Legendre polynomial. Uncertainties in the values of the correlation function $C_l(t)$, calculated from the MD trajectory, depend on the characteristic time of the intramolecular dynamic processes τ_e and on the trajectory length t_{MD} [102]:

$$\Delta C(t) = C(t)(1 - C(t))\sqrt{2\tau_e/t_{MD}}. \quad (3.16)$$

The model-free order parameter S^2 (Section 3.2) can be calculated from a MD trajectory using plateau values of the correlation function (Eq. (3.15)) or directly from the distribution of the directions of the relaxation relevant vectors (see Eq. (3.9a)):

$$S^2 = \frac{1}{N^2}\sum_{i=1}^{N}\sum_{j=1}^{N} P_2(\boldsymbol{\mu}_i\boldsymbol{\mu}_j), \quad (3.17)$$

where indexes i and j run over all N snapshots of the trajectory. Examples of correlation functions $C_l(t)$ calculated from an MD trajectory are shown in Fig. 16. Order parameters and correlation times of internal motions derived from MD trajectories have often been compared with the results of model-free analyses of relaxation data [102,156,174,221–230].

3.5.3. Motions affecting NMR relaxation revealed by MD simulations

3.5.3.1. Femtosecond–picosecond time scale motions. The best characterisation by correlation functions and order parameters from MD simulations is for fast motions occurring in the femto to picosecond time-scales. Backbone NH and $C^{\alpha}H$ order parameters for such motions usually compare well with those obtained from model-free analyses of relaxation data (see, e.g. [225]). The correlation functions of internal motions, $C_l(t)$, for the backbone NH vectors usually decay during the first 50–100 fs to values around 0.85–0.9 (Fig. 16a). These values correspond to the order parameters of fast internal motions obtained from experimental data for ordered regions of proteins.

The oscillating behaviour of $C_l(t)$ (Fig. 16a) in the femtosecond time-scale results from local correlated vibrations of torsion angles (backbone φ, ψ and side-chain χ_1) as well as from vibrations of bond lengths and bond angles. At room temperature, fast vibrations of the backbone NH vector occur, relative to a molecular co-ordinate frame, in a cone with angular amplitudes of about 20° [174,223,226]. In the co-ordinate frame attached to the peptide plane the angular amplitudes of in-plane and out-of-plane NH vector vibrations are 3–5° and 10–12°, respectively [223], which corresponds approximately to order parameters S^2 of 0.95–0.96. This value might be regarded as an upper limit for NH order parameters at room temperature. It is notable that vibrations at lowest quantum vibrational level, which are not accounted for by the classical Newton equations used in MD simulations, would result in an additional decrease in order parameters. This effect may partially account for overestimation of MD derived order parameters with respect to the experimental values [102,224].

Order parameters derived from MD simulations for $C^{\alpha}H$ bonds are usually higher than those observed for backbone NH vectors [224,231]. Qualitatively, this can be explained by the restriction of $C^{\alpha}H$ mobility due to the side-chain. Daragan and Mayo [231] showed that the differences in NH and $C^{\alpha}H$ order parameters are associated with the correlated vibrations observed for the backbone torsion angles φ and ψ of neighbour residues.[6] In particular, S^2_{CH} increases and S^2_{NH} decreases with an increasing correlation coefficient $c(\varphi_i,\psi_i)$ and a decreasing $c(\psi_i,\varphi_{i+1})$. The analysis of MD trajectories shows that the motions of ψ_i and φ_{i+1} are strongly anti-correlated i.e. $c(\psi_i,\varphi_{i+1}) < -0.5$. For α-helices the vibrations of φ_i and ψ_i are also slightly correlated, whereas for a β-structure the correlation coefficient $c(\varphi_i,\psi_i)$ is closed to zero.

3.5.3.2. Sub-nanosecond time-scale motions. The internal motions resulting in a decay of $C_l(t)$ in the time-scale longer than 1 ps but shorter than 100 ps–1.0 ns are also well characterised from MD simulations (see, e.g. Refs. [174,224,226]). The motions of $C^{\alpha}H$ and NH vectors in this time-scale strongly depend on the secondary structure of the protein, in particular on over-damped quasi-harmonic motions such as twisting of β-sheets or bending of α-helices [226], local conformation transitions such as jumps between side-chain rotamers or simultaneous flips of the backbone torsion angles ψ_i and φ_{i+1} resulting in changes of the peptide plane orientation [226,232], local changes in the hydrogen bond network such as the formation of bifurcated $\alpha - 3_{10}$

[6] These torsion angles vibrations are correlated such that positional fluctuations of the neighbouring atoms are minimised.

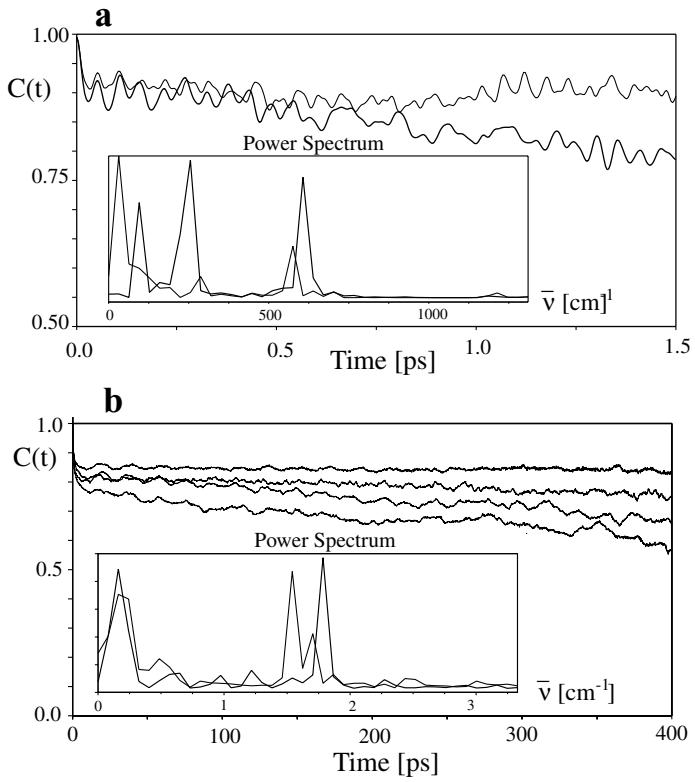

Fig. 16. Correlation functions $C_l(t)$ obtained from 0.5 ns in vacuo MD trajectory of the fragment (1–71) bacteriorhodopsin [226]. (a) $C_l(t)$ for fast femtosecond motions of NH vectors of the residues Trp10 and Val49. (b) $C_l(t)$ for picosecond motions for NH Val49, Leu61, Trp10 and Val34 (from top to bottom). The Fourier transform of $C_l(t)$ are shown in the insets to the figures — Trp10 (bold line) and Val49 (thin line). To remove the peak at zero frequency the baseline correction of $C_l(t)$ was performed before the Fourier transform. Reproduced from [226] with kind permission from Kluwer Academic Press.

hydrogen bonds (see, e.g. Ref. [233]) and on conformational transitions in the disordered parts of the protein molecule. Some picosecond oscillations may be observed from $C_l(t)$ functions calculated from in vacuo MD trajectories (Fig. 16b). These oscillations usually disappear when the effects of viscous damping are taken into account.

MD simulations and the experimental relaxation data (in particular, large $^{15}N\{^1H\}$ NOEs) suggest that the mobility of secondary structure elements of proteins in the sub-nanosecond time-scale is substantially reduced. The correlation functions $C_l(t)$ for $C^{\alpha}H$ and NH vectors usually reach a plateau value of about 0.8 (determined mainly by the initial femtosecond decay) during the first tens of picoseconds (Fig. 16b). This can justify the application of simple one- (S^2) or two-parametric (S^2, τ_e) forms of a spectral density function (Eq. (3.8a)–(3.8c)) upon the model-free analysis of relaxation data [164,165]. The intramolecular motions in flexible regions of proteins (e.g. in N- and C-terminal parts of the molecule or linker regions between the elements of secondary structure) are more complex and include both fast femtosecond–picosecond quasi-harmonic vibrations and relatively slow conformation transitions in the sub-nanosecond time-scale, including concerted flips of backbone and side-chain rotamers or formation of ordered structures stabilised by transient hydrogen bonds. Usually, the 'extended' three- (S_f^2, S_s^2, τ_s) or even four-parameter ($S_f^2, S_s^2, \tau_s, \tau_f$) form of a spectral density function

(Eqs. (3.10c), (3.10d)) [166] is required for model-free analysis of the relaxation data for the backbone NHs from the disordered regions. Using a plateau value for the correlation function $C_I(t)$ for calculations of the order parameters of intermediate motions S_s^2 (with correlation times $\tau_s > 100$ ps) is often complicated. In this case S_s^2 may be estimated from the distribution of the NH vector directions (Eq. (3.17)). Examples of the distributions of the backbone NH vector directions obtained from MD simulations are shown in Fig. 17.

3.5.3.3. Nanosecond time-scale motions. Although the predictive capacities of MD with respect to fast femtosecond–picosecond dynamics have been repeatedly demonstrated, the method still fails in describing slow nanosecond motions [227,228]. Protein dynamics in this time-scale includes global conformational rearrangements such as changes in packing of secondary structure elements and early events of protein folding such as α-helix growth or breathing of β-sheets. An example of a folding event affecting the relaxation of ^{15}N nuclei is the helix–coil transition in a transmembrane segment of (1–36) bacteriorhodopsin [78,204,205]. The rare occurrence of such events in MD trajectories, however, can not provide a statistically meaningful description of nanosecond time-scale motions. Thus, the question of whether the rare events detected in MD trajectories are a consequence of an inaccurate MD procedure still remains unclear (see [225]).

3.5.4. Analytical models for relaxation data analysis derived from MD simulations

MD simulations can help in the selection of an adequate analytical motional model for the description of NMR relaxation data. A general strategy for this selection was proposed by Bremi et al. [162] in their detailed analysis of the internal dynamics of the cyclic decapeptide antamanide: (i) Set up a MD simulation, with a length that ideally exceeds the maximal intramolecular correlation time by a factor of about ten. In the case of slowly exchanging species, several MD starts with different initial structures may be required. (ii) Select an analytical motional model or a combination of models suitable for the analysis of the relaxation data. Different approaches for this selection might be used: visual analysis of the trajectory, analysis of the distributions of vector directions, study of motional correlations or calculation of free energy surfaces for different motional degrees of freedom. (iii) Derive analytical expressions for correlation functions of intramolecular motions, $C_I(t)$, depending on a relatively small number of parameters. (iv) Calculate the model relaxation rates from the MD trajectory, and check the sensitivity of the model parameters with respect to the uncertainties of the experimental data; if possible simplify the model. (v) Analyse the experimental data. If the model parameters calculated from the experimental data are in good correspondence with those derived from the MD trajectory then the selected motional model might be regarded as appropriate and the MD setup as correct. The proposed strategy was used for the analysis of a MD trajectory of the cyclic decapeptide antamanide [162]. It was shown that the Gaussian axial fluctuation (GAF) model [234] for fast motions within side-chain rotameric states and a jump model for slow transitions between rotamers were suitable for the analysis of ^{13}C relaxation in phenylalanine side-chains. Apart from the model selection and checking the correctness of the MD procedure the proposed strategy might also be used for planning of an NMR experiment (i.e. for the selection of the optimal set of relaxation data suitable for consideration of the particular type of intramolecular motions). For example, Bremi and Bruschweiler [235] showed that the motions of peptide planes could be considered as superpositions of the restricted rotations about three orthogonal axes (three-dimensional GAF model). The parameters of these rotations might be obtained from ^{15}N R_1, NOE and $^{13}C'$ R_1 data measured at several magnetic fields.

3.5.5. Normal mode analysis and NMR relaxation data

Another computational method of bio-molecular dynamics studies, normal mode analysis, is also widely used for the interpretation of NMR relaxation data [102,161,236,237]. In normal mode analysis the potential energy surface $V(\mathbf{r}_1,\ldots,\mathbf{r}_N)$ is approximated by harmonic potentials, depending on second moments of $V(\mathbf{r}_1,\ldots,\mathbf{r}_N)$ calculated at its minimum. The dynamics of the molecule is represented by superposition of the vibrations occurring with frequencies ω_i along $3N-6$ orthogonal directions $\mathbf{Q}_i$ in $3N$ dimensional co-ordinate space (three

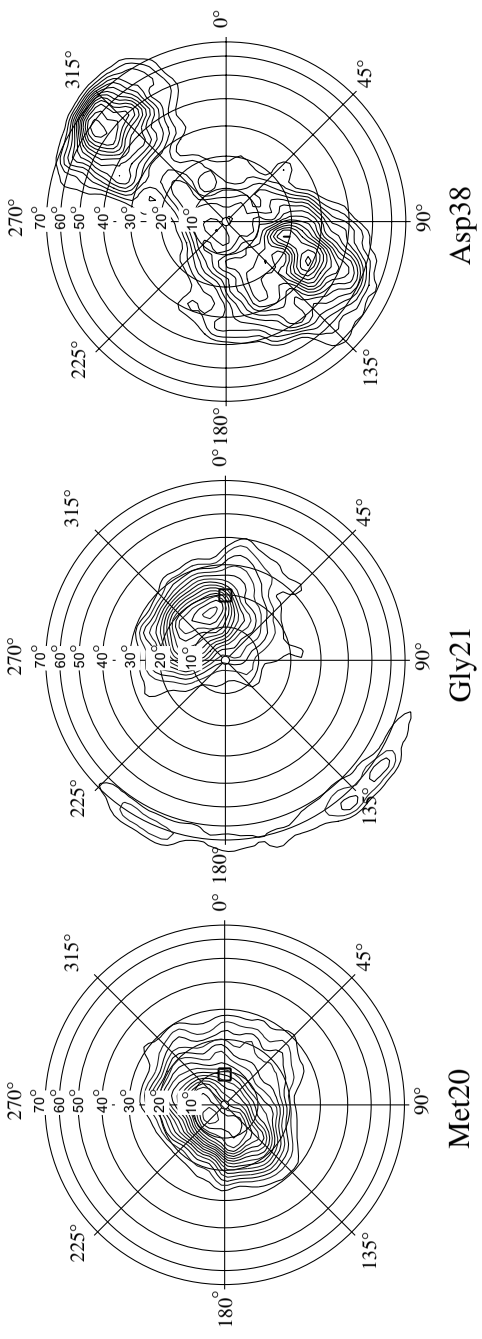

Fig. 17. Distributions of the NH vector directions for the residues Met20 and Gly21 from 0.5 ns in vacuo MD trajectory of (1–36) bacteriorhodopsin and NH Asp38 from 0.5 ns in vacuo MD of (1–71) bacterorhodopsin [226]. The residues Met20 and Gly21 are from the central part of α-helix 8–32. Asp38 belongs to the disordered loop region connecting the transmembrane helices 8–32 and 42–64. The several maxima in distribution for Gly21 are due to the local conformational transition — simultaneous flip of ψ Met20 and φ Gly21 backbone angles resulting in change of orientation of the corresponding peptide plane. The several maxima in distribution for Asp38 point on complex dynamics of the disordered region of the molecule. Reproduced from [226] with kind permission from Kluwer Academic Press.

translational and three rotational degrees of freedom should also be considered). The normal modes $\mathbf{Q}_i$ are calculated from the equations:

$$\mathbb{M}^{1/2}\mathbf{F}\mathbb{M}^{1/2}\mathbf{Q}_i = \omega_i^2\mathbf{Q}_i \tag{3.18a}$$

$$\mathbf{Q}_i\mathbf{Q}_j = \delta_{ij}, \tag{3.18b}$$

where $\mathbb{M}$ is a diagonal matrix with atomic masses, $\mathbf{F}$ the matrix of the second derivative of potential energy $V(\mathbf{r}_1,\ldots,\mathbf{r}_N)$. For a classical system interacting with the thermal bath the fluctuations in harmonic potential walls are described by the following equations:

$$\langle q_i(0)q_j(t)\rangle = \delta_{ij}\frac{k_BT}{\omega_i^2}\cos(\omega_i t), \tag{3.19a}$$

$$\sigma_i^2 = \frac{k_BT}{\omega_i^2}, \tag{3.19b}$$

where, q_i and q_j are mass-weighted deviations of i-th and j-th normal coordinates from their equilibrium positions, T is the temperature, k_B is the Boltzmann's constant, δ is the Kronecker's delta and σ is the vibration amplitude. For a quantum-mechanical system these equations have the form:

$$\langle q_i(0)q_j(t)\rangle = \delta_{ij}\frac{\hbar}{2\omega_i}\coth\left(\frac{\hbar\omega_i}{2k_BT}\right)\cos(\omega_i t) \tag{3.20a}$$

$$\sigma_i^2 = \frac{\hbar}{2\omega_i}\coth\left(\frac{\hbar\omega_i}{2k_BT}\right). \tag{3.20b}$$

In some cases it is convenient to use the torsion angle co-ordinate space instead of the conventional Cartesian space for the normal mode analysis of proteins [237].

The description of molecular motions provided by normal mode analysis does not account for the effects of the surrounding medium. A useful modification of the normal mode analysis accounting for the viscous damping, Langevin mode analysis, was proposed by Lamm and Szabo, [123]. In Langevin mode analysis the frequencies of the vibrations are given by complex numbers. The method is appropriate for studies of protein harmonic motions since the protein vibrations with frequencies less than 75–100 cm^{-1} are over-damped [236,238]. The set of molecular normal or 'essential' modes might be obtained from MD trajectories by diagonalisation of the covariance matrix for positional fluctuations of protein atoms (quasi-harmonic and essential mode analysis) [239–241]. Although at 300 K more than 70% of the root mean square deviations of protein atoms from their equilibrium positions are accounted for by conformational transitions (i.e. by inharmonic motions), vibration analysis (normal or Langevin mode) is useful for the understanding of some aspects of protein dynamics (in particular quantum effects, see, e.g. Ref. [238]).

From (Eqs. (3.18a)–(3.20b)) one can easily calculate the auto- and cross-correlation functions for any quantites depending on the co-ordinates of protein atoms [102,238]. Palmer and Case [102] used normal mode analysis for calculations of correlation functions $C_l(t)$ and order parameters S^2 for fast femtosecond–picosecond motions of backbone NH and $C^{\alpha}H$ vectors. It was shown that the order parameters calculated with the assumption of a classical nature of protein motions exceed those calculated for a quantum-mechanical system (the difference is of about 0.05–0.06). This is explained by the fact that in the classical case the amplitude of high-frequency vibrations might be substantially lower than those expected for quantum vibrations.

Acknowledgements

This work was supported by research grant 00-04-48318 from the Russian Foundation of Basic Research to D.M.K., a research grant from the Royal Swedish Academy of Sciences to M.B., a postdoctoral fellowship from Wenner-Gren Foundation (Sweden) to D.M.K. This work is partially based on the PhD thesis of D.M.K., Moscow Institute of Physics and Technology, 1999.

Appendix A

A.1. Spherical harmonics

Spherical harmonics of rank l are given by (see Ref. [242]):

$$Y_{lm}(\theta,\varphi) = \Theta_{lm}(\theta)\Phi_m(\varphi), \tag{A1a}$$

where θ $(0,\pi)$ and φ $(0,2\pi)$ are the polar angles; $|m| \leq l$

$$\Phi_m(\varphi) = (2\pi)^{1/2}\, \mathrm{e}^{\mathrm{i}m\varphi} \tag{A1b}$$

$\Theta_{lm}(\theta)$ are given by:

$$\Theta_{lm}(\theta) = (-1)^m \left[\frac{2l+1}{2} \frac{(l-m)!}{(l+m)!} \right]^{1/2} P_l^m(\cos\,\theta), \tag{A1c}$$

where

$$P_l^m(\cos\,\theta) = (\sin\,\theta)^m \left[\frac{d}{d\cos\,\theta} \right]^m P_l(\cos\,\theta),$$

$$P_l(\cos\,\theta) = \frac{1}{2^l l!} \left[\frac{d}{d\cos\,\theta} \right]^l ((\cos\,\theta)^2 - 1)^l,$$

$P_l(\cos\theta)$ is a Legendere polynomial of rank l.

The spherical harmonics are normalised on a unit sphere

$$\int_0^{2\pi} \mathrm{d}\varphi \int_0^{\pi} Y_{lm}^*(\theta,\varphi) Y_{l'm'}(\theta,\varphi) \sin\,\theta\, \mathrm{d}\theta = \delta_{l,l'}\delta_{m,m'}. \tag{A2a}$$

Other useful properties of spherical harmonics are

$$Y_{lm}^*(\theta,\varphi) = (-1)^m Y_{l,-m}(\theta,\varphi),$$
$$Y_{lm}(-\theta,-\varphi) = (-1)^m Y_{lm}^*(\theta,\varphi), \tag{A2b}$$

$$Y_{l0}(\theta,\varphi) = \left(\frac{2l+1}{4\pi} \right)^{1/2} P_l(\cos\,\theta).$$

One of the most useful relationships is an addition theorem for spherical harmonics

$$P_l(\cos\,\theta_{ij}) = \frac{4\pi}{2l+1} \sum_{m=-l}^{l} Y_{lm}^*(\theta_i,\varphi_i) Y_{lm}(\theta_j,\varphi_j) \tag{A2c}$$

Finally, let us write explicit expressions for some spherical harmonics and Legendre polynomials

$$P_0(\cos\,\theta) = 1 \qquad P_1(\cos\,\theta) = \cos\,\theta$$
$$P_2(\cos\,\theta) = \tfrac{1}{2}(3\cos^2\,\theta - 1) \tag{A3a}$$

$$Y_{00} = \frac{1}{\sqrt{4\pi}} \tag{A3b}$$

$$Y_{10} = \sqrt{\frac{3}{4\pi}} \cos\,\theta \qquad Y_{1,\pm1} = \mp\sqrt{\frac{3}{8\pi}}\, \mathrm{e}^{\pm\mathrm{i}\varphi} \sin\,\theta \tag{A3c}$$

$$Y_{20} = \sqrt{\frac{5}{16\pi}} (3\cos^2\theta - 1)$$
$$Y_{2,\pm1} = \mp\sqrt{\frac{15}{8\pi}}\, \mathrm{e}^{\pm\mathrm{i}\varphi} \sin\,\theta\cos\,\theta \tag{A3d}$$

$$Y_{2,\pm2} = \sqrt{\frac{15}{32\pi}}\, \mathrm{e}^{\pm 2i\varphi} \sin^2\theta.$$

A.2. Transformational properties of spherical harmonics. Wigner functions

Rotations in space are parameterised by Euler's angles α, β and γ. Under the rotations the spherical harmonics $Y_{lm}(\theta,\ \varphi)$ are transformed through the Wigner functions $D^l_{m'm}$, depending on α, β and γ (see [242]):

$$Y_{lm}(\theta',\varphi') = \sum_{m'=-l}^{l} D^l_{m'm}(\alpha,\beta,\gamma) Y_{lm'}(\theta,\varphi). \tag{A4}$$

The Wigner functions $D^l_{m'm}$ are given by

$$D^l_{m'm} = \mathrm{e}^{-\mathrm{i}m'\alpha} d^l_{m'm}(\beta)\, \mathrm{e}^{-\mathrm{i}m'\gamma} \tag{A5}$$

$$d^l_{m'm}(\beta) = \sum_s \frac{(-1)^s [(l+m)!(l-m)!(l+m')!(l-m')!]^{1/2}}{(l-m'-s)!(l+m-s)!(s+m'-m)!s!} \times \left(\cos\frac{\beta}{2} \right)^{2l+m-m'-2s} \left(-\sin\frac{\beta}{2} \right)^{m'-m+2s}.$$

The Wigner functions are orthogonal

$$\int_0^{2\pi} \mathrm{d}\gamma \int_0^{\pi} \sin\beta\, \mathrm{d}\beta \int_0^{2\pi} \mathrm{d}\alpha D^{l^*}_{mk}(\alpha,\beta,\gamma) D^{l'}_{m'k'}(\alpha,\beta,\gamma) = \frac{8\pi^2}{2l+1}\delta_{l,l'}\delta_{m,m'}\delta_{k,k'}. \quad \text{(A6a)}$$

Other useful properties of Wigner functions are:

$$D^{l}_{mm'}(-\gamma,-\beta,-\alpha) = D^{l^*}_{m'm}(\alpha,\beta,\gamma) \quad \text{(A6b)}$$

$$D^{l}_{m0}(\alpha,\beta,\gamma) = \left(\frac{4\pi}{2l+1}\right)^{1/2} Y^{*}_{lm}(\beta,\alpha)$$

$$D^{l}_{0m}(\alpha,\beta,\gamma) = (-1)^m \left(\frac{4\pi}{2l+1}\right)^{1/2} Y^{*}_{lm}(\beta,\gamma).$$

A.3. Irreducible tensor operators

The irreducible tensor operator $\mathbf{T}_l$ of rank l comprises the set of $2l+1$ operators T_{lm} (m is ranged from $-l$ to l) transformed under spatial rotations through the Wigner functions (Eq. (A4)), i.e. transformational properties of T_{lm} are similar to those of spherical harmonics. This definition is equivalent to the definition of irreducible tensor operator through commutation relationships (see [242]):

$$[I_z, T_{lm}] = mT_{lm}$$
$$[I_x \pm \mathrm{i}I_y, T_{lm}] = (l(l+1) - m(m\pm 1))^{1/2} T_{l,m\pm 1}, \quad \text{(A7)}$$

where I_x, I_y and I_z are the components of the angular momentum operator. An example of irreducible tensor operator of rank 1 is operator with components:

$$I_{-1} = \frac{I_x - \mathrm{i}I_y}{\sqrt{2}} = \frac{I_-}{\sqrt{2}} \qquad I_0 = I_z$$
$$I_1 = -\frac{I_x + \mathrm{i}I_y}{\sqrt{2}} = -\frac{I_+}{\sqrt{2}}. \quad \text{(A8)}$$

From two commuting tensor operators $\mathbf{A}_{l_1}$ of rank l_1 and $\mathbf{B}_{l_2}$ of rank l_2 one can compose an irreducible tensor operator $\mathbf{C}_l$ of rank l using the following relationship

$$C_{lm} = \sum c(l_1, l_2, l; m_1, m_2, m) A_{l_1 m_1} B_{l_2 m_2}, \quad \text{(A9)}$$

where the $c(l_1, l_2, l; m_1, m_2, m)$ are Clebsch–Gordan coefficients [242]. For example, from the two irreducible tensor operators $\mathbf{A}_1$ and $\mathbf{B}_1$ of rank 1 one can compose an irreducible tensor operator $\mathbf{C}_2$ of rank 2 with the components:

$$C_{20} = \frac{1}{\sqrt{6}}[2A_{10}B_{10} + (A_{11}B_{1,-1} + A_{1,-1}B_{11})] \quad \text{(A10a)}$$
$$C_{2,\pm 1} = \frac{1}{\sqrt{2}}[A_{10}B_{1,\pm 1} + A_{1,\pm 1}B_{10}]$$
$$C_{2,\pm 2} = A_{1,\pm 1}B_{1,\pm 1},$$

or, e.g. the irreducible tensor operator $\mathbf{C}_0$ of rank 0 with the component

$$C_{00} = -\frac{1}{\sqrt{3}}[A_{10}B_{10} - (A_{11}B_{1,-1} + A_{1,-1}B_{11}]. \quad \text{(A10b)}$$

References

[1] F. Bloch, Phys. Rev. 70 (1946) 460.
[2] N. Blombergen, E.M. Purcell, R.V. Pound, Phys. Rev. 73 (1948) 679.
[3] A.G. Redfield, IBM J Res. Dev. 1 (1957) 19.
[4] A.G. Redfield, Adv. Magn. Reson. 1 (1965) 1.
[5] A. Abragam, The principles of nuclear magnetism, Clarendon Press, Oxford, 1961.
[6] C.P. Slichter, Principles of magnetic resonance, Springer, Berlin, 1978.
[7] J. McConnell, Theory of nuclear magnetic relaxation in liquids, Cambridge University Press, Cambridge, 1987.
[8] J. Cavanagh, Protein NMR spectroscopy: principles and practice, Academic Press, New York, 1996.
[9] K. Blum, Density matrix theory and applications, Plenum Press, New York, 1981.
[10] R.R. Ernst, G. Bodenhausen, A. Wokaun, Principles of nuclear magnetic resonance in one and two dimensions, Oxford University Press, Oxford, 1987.
[11] P.S. Hubbard, Phys. Rev. 180 (1969) 319.
[12] J. Tropp, J. Chem. Phys. 72 (1980) 6035.
[13] H. Kessler, C. Griesinger, J. Lautz, A. Muller, W.F. van Gunsteren, H.J.C. Berendsen, J. Am. Chem. Soc. 110 (1988) 3393.
[14] D.M. Grant, in: D.M. Grant, R.K. Harris (Eds.), Encyclopedia of nuclear magnetic resonance, Wiley, New York, 1996 (1298 pp).
[15] M. Goldman, J. Magn. Reson. 60 (1984) 437.
[16] L. Werbelow, D.M. Grant, Adv. Magn. Reson. 9 (1977) 189.
[17] N. Tjandra, A. Szabo, A. Bax, J. Am. Chem. Soc. 118 (1996) 6986.
[18] E.L. Mackor, C. MacLean, Prog. Nucl. Magn. Reson. Spectrosc. 3 (1967) 129.

[19] K. Pervushin, R. Riek, G. Wider, K. Wuthrich, Proc. Natl. Acad. Sci. USA 94 (1997) 12 366.
[20] K. Pervushin, R. Riek, G. Wider, K. Wuthrich, J. Am. Chem. Soc. 120 (1998) 6394.
[21] K.V. Pervushin, G. Wider, R. Riek, K. Wuthrich, Proc. Natl. Acad. Sci. USA 96 (1999) 9607.
[22] D. Fushman, N. Tjandra, D. Cowburn, J. Am. Chem. Soc. 120 (1998) 10 947.
[23] D. Fushman, D. Cowburn, J. Am. Chem. Soc. 120 (1998) 7109.
[24] T.J. Norwood, M.L. Tillett, L.Y. Lian, Chem. Phys. Lett. 300 (1999) 429.
[25] M. Pellecchia, Y.X. Pang, L.C. Wang, A.V. Kurochkin, A. Kumar, E.R.P. Zuiderweg, J. Am. Chem. Soc. 121 (1999) 9165.
[26] M. Tessari, G.W. Vuister, J. Biomol. NMR 16 (2000) 171.
[27] H. Desvaux, P. Berthault, Prog. Nucl. Magn. Reson. Spectrosc. 35 (1999) 295.
[28] J.W. Peng, V. Thanabal, G. Wagner, J. Magn. Reson. 94 (1991) 82.
[29] J.W. Peng, G. Wagner, J. Magn. Reson. 98 (1992) 308.
[30] M. Guenneugues, P. Berthault, H. Desvaux, M. Goldman, J. Biomol. NMR 15 (1999) 295.
[31] E.L. Hahn, D.E. Maxwell, Phys. Rev. 88 (1952) 1070.
[32] H.M. McConnell, J. Chem. Phys. 28 (1958) 430.
[33] D.E. Woessner, J. Chem. Phys. 35 (1961) 41.
[34] C. Deverell, R.E. Morgan, J.H. Strange, Mol. Phys. 18 (1970) 553.
[35] H. Wennerstrom, Mol. Phys. 24 (1972) 69.
[36] D.G. Davis, M.E. Perlman, R.E. London, J. Magn. Reson. B 104 (1994) 266.
[37] N.Y. Carr, E.M. Purcell, Phys. Rev. 94 (1954) 30.
[38] S. Meiboom, D. Gill, Rev. Sci. Instrum. 29 (1958) 688.
[39] M. Bloom, L.W. Reeves, E.J. Wells, J. Chem. Phys. 42 (1965) 1615.
[40] A. Allerhand, H.S. Gutowsky, J. Chem. Phys. 42 (1965) 1587.
[41] A. Allerhand, E. Thiele, J. Chem. Phys. 45 (1966) 902.
[42] J. Jen, J. Magn. Reson. 30 (1978) 111.
[43] Z. Luz, S. Meiboom, J. Chem. Phys. 39 (1963) 366.
[44] V.Y. Orekhov, K.V. Pervushin, A.S. Arseniev, Eur. J. Biochem. 219 (1994) 887.
[45] A.G. Palmer, J. Williams, A. McDermott, J. Phys. Chem. 100 (1996) 13 293.
[46] J.P. Carver, R.E. Richards, J. Magn. Reson. 6 (1972) 89.
[47] T. Yamazaki, R. Muhandiram, L.E. Kay, J. Am. Chem. Soc. 116 (1994) 8266.
[48] J. Engelke, H. Ruterjans, J. Biomol. NMR 5 (1995) 173.
[49] L.E. Kay, D.A. Torchia, A. Bax, Biochemistry 28 (1989) 8972.
[50] M.J. Stone, W.J. Fairbrother, A.G. Palmer, J. Reizer, M.H. Saier, P.E. Wright, Biochemistry 31 (1992) 4394.
[51] N.A. Farrow, R. Muhandiram, A.U. Singer, S.M. Pascal, C.M. Kay, G. Gish, S.E. Shoelson, T. Pawson, J.D. Forman-Kay, L.E. Kay, Biochemistry 33 (1994) 5984.
[52] J.W. Peng, G. Wagner, Meth. Enzymol. 239 (1994) 563.
[53] K.T. Dayie, G. Wagner, J. Magn. Reson. A 111 (1994) 121.
[54] M. Tessari, H. Vis, R. Boelens, R. Kaptein, G.W. Vuister, J. Am. Chem. Soc. 119 (1997) 8985.
[55] C.D. Kroenke, J.P. Loria, L.K. Lee, M. Rance, A.G. Palmer, J. Am. Chem. Soc. 120 (1998) 7905.
[56] G.A. Morris, R. Freeman, J. Am. Chem. Soc. 101 (1979) 760.
[57] J. Cavanagh, A.G. Palmer, P.E. Wright, M. Rance, J. Magn. Reson. 91 (1991) 429.
[58] A.G. Palmer, J. Cavanagh, P.E. Wright, M. Rance, J. Magn. Reson. 93 (1991) 151.
[59] L.E. Kay, P. Keifer, T. Saarinen, J. Am. Chem. Soc. 114 (1992) 10 663.
[60] L.E. Kay, Prog. Biophys. Mol. Biol. 63 (1995) 277.
[61] L.E. Kay, Curr. Opin. Struct. Biol. 5 (1995) 674.
[62] R. Freeman, E. Kupce, NMR. Biomed. 10 (1997) 372.
[63] F.A.A. Mulder, R.A. de Graaf, R. Kaptein, R. Boelens, J. Magn. Reson. 131 (1998) 351.
[64] A. Bax, S.S. Pochapsky, J. Magn. Reson. 99 (1992) 638.
[65] N.J. Skelton, A.G. Palmer, M. Akke, J. Kordel, M. Rance, W.J. Chazin, J. Magn. Reson. B 102 (1993) 253.
[66] J. Boyd, U. Hommel, I.D. Campbell, Chem. Phys. Lett. 175 (1990) 477.
[67] A.G. Palmer, N.J. Skelton, W.J. Chazin, P.E. Wright, M. Rance, Mol. Phys. 75 (1992) 699.
[68] A. Ross, M. Czisch, G.C. King, J. Magn. Reson. 124 (1997) 355.
[69] D.M. Korzhnev, E.V. Tischenko, A.S. Arseniev, J. Biomol. NMR 17 (2000) 257.
[70] S. Zinn-Justin, P. Berthault, M. Guenneugues, H. Desvaux, J. Biomol. NMR 10 (1997) 363.
[71] M. Akke, A.G. Palmer, J. Am. Chem. Soc. 118 (1996) 911.
[72] M. Guenneugues, P. Berthault, H. Desvaux, J. Magn. Reson. 136 (1999) 118.
[73] J.L. Markley, W.J. Horsley, M.P. Klein, J. Chem. Phys. 55 (1971) 3604.
[74] S. Grzesiek, A. Bax, J. Am. Chem. Soc. 115 (1993) 12 593.
[75] Y.C. Li, G.T. Montelione, J. Magn. Reson. Ser. B 105 (1994) 45.
[76] A.C. Wang, A. Bax, J. Biomol. NMR 3 (1993) 715.
[77] S.M. Gagne, S. Tsuda, L. Spyracopoulos, L.E. Kay, B.D. Sykes, J. Mol. Biol. 278 (1998) 667.
[78] V.Y. Orekhov, D.M. Korzhnev, T. Diercks, H. Kessler, A.S. Arseniev, J. Biomol. NMR 14 (1999) 345.
[79] C. Bracken, P.A. Carr, J. Cavanagh, A.G. Palmer, J. Mol. Biol. 285 (1999) 2133.
[80] F.A.A. Mulder, P.J.A. van Tilborg, R. Kaptein, R. Boelens, J. Biomol. NMR 13 (1999) 275.
[81] R.H. Havlin, H.B. Le, D.D. Laws, A.C. deDios, E. Oldfield, J. Am. Chem. Soc. 119 (1997) 11 951.
[82] J. Heller, D.D. Laws, M. Tomaselli, D.S. King, D.E. Wemmer, A. Pines, R.H. Havlin, E. Oldfield, J. Am. Chem. Soc. 119 (1997) 7827.
[83] N. Tjandra, A. Bax, J. Am. Chem. Soc. 119 (1997) 9576.
[84] D. Sitkoff, D.A. Case, Prog. Nucl. Magn. Reson. Spectrosc. 32 (1998) 165.
[85] N. Tjandra, P. Wingfield, S. Stahl, A. Bax, J. Biomol. NMR 8 (1996) 273.
[86] M. Ottiger, N. Tjandra, A. Bax, J. Am. Chem. Soc. 119 (1997) 9825.

[87] J. Boyd, C. Redfield, J. Am. Chem. Soc. 121 (1999) 7441.
[88] C.D. Kroenke, M. Rance, A.G. Palmer, J. Am. Chem. Soc. 121 (1999) 10 119.
[89] C. Scheurer, N.R. Skrynnikov, S.F. Lienin, S.K. Straus, R. Bruschweiler, R.R. Ernst, J. Am. Chem. Soc. 121 (1999) 4242.
[90] D. Fushman, N. Tjandra, D. Cowburn, J. Am. Chem. Soc. 121 (1999) 8577.
[91] A.E. Walling, R.E. Pargas, A.C. deDios, J. Phys. Chem. A 101 (1997) 7299.
[92] S. Kuroki, N. Asakawa, S. Ando, I. Ando, A. Shoji, T. Ozaki, J. Mol. Struct. 245 (1991) 69.
[93] M. Tessari, F.A.A. Mulder, R. Boelens, G.W. Vuister, J. Magn. Reson. 127 (1997) 128.
[94] N. Tjandra, A. Bax, J. Am. Chem. Soc. 119 (1997) 8076.
[95] C.H. Wu, A. Ramamoorthy, L.M. Gierasch, S.J. Opella, J. Am. Chem. Soc. 117 (1995) 6148.
[96] R. Gerald, T. Bernhard, U. Haeberlen, J. Rendell, S. Opella, J. Am. Chem. Soc. 115 (1993) 777.
[97] G.A. Jeffrey, W. Saenger, Hydrogen bonding in biological structures, Springer, Berlin, 1994.
[98] D.A. Case, J. Biomol. NMR 15 (1999) 95.
[99] J.E. Roberts, G.S. Harbison, M.G. Munowitz, J. Herzfeld, R.G. Griffin, J. Am. Chem. Soc. 109 (1987) 4163.
[100] G.A. Jeffrey, in: A. Domenicano, I. Hargittai (Eds.), International Union of Crystallography Monographs on Crystallography, vol. 1, Oxford University Press, Oxford, 1992 (270 pp).
[101] M. Ottiger, A. Bax, J. Am. Chem. Soc. 120 (1998) 12 334.
[102] A.G. Palmer, D.A. Case, J. Am. Chem. Soc. 114 (1992) 9059.
[103] S. Kuroki, S. Ando, I. Ando, A. Shoji, T. Ozaki, G.A. Webb, J. Mol. Struct. 240 (1990) 19.
[104] V.Y. Orekhov, P.V. Dubovskii, H. Yamada, K. Akasaka, A.S. Arseniev, J. Biomol. NMR 17 (2000) 231.
[105] J.M. Schurr, H.P. Babcock, B.S. Fujimoto, J. Magn. Reson. Ser. B 105 (1994) 211.
[106] D.M. Korzhnev, V.Y. Orekhov, A.S. Arseniev, J. Magn. Reson. 127 (1997) 184.
[107] D.E. Woessner, J. Chem. Phys. 37 (1962) 647.
[108] W.T. Huntress, J. Chem. Phys. 48 (1968) 3524.
[109] L.D. Favro, Phys. Rev. 119 (1960) 53.
[110] R.F. Goldstein, Biopolymers 33 (1993) 409.
[111] W.T. Huntress, Adv. Magn. Reson. 4 (1970) 1.
[112] D.M. Grant, R.A. Brown, Encyclopedia of Nuclear Magnetic Resonance, in: Wiley, New York, 1996 (4003 pp).
[113] H. Brenner, J. Colloid. Interface. Sci. 23 (1967) 407.
[114] I.S. Beloborodov, V.Y. Orekhov, A.S. Arseniev, J. Magn. Reson. 132 (1998) 328.
[115] D. Brune, S. Kim, Proc. Natl. Acad. Sci. USA 90 (1993) 3835.
[116] J.G. de la Torre, V.A. Bloomfield, Biopolymers 16 (1977) 1747.
[117] J.G. de la Torre, V.A. Bloomfield, Biopolymers 16 (1977) 1765.
[118] J.G. de la Torre, V.A. Bloomfield, Q. Rev. Biophys. 14 (1981) 81.
[119] J. Happel, H. Brenner, Low Reynolds number hydrodynamics, with special applications to particulate media, Noordhoff, Leiden, 1973.
[120] J.M.G. Bernal, J.G. de la Torre, Biopolymers 19 (1980) 751.
[121] J. Rotne, S. Prager, J. Chem. Phys. 50 (1969) 4831.
[122] H. Yamakawa, J. Chem. Phys. 53 (1970) 436.
[123] G. Lamm, A. Szabo, J. Chem. Phys. 85 (1986) 7334.
[124] J.G. de la Torre, M.L. Huertas, B. Carrasco, Biophys. J. 78 (2000) 719.
[125] R.W. Pastor, M. Karplus, J. Phys. Chem. 92 (1988) 2636.
[126] R.W. Pastor, R. Zwanzig, J. Chem. Phys. 90 (1989) 5729.
[127] R.M. Venable, R.W. Pastor, Biopolymers 27 (1988) 1001.
[128] E. Ilyina, V. Roongta, H. Pan, C. Woodward, K.H. Mayo, Biochemistry 36 (1997) 3383.
[129] W.S. Price, F. Tsuchiya, Y. Arata, J. Am. Chem. Soc. 121 (1999) 11 503.
[130] M. HernandezContreras, O. AlarconWaess, M. Medina-Noyola, J. Chem. Phys. 106 (1997) 2492.
[131] G. Chirico, S. Beretta, G. Baldini, J. Chem. Phys. 110 (1999) 2297.
[132] J.O.M. Bockris, A.K.N. Reddy, Modern Electrochemistry, Plenum Press, New York, 1998.
[133] P. Stilbs, Prog. Nucl. Magn. Reson. Spectrosc. 19 (1987) 1.
[134] W.S. Price, Concepts. Magn. Reson. 9 (1997) 299.
[135] W.S. Price, Concepts. Magn. Reson. 10 (1998) 197.
[136] M.L. Tillett, L.Y. Lian, T.J. Norwood, J. Magn. Reson. 133 (1998) 379.
[137] V.P. Denisov, B. Halle, Faraday. Discuss. (1996) 227.
[138] G. Otting, Prog. Nucl. Magn. Reson. Spectrosc. 31 (1997) 259.
[139] B.M. Pettitt, V.A. Makarov, B.K. Andrews, Curr. Opin. Struct. Biol. 8 (1998) 218.
[140] G. Wider, Prog. Nucl. Magn. Reson. Spectrosc. 32 (1998) 193.
[141] C.R. Cantor, Biophysical Chemistry, Freeman, San Francisco, 1980.
[142] I.D. Kuntz Jr., W. Kauzmann, Adv. Protein Chem. 28 (1974) 239.
[143] J.S. Jiang, A.T. Brunger, J. Mol. Biol. 243 (1994) 100.
[144] H.X. Zhou, Biophys. J. 69 (1995) 2286.
[145] S.A. Allison, V.T. Tran, Biophys. J. 68 (1995) 2261.
[146] G. Barbato, M. Ikura, L.E. Kay, R.W. Pastor, A. Bax, Biochemistry 31 (1992) 5269.
[147] J.J. Muller, Biopolymers 31 (1991) 149.
[148] V.Y. Orekhov, D.M. Korzhnev, K.V. Pervushin, E. Hoffmann, A.S. Arseniev, J. Biomol. Struct. Dyn. 17 (1999) 157.
[149] G. Chirico, S. Beretta, Phys. Rev. E 60 (1999) 2148.
[150] R.J. Tough, Dynamic Light Scattering: Applications of Photon Correlation Spectroscopy, Plenum Press, New York, 1985.
[151] A. Van Blaaderen, J. Peetermans, G. Maret, J.K.G. Dhont, J. Chem. Phys. 96 (1992) 4591.
[152] C.L. Bon, T. Nicolai, M.E. Kuil, J.G. Hollander, J. Phys. Chem. B 103 (1999) 10 294.
[153] I.V. Ermolina, V.D. Fedotov, Y.D. Feldman, Physica A 249 (1998) 347.

[154] P. Barthe, N. Declerck, M.A. Delsuc, J.F. Lefevre, C. Roumestand, J. Chim. Phys: Chim. Biol. 96 (1999) 1585.
[155] W.X. Zhang, T.E. Smithgall, W.H. Gmeiner, Biochemistry 37 (1998) 7119.
[156] D. Fushman, S. Cahill, D. Cowburn, J. Mol. Biol. 266 (1997) 173.
[157] M. Karplus, J.A. McCammon, Annu. Rev. Biochem. 52 (1983) 263.
[158] V.A. Daragan, K.H. Mayo, Prog. Nucl. Magn. Reson. Spectrosc. 31 (1997) 63.
[159] K. Kinosita, S. Kawato, A. Ikegami, Biophys. J. 20 (1977) 289.
[160] R.J. Wittebort, A. Szabo, J. Chem. Phys. 69 (1978) 1722.
[161] R. Bruschweiler, D.A. Case, Phys. Rev. Lett. 72 (1994) 940.
[162] T. Bremi, R. Bruschweiler, R.R. Ernst, J. Am. Chem. Soc. 119 (1997) 4272.
[163] R. King, O. Jardetzky, Chem. Phys. Lett. 55 (1978) 15.
[164] G. Lipari, A. Szabo, J. Am. Chem. Soc. 104 (1982) 4546.
[165] G. Lipari, A. Szabo, J. Am. Chem. Soc. 104 (1982) 4559.
[166] G.M. Clore, A. Szabo, A. Bax, L.E. Kay, P.C. Driscoll, A.M. Gronenborn, J. Am. Chem. Soc. 112 (1990) 4989.
[167] J.W. Peng, G. Wagner, Biochemistry 31 (1992) 8571.
[168] W.H. Press, S.A. Tenkolsky, W.T. VeHerling, B.P. Flannery, Numerical Recipes in C: The Art of Scientific Computing, Cambridge University Press, Cambridge, 1997.
[169] D.Q. Jin, F. Figueirido, G.T. Montelione, R.M. Levy, J. Am. Chem. Soc. 119 (1997) 6923.
[170] D.Q. Jin, M. Andrec, G.T. Montelione, R.M. Levy, J. Biomol. NMR 12 (1998) 471.
[171] M.T. McMahon, E. Oldfield, J. Biomol. NMR 13 (1999) 133.
[172] E. Lloyd, Handbook of applicable mathematics. Statistics, Part A, Wiley, New York, 1980.
[173] A.M. Mandel, M. Akke, A.G. Palmer, J. Mol. Biol. 246 (1995) 144.
[174] K. Yamasaki, M. Saito, M. Oobatake, S. Kanaya, Biochemistry 34 (1995) 6587.
[175] M. Andrec, G.T. Montelione, R.M. Levy, J. Magn. Reson. 139 (1999) 408.
[176] D.E. Woessner, J. Chem. Phys. 36 (1962) 1.
[177] O. Millet, J.P. Loria, C.D. Kroenke, M. Pons, A.G. Palmer, J. Am. Chem. Soc. 122 (2000) 2867.
[178] G.M. Clore, P.C. Driscoll, P.T. Wingfield, A.M. Gronenborn, Biochemistry 29 (1990) 7387.
[179] J.J. Barchi, B. Grasberger, A.M. Gronenborn, G.M. Clore, Protein. Sci. 3 (1994) 15.
[180] N. Tjandra, H. Kuboniwa, H. Ren, A. Bax, Eur. J. Biochem. 230 (1995) 1014.
[181] K.A. Williams, N.A. Farrow, C.M. Deber, L.E. Kay, Biochemistry 35 (1996) 5145.
[182] V.Y. Orekhov, D.E. Nolde, A.P. Golovanov, D.M. Korzhnev, A.S. Arseniev, Appl. Magn. Reson. 9 (1995) 581.
[183] V.Y. Orekhov, K.V. Pervushin, D.M. Korzhnev, A.S. Arseniev, J. Biomol. NMR 6 (1995) 113.
[184] N. Tjandra, S.E. Feller, R.W. Pastor, A. Bax, J. Am. Chem. Soc. 117 (1995) 12 562.
[185] Z.W. Zheng, J. Czaplicki, O. Jardetzky, Biochemistry 34 (1995) 5212.
[186] R. Bruschweiler, X.B. Liao, P.E. Wright, Science 268 (1995) 886.
[187] L.K. Lee, M. Rance, W.J. Chazin, A.G. Palmer, J. Biomol. NMR 9 (1997) 287.
[188] J.P. Mackay, G.L. Shaw, G.F. King, Biochemistry 35 (1996) 4867.
[189] I.Q.H. Phan, J. Boyd, I.D. Campbell, J. Biomol. NMR 8 (1996) 369.
[190] F. Cordier, M. Caffrey, B. Brutscher, M.A. Cusanovich, D. Marion, M. Blackledge, J. Mol. Biol. 281 (1998) 341.
[191] B.M. Lee, R.N. De Guzman, B.G. Turner, N. Tjandra, M.F. Summers, J. Mol. Biol. 279 (1998) 633.
[192] H. Vis, C.E. Vorgias, K.S. Wilson, R. Kaptein, R. Boelens, J. Biomol. NMR 11 (1998) 265.
[193] M. Blackledge, F. Cordier, P. Dosset, D. Marion, J. Am. Chem. Soc. 120 (1998) 4538.
[194] P. Luginbuhl, K.V. Pervushin, H. Iwai, K. Wuthrich, Biochemistry 36 (1997) 7305.
[195] A.G. Palmer, Curr. Opin. Struct. Biol. 7 (1997) 732.
[196] L.E. Kay, Nat. Struct. Biol. 5 (1998) 513.
[197] A.L. Lee, A.J. Wand, J. Biomol. NMR 13 (1999) 101.
[198] J. Habazettl, L.C. Myers, F. Yuan, G.L. Verdine, G. Wagner, Biochemistry 35 (1996) 9335.
[199] B. Brutscher, R. Bruschweiler, R.R. Ernst, Biochemistry 36 (1997) 13 043.
[200] D. Fushman, D. Cowburn, J. Biomol. NMR 13 (1999) 139.
[201] L. Spyracopoulos, S.M. Gagne, M.X. Li, B.D. Sykes, Biochemistry 37 (1998) 18 032.
[202] J.R. Tolman, J.M. Flanagan, M.A. Kennedy, J.H. Prestegard, Nat. Struct. Biol. 4 (1997) 292.
[203] A. Bax, N. Tjandra, Nat. Struct. Biol. 4 (1997) 254.
[204] D.M. Korzhnev, V.Y. Orekhov, A.S. Arseniev, R. Gratias, H. Kessler, J. Phys. Chem. B 103 (1999) 7036.
[205] D.M. Korzhnev, V.Y. Orekhov, A.S. Arseniev, J. Biomol. NMR 14 (1999) 357.
[206] J.W. Peng, G. Wagner, Biochemistry 34 (1995) 16 733.
[207] N.A. Farrow, O.W. Zhang, A. Szabo, D.A. Torchia, L.E. Kay, J. Biomol. NMR 6 (1995) 153.
[208] R. Ishima, K. Nagayama, J. Magn. Reson. B 108 (1995) 73.
[209] R. Ishima, K. Nagayama, Biochemistry 34 (1995) 3162.
[210] J.F. Lefevre, K.T. Dayie, J.W. Peng, G. Wagner, Biochemistry 35 (1996) 2674.
[211] T. Szyperski, P. Luginbuhl, G. Otting, P. Guntert, K. Wuthrich, J. Biomol. NMR 3 (1993) 151.
[212] M. Akke, J. Liu, J. Cavanagh, H.P. Erickson, A.G. Palmer, Nat. Struct. Biol. 5 (1998) 55.
[213] J.P. Loria, M. Rance, A.G. Palmer, J. Am. Chem. Soc. 121 (1999) 2331.
[214] R. Ishima, D.A. Torchia, J. Biomol. NMR 14 (1999) 369.
[215] W.F. van Gunsteren, X. Daura, A.E. Mark, Enc. Comput. Chem. 2 (1998) 1211.
[216] W.F. van Gunsteren, H.J.C. Berendsen, Angew. Chem: Int. Ed. Engl. 29 (1990) 992.
[217] T. Darden, D. York, L. Pedersen, J. Chem. Phys. 98 (1993) 10 089.
[218] J.P. Ryckaert, G. Ciccotti, H.J.C. Berendsen, J. Comput. Phys. 23 (1977) 327.

[219] H.J.C. Berendsen, J.P.M. Postma, W.F. van Gunsteren, A. Dinola, J.R. Haak, J. Chem. Phys. 81 (1984) 3684.
[220] R. Ishima, K. Yamasaki, M. Saito, K. Nagayama, J. Biomol. NMR 6 (1995) 217.
[221] M.A.L. Eriksson, H. Berglund, T. Hard, L. Nilsson, Proteins 17 (1993) 375.
[222] J. Kordel, O. Teleman, J. Am. Chem. Soc. 114 (1992) 4934.
[223] D. Fushman, O. Ohlenschlager, H. Ruterjans, J. Biomol. Struct. Dyn. 11 (1994) 1377.
[224] M. Philippopoulos, C. Lim, J. Mol. Biol. 254 (1995) 771.
[225] M. Philippopoulos, A.M. Mandel, A.G. Palmer, C. Lim, Proteins 28 (1997) 481.
[226] K.V. Pervushin, V.Y. Orekhov, D.M. Korzhnev, A.S. Arseniev, J. Biomol. NMR 5 (1995) 383.
[227] L.J. Smith, A.E. Mark, C.M. Dobson, W.F. van Gunsteren, Biochemistry 34 (1995) 10 918.
[228] P.E. Smith, R.C. Vanschaik, T. Szyperski, K. Wuthrich, W.F. van Gunsteren, J. Mol. Biol. 246 (1995) 356.
[229] M.R. Gryk, R. Abseher, B. Simon, M. Nilges, H. Oschkinat, J. Mol. Biol. 280 (1998) 879.
[230] K.B. Wong, V. Daggett, Biochemistry 37 (1998) 11 182.
[231] V.A. Daragan, K.H. Mayo, J. Phys. Chem. 100 (1996) 8378.
[232] L.K. Iyer, S. Vishveshwara, Biopolymers 38 (1996) 401.
[233] V. Daggett, M. Levitt, J. Mol. Biol. 223 (1992) 1121.
[234] R. Bruschweiler, P.E. Wright, J. Am. Chem. Soc. 116 (1994) 8426.
[235] T. Bremi, R. Bruschweiler, J. Am. Chem. Soc. 119 (1997) 6672.
[236] R. Bruschweiler, J. Am. Chem. Soc. 114 (1992) 5341.
[237] S. Sunada, N. Go, P. Koehl, J. Chem. Phys. 104 (1996) 4768.
[238] D.A. Case, Curr. Opin. Struct. Biol. 4 (1994) 285.
[239] M. Karplus, J.N. Kushick, Macromolecules 14 (1981) 325.
[240] R.M. Levy, M. Karplus, J. Kushick, D. Perahia, Macromolecules 17 (1984) 1370.
[241] A. Amadei, A.B.M. Linssen, H.J.C. Berendsen, Proteins 17 (1993) 412.
[242] R.N. Zare, Angular Momentum: Understanding Spatial Aspects in Chemistry and Physics, Wiley, New York, 1988.
[243] C.J. Hartzell, M. Whitfield, T.G. Oas, G.P. Drobny, J. Am. Chem. Soc. 109 (1987) 5966.
[244] T.G. Oas, C.J. Hartzell, F.W. Dahlquist, G.P. Drobny, J. Am. Chem. Soc. 109 (1987) 5962.
[245] A. Shoji, T. Ozaki, T. Fujito, K. Deguchi, S. Ando, I. Ando, Macromolecules 22 (1989) 2860.
[246] M. Ashikawa, A. Shoji, T. Ozaki, I. Ando, Macromolecules 32 (1999) 2288.
[247] D.K. Lee, R.J. Wittebort, A. Ramamoorthy, J. Am. Chem. Soc. 120 (1998) 8868.
[248] L.W. Jelinski, D.A. Torchia, J. Mol. Biol. 133 (1979) 45.
[249] D.K. Lee, J.S. Santos, A. Ramamoorthy, J. Phys. Chem. B 103 (1999) 8383.
[250] Y. Hiyama, C.H. Niu, J.V. Silverton, A. Bavoso, D.A. Torchia, J. Am. Chem. Soc. 110 (1988) 2378.
[251] A. Naito, A. Fukutani, M. Uitdehaag, S. Tuzi, H. Saito, J. Mol. Struct. 441 (1998) 231.
[252] M. Munowitz, W.P. Aue, R.G. Griffin, J. Chem. Phys. 77 (1982) 1686.
[253] G.S. Harbison, L.W. Jelinski, R.E. Stark, D.A. Torchia, J. Herzfeld, R.G. Griffin, J. Magn. Reson. 60 (1984) 79.
[254] A. Shoji, T. Ozaki, T. Fujito, K. Deguchi, I. Ando, J. Magoshi, J. Mol. Struct. 441 (1998) 251.
[255] D.K. Lee, J.S. Santos, A. Ramamoorthy, Chem. Phys. Lett. 309 (1999) 209.
[256] G.C. Levy, R.L. Lichter, Nitrogen-15 Nuclear Magnetic Resonance Spectroscopy, Wiley, New York, 1979.
[257] R.T. Clubb, J.G. Omichinski, K. Sakaguchi, E. Appella, A.M. Gronenborn, G.M. Clore, Protein Sci. 4 (1995) 855.
[258] J.T. Stivers, C. Abeygunawardana, A.S. Mildvan, C.P. Whitman, Biochemistry 35 (1996) 16036.